Supporting Information

A General Method for Selective Recognition of Monosaccharides and Oligosaccharides in Water

Roshan W. Gunasekara, and Yan Zhao*

Department of Chemistry, Iowa State University, Ames, Iowa 50011-3111, USA

Table of Contents

General Method

Methanol, methylene chloride, and ethyl acetate were of HPLC grade and were purchased from Fisher Scientific. The blood group H disaccharide, blood group A trisaccharide, and blood group B trisaccharide were bought from Carbosynth. All other reagents, sugars, and solvents were of ACS-certified grade or higher, and were used as received from the commercial suppliers. Routine ^{1}H and ^{13}C NMR spectra were recorded on a Bruker DRX-400, on a Bruker AV II 600 or on a Varian VXR-400 spectrometer. ESI-MS mass was recorded on Shimadzu LCMS-2010 mass spectrometer. Dynamic light scattering (DLS) data were recorded at 25 °C using PDDLS/ CoolBatch 90T with PD2000DLS instrument. Isothermal titration calorimetry (ITC) was performed using a MicroCal VP-ITC Microcalorimeter with Origin 7 software and VPViewer2000 (GE Healthcare, Northampton, MA).

Scheme 1S

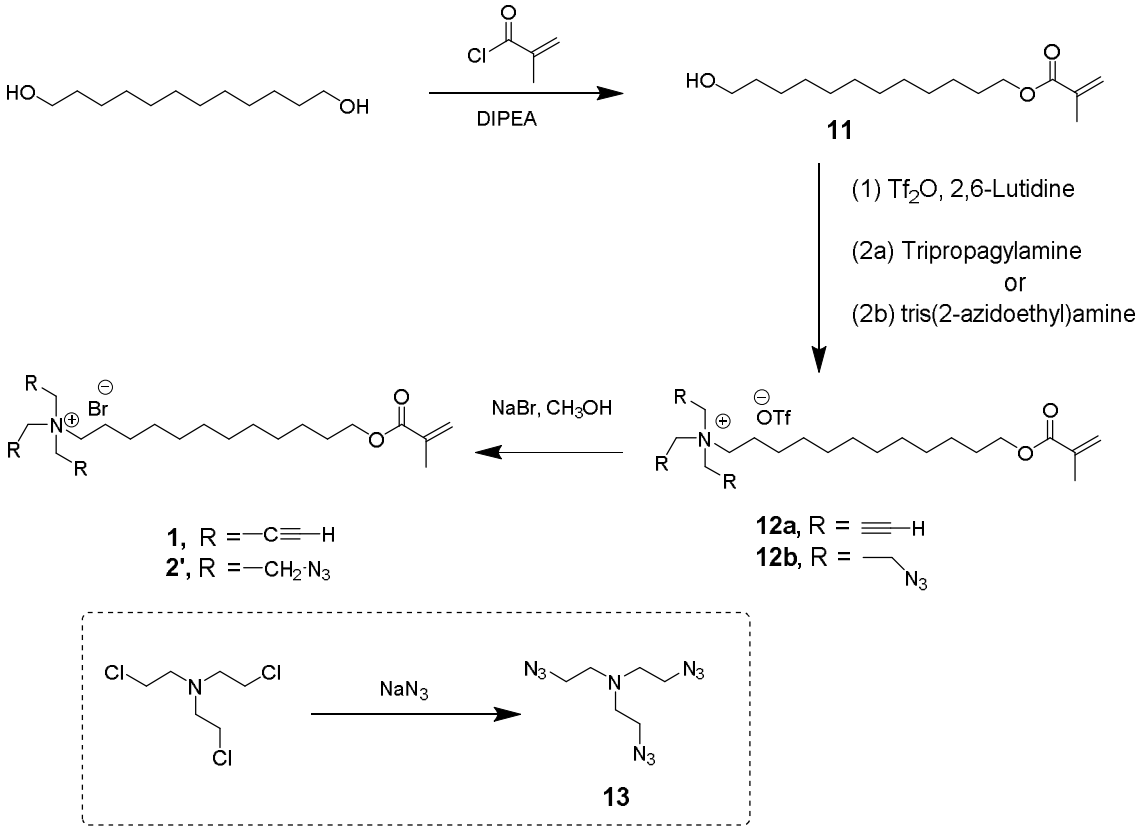

Scheme 2S

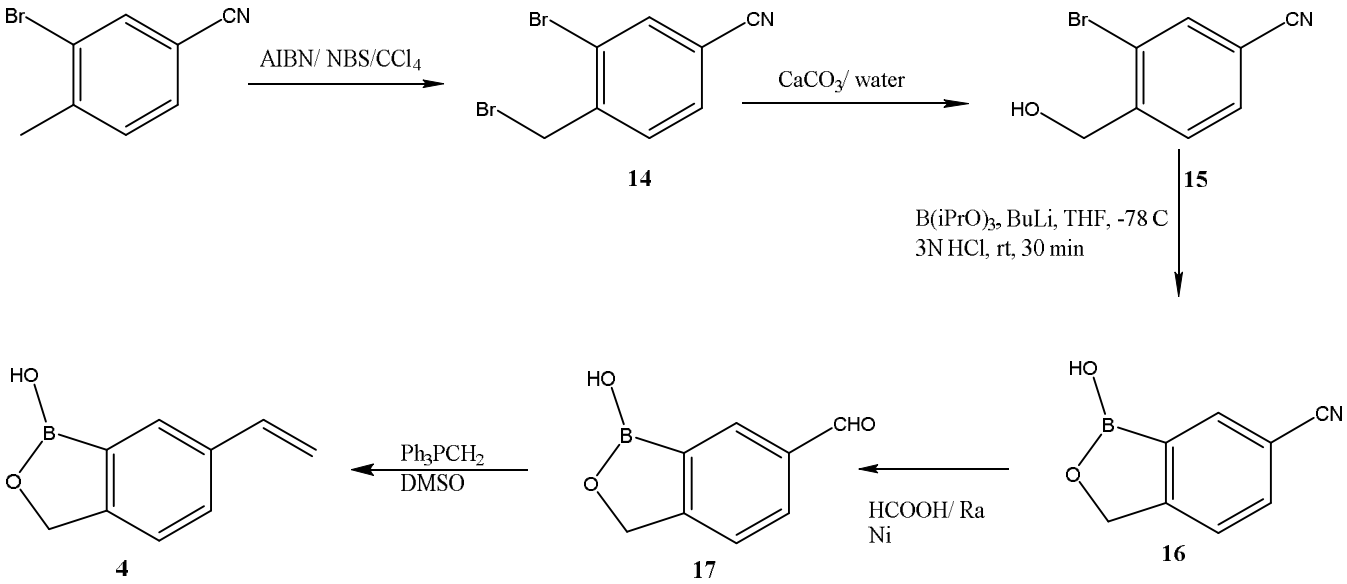

Scheme 3S

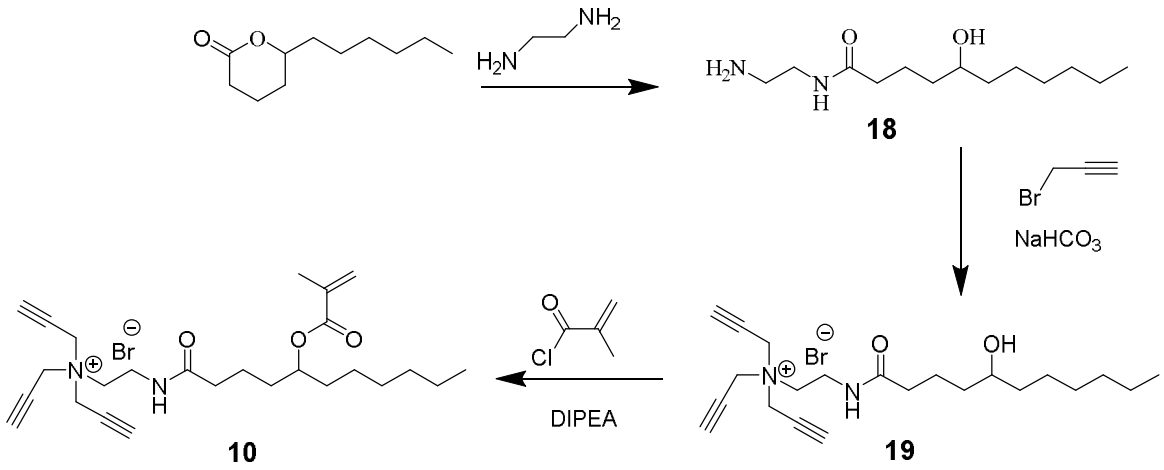

Syntheses

Compounds **1**,[1] **11**,[1] **12a**,[1] **13**,[2] **14**,[3] **15**,[4] **16**,[3] **17**,[3] **4**,[3] **18**,[5] **19**,[5] and **10**[5] were synthesized following reported procedures.

Compound 2'. Triflic anhydride (0.40 mL, 2.4 mmol) and 2,6-lutidine (0.26 mL, 2.4 mmol) were added to 7 mL of dry dichloromethane, which was cooled at -20 °C. The cooling bath was removed and compound **11** (0.50 g, 1.8 mmol) in CH_2Cl_2 (3 mL) was added dropwise to the stirred solution. After being stirred at room temperature for 90 min, the reaction mixture was diluted with CH_2Cl_2 (5 mL). The organic layer was washed with 1 M HCl (10 mL) and water (2 × 10 mL), dried with magnesium sulfate, filtered, and concentrated by rotary evaporation to give the triflate as a yellowish oil (680 mg, 94 %). The oil was dissolved in dry THF (5 mL) and compound **13** (0.88 mL, 2.2 mmol) was added dropwise. After being stirred at room temperature overnight, the reaction mixture was concentrated by rotary evaporation and the residue was purified by column chromatography over silica

[1] Awino, J. K.; Zhao, Y. *J. Am. Chem. Soc*. **2013**, *135*, 12552.
[2] Michaels, H.A.; Zhu L. *Chem Asian J*., **2011**, *6*, 2825.
[3] Boron-containing small molecules as antiprotozoal agents- WO2011022337 A1.
[4] Kim, H.; Kang, Y.J.; Kang, S.; Kim K.T. *J. Am. Chem. Soc.*, **2012**, *134*, 4030.
[5] Arifuzzaman, M. D.; Zhao, Y. *J. Org. Chem.* **2016**, *81*, 7518.

gel using 1:10 methanol/ CH_2Cl_2 as eluent to afford yellowish oil (compound **12b,** 869 mg, 77 %). This oil was dissolved in methanol (5 mL), followed by the addition of excess sodium bromide solution in 5 mL of water (3.86 g, 37.5 mmol). After being stirred for 6 h, the reaction mixture was diluted with CH_2Cl_2 (10 mL). The organic layer was washed with water (2 × 30 mL), dried with sodium sulfate, and concentrated by rotary evaporation. The process was repeated once to afford a yellowish oil (770, 100 %). ^{1}H NMR (400 MHz, $CDCl_3$, δ): 6.09 (s, 1H), 5.54 (s, 1H), 4.13 (t, *J* = 6.7 Hz, 2H), 3.40 (d, *J* = 5.3 Hz, 14H), 1.94 (s, 3H), 1.42 – 1.15 (m, 20H). ^{13}C NMR (100 MHz, $CDCl_3$, δ): 167.4, 136.4, 125.1, 77.2, 77.1, 70.6, 70.5, 70.5, 70.5, 70.5, 70.5, 70.5, 70.5, 70.5, 64.7, 53.8, 53.8, 29.4, 29.4, 29.4, 29.4, 29.4, 28.5, 26.4, 26.4, 26.4, 26.4, 26.4, 26.4, 26.4, 26.4, 26.4, 26.4, 26.4, 26.4, 26.3, 26.3, 26.3, 26.3, 18.2. ESI-HRMS (m/z): $[M\text{-}Br]^+$ calcd for $C_{22}H_{41}N_{10}O_2$, 477.3408; found, 477.3402.

Compound 14. 3-bromo-4-methylbenzonitrile (1.00 g, 5.1 mmol) was added to 2,2′-azobis(2-methylpropionitrile) (AIBN, 42 mg, 0.25 mmol) and N-bromosuccinimide (NBS, 1.00 g, 5.61 mmol) in CCl4 (40 mL). The mixture was refluxed for 18 h and cooled to room temperature. The residue was mixed with water (10 mL) and extracted with DCM (3×15 mL), dried with anhydrous Na_2SO_4, and concentrated in vacuo to obtain white powder (1.10 g, 80%). 1H NMR (600 MHz, CDCl3, δ): 7.87 (d, J = 1.5 Hz, 1H), 7.58 (m, 2H), 4.58 (s, J = 1.7 Hz, 2H).

Compound 15. 3-bromo-4-bromomethylbenzonitrile (1.50 g, 5.45 mmol) was added to a suspension of $CaCO_3$ (2.5 g, 25 mmol) in dioxane/water (2:3 v/v, 60 mL). This mixture was stirred at 100 °C for 28 h. After cooling to room temperature, the reaction mixture was extracted with diethyl ether (3×20 mL). The combined organic phase was washed with brine (15 mL), water (20 mL), dried over anhydrous $MgSO_4$, and concentrated *in vacuo*. The resulting solid was recrystallized with CH_2Cl_2/MeOH (80:10, v/v) to obtained white powder (0.89 g, 77%). ^{1}H NMR (600 MHz, CD_3OD, δ): 7.94 (s, 1H), 7.74 (m, 2H), 4.69 (s, 2H).

Compound 16. Compound **15** (422 mg, 2.0 mmol) and triisopropyl borate (0.92 mL, 4.0 mmol) in anhydrous THF (10 mL) at N_2 atmosphere was cooled at -78 °C for 20 min. 2M n-BuLi in hexane (2.25 mL, 4.50 mmol) was added dropwise at-78° C. Then the mixture was allowed to warm to room temperature and stirred at room temperature for overnight under N_2 atmosphere. The mixture was quenched with IN HCl and extracted with ethyl acetate (3×10 mL). The combined organic layers were washed with brine (20 mL), dried over anhydrous $MgSO_4$, concentrated *in vacuo*. The residue was purified by a flash column chromatograph over silica gel with 4:1 dichloromethane/methanol as the eluent to give a yellow powder (0.22, 69%). ^{1}H NMR (600 MHz, CD_3OD, δ): 7.99 (s, 1H), 7.81 (dt, *J* = 7.9, 1.5 Hz, 1H), 7.59 (d, *J* = 7.9 Hz, 1H), 5.17 (s, 2H).

Compound 17. Compound **16** (0.1 g, 0.63 mmol) in HCOOH/water/THF (16:2:12 v/v/v, 30 mL) was added to Raney-Ni (0.85 g) and refluxed for 3 h. The reaction mixture was cooled and filtered through Celite and concentrated *in vacuo*. The filtrate was extracted with ethyl acetate (3×5 mL), washed with brine (5 mL), dried with anhydrous $MgSO_4$ and concentrated *in vacuo*. The residue was purified by a flash column chromatograph over silica gel with 20:1 dichloromethane/methanol as the eluent to give a white powder (81 mg, 80%). ^{1}H NMR (600 MHz, CD_3OD, δ): 10.01 (s, 1H), 8.25 (s, 1H), 8.01 (dt, *J* = 7.9, 1.5 Hz, 1H), 7.59 (d, *J* = 7.9 Hz, 1H), 5.11 (s, 2H).

Compound 4. Methyltriphenylphosphonium bromide (1.0 g, 2.8 mmol) and potassium t-butoxide (0.38 g, 3.30 mmol) was mixed in DMSO (4 mL) and stirred 4 h before adding compound **17** (0.3 g, 1.85 mmol) in THF (6 mL). The reaction was stirred 14 h and quenched with aqueous HCl and extracted with ethyl acetate (3×10 mL), washed with brine (5 mL), dried with anhydrous $MgSO_4$ and concentrated *in vacuo*. The residue was purified by a flash column chromatograph over silica gel with 20:1 dichloromethane/methanol as the eluent to give a white powder (0.21, 72%). ^{1}H NMR (400 MHz, $DMSO_4$-D_6, δ): 9.17 (s, 1H), 7.75 (d, *J* = 1.5 Hz, 1H), 7.56 (d, *J* = 8.0 Hz, 1H), 7.35 (d, *J* = 7.9 Hz,

1H), 6.76 (dd, *J* = 17.6, 10.9 Hz, 1H), 5.78 (d, *J* = 17.7 Hz, 1H), 5.22 (d, *J* = 11.0 Hz, 1H), 4.94 (s, 2H).

Synthesis of monosaccharide MINPs. A solution of 6-vinylbenzoxaborole (**4**) in methanol (10 µL of a 6.4 mg/mL, 0.0004 mmol) was added to glucose in methanol (10 µL of 7.20 mg/mL, 0.0004 mmol) in a vial containing methanol (5 mL). After the mixture was stirred for 6 h at room temperature, methanol was removed *in vacuo*. A micellar solution of **1** (0.03 mmol), **2'** (0.02 mmol), divinylbenzene (DVB, 2.8 µL, 0.02 mmol), and 2,2-dimethoxy-2-phenylacetophenone (DMPA,10 µL of a 12.8 mg/mL solution in DMSO, 0.0005 mmol) in D_2O (2.0 mL) was added to the sugar–boronate complex. (D_2O instead of H_2O was used to allow the reaction progress to be monitored by ^1H NMR spectroscopy.) The mixture was subjected to ultrasonication for 10 min before $CuCl_2$ (10 µL of a 6.7 mg/mL solution in D_2O, 0.0005 mmol) and sodium ascorbate (10 µL of a 99 mg/mL solution in D_2O, 0.005 mmol) were added. After the reaction mixture was stirred slowly at room temperature for 12 h, the reaction mixture was transferred into a glass vial, purged with nitrogen for 15 min, sealed with a rubber stopper, and irradiated in a Rayonet reactor for 8 h. Compound **3** (10.6 mg, 0.04 mmol), $CuCl_2$ (10 µL of a 6.7 mg/mL solution in D_2O, 0.0005 mmol), and sodium ascorbate (10 µL of a 99 mg/mL solution in D_2O, 0.005 mmol) were added. After being stirred for another 6 h at room temperature, the reaction mixture was poured into acetone (8 mL). The precipitate collected by centrifugation was washed with a mixture of acetone/water (5 mL/1 mL), and methanol/acetic acid (5 mL/0.1 mL) for three times and finally with acetone (1×5 mL) to neutral before being dried in air to afford the final MINPs.

Table 1S. Monosaccharide mixing method

Entry	MINP	Amount of 0.04 M Sugar / µL	Amount of 0.04 M 6-vinylbenzoxoborole / µL	Ratio (Sugar:benzoxoborole)
1	MINP(glucose)	10	10	1:1
2	MINP(glucose)	10	20	1:2
3	MINP(glucose)	10	30	1:3
4	NINP[a]	-	-	-
5	NINP[b]	-	20	-
6	MINP(mannose)	10	20	1:2
7	MINP(galactose)	10	20	1:2
8	MINP(**5**)	10	10	1:1

[a] The nonimprinted nanoparticles were prepared without functional monomer **4** and sugar. [b] The nonimprinted nanoparticles were prepared with functional monomer **4** but without sugar.

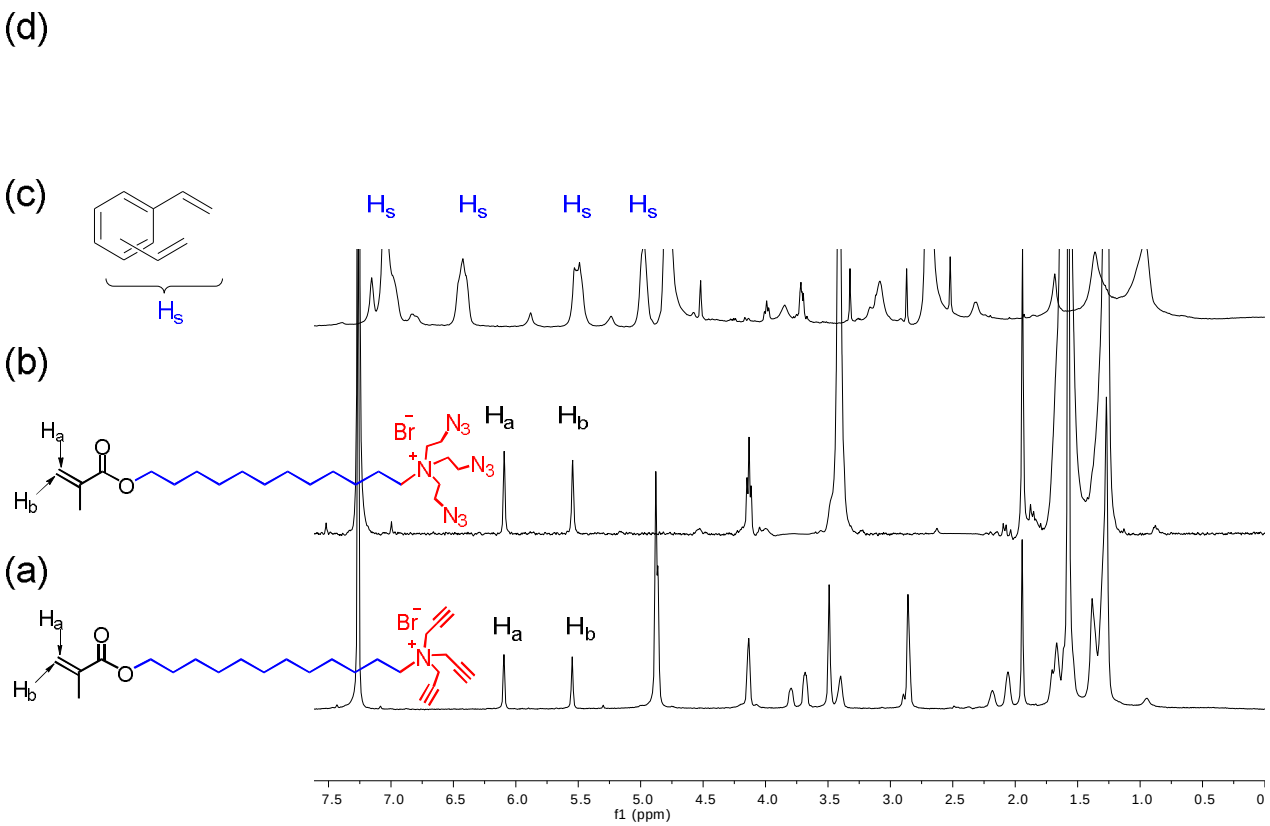

Figure 1S. ^{1}H NMR spectra of (a) Compound **1** in $CDCl_3$, (b) Compound **2'** in $CDCl_3$, (c) alkynyl-SCM in D_2O, and (d) MINP(glucose) in D_2O at 298 K. The data correspond to entry 1 in Table 1S.

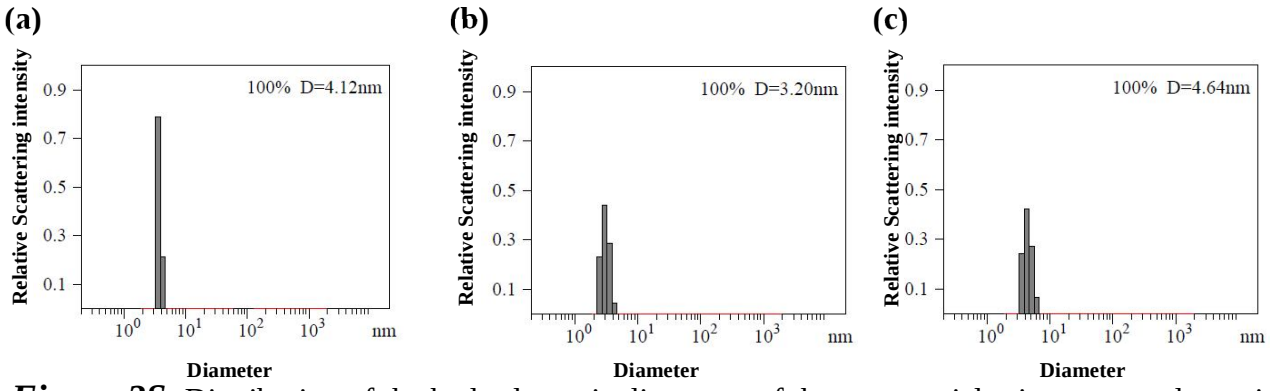

Figure 2S. Distribution of the hydrodynamic diameters of the nanoparticles in water as determined by DLS for the synthesis of MINP(glucose) (a) alkynyl-SCM, (b) core-cross-linked SCM, and (c) surface-functionalized MINP(glucose) after purification. The data correspond to entry 1 in Table 1S.

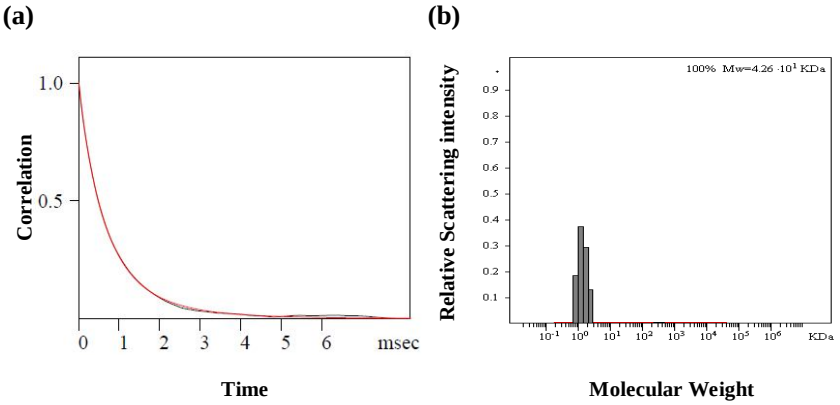

Figure 3S. The correlation curve and the distribution of the molecular weight for MINP(glucose) from the DLS. The data correspond to entry 1 in Table 1S. The PRECISION DECONVOLVE program assumes the intensity of scattering is proportional to the mass of the particle squared. If each unit of building block for the MINP(glucose) is assumed to contain 0.6 molecules of compound **1** (MW = 465 g/mol), 0.4 molecules of compound **2'** (MW = 558 g/mol), 0.6 molecules of compound **3** (MW = 264 g/mol), one molecule of DVB (MW = 130 g/mol), and 0.02 molecules of 6-vinylbenzoxaborole (MW = 160 g/mol), the molecular weight of MINP(glucose) translates to 54 [= 42600 / (0.6×465 +0.4×558 +0.6×264 +130 +0.02×160)] of such units.

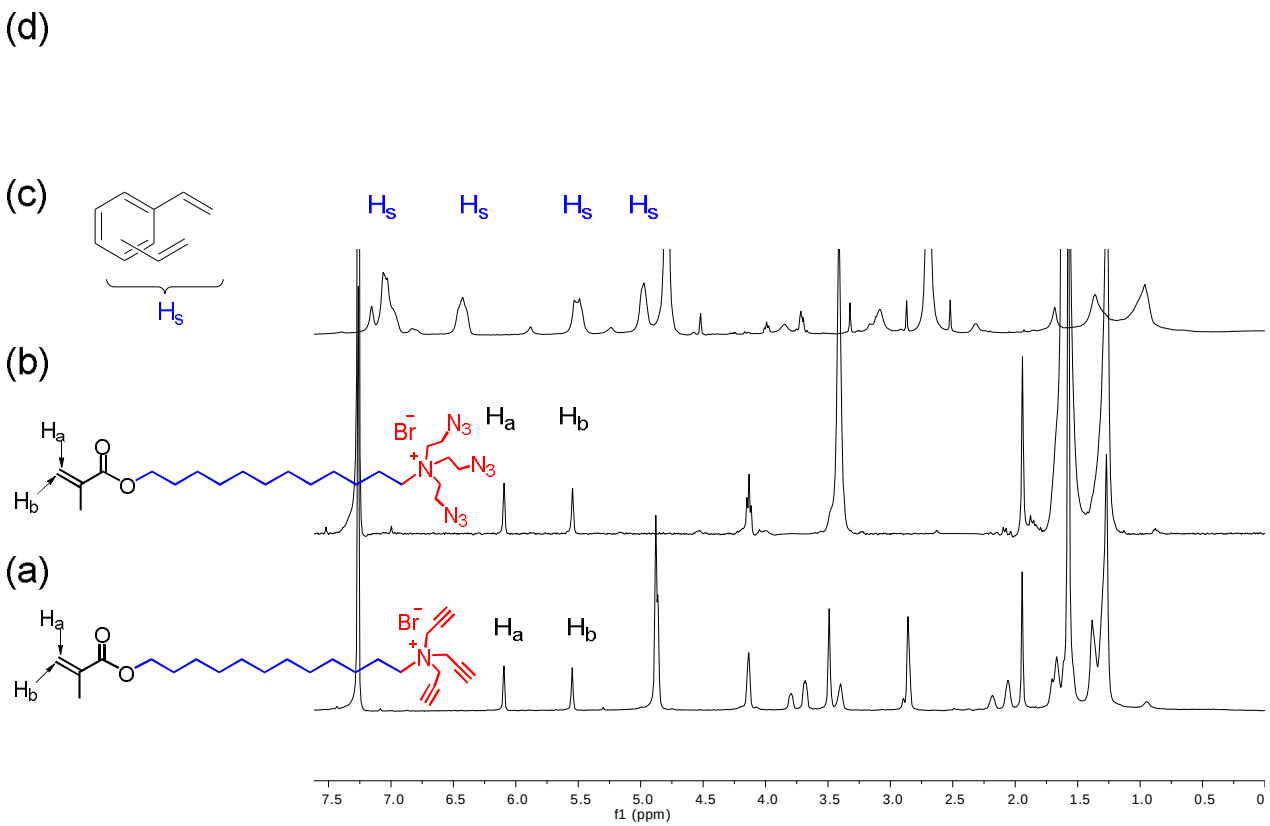

Figure 4S. ^{1}H NMR spectra of (a) Compound **1** in $CDCl_3$, (b) Compound **2'** in $CDCl_3$, (c) alkynyl-SCM in D_2O, and (d) MINP(glucose) in D_2O at 298 K. The data correspond to entry 2 in Table 1S.

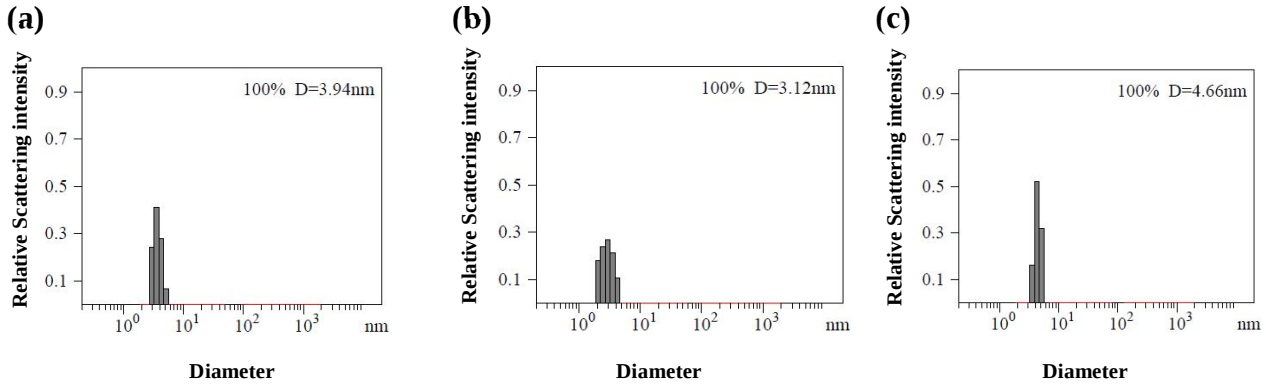

Figure 5S. Distribution of the hydrodynamic diameters of the nanoparticles in water as determined by DLS for the synthesis of MINP(glucose) (a) alkynyl-SCM, (b) core-cross-linked-SCM, and (c) surface-functionalized MINP(glucose) after purification. The data correspond to entry 2 in Table 1S.

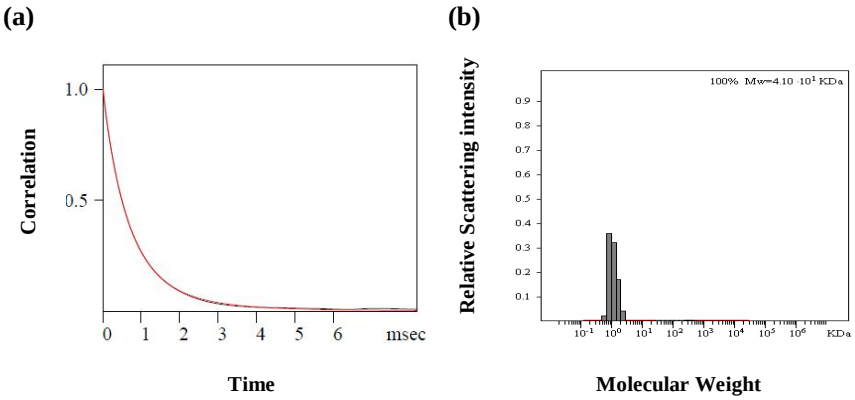

Figure 6S. The correlation curve and the distribution of the molecular weight for MINP(glucose) from the DLS. The data correspond to entry 2 in Table 1S. The PRECISION DECONVOLVE program assumes the intensity of scattering is proportional to the mass of the particle squared. If each unit of building block for the MINP(glucose) is assumed to contain 0.6 molecules of compound **1** (MW = 465 g/mol), 0.4 molecules of compound **2'** (MW = 558 g/mol), 0.6 molecules of compound **3** (MW = 264 g/mol), one molecule of DVB (MW = 130 g/mol), and 0.04 molecules of 6-vinylbenzoxaborole (MW = 160 g/mol), the molecular weight of MINP(glucose) translates to 51 [= 41000 / (0.6×465 +0.4×558 +0.6×264 +130 +0.04×160)] of such units.

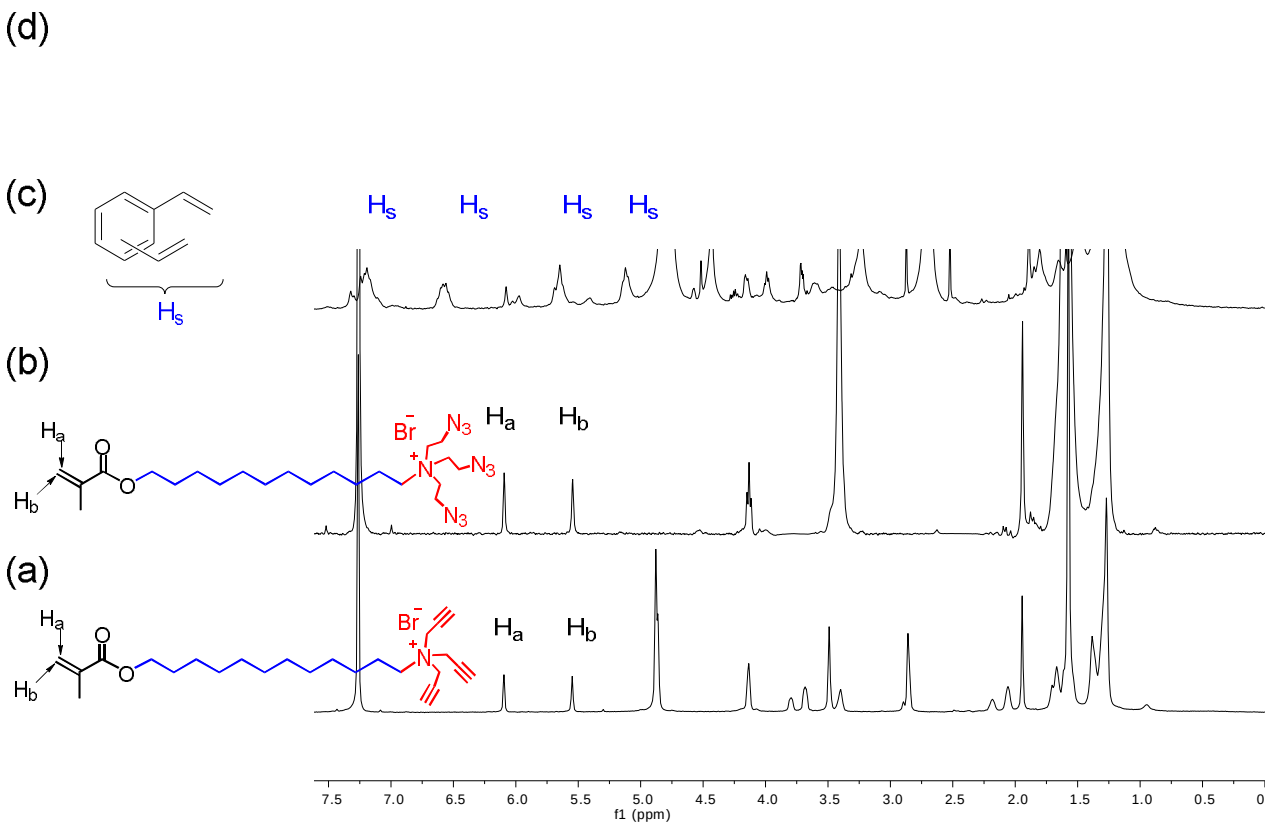

Figure 7S. ^{1}H NMR spectra of (a) Compound **1** in $CDCl_3$, (b) Compound **2'** in $CDCl_3$, (c) alkynyl-SCM in D_2O, and (d) MINP(glucose) in D_2O at 298 K. The data correspond to entry 3 in Table 1S.

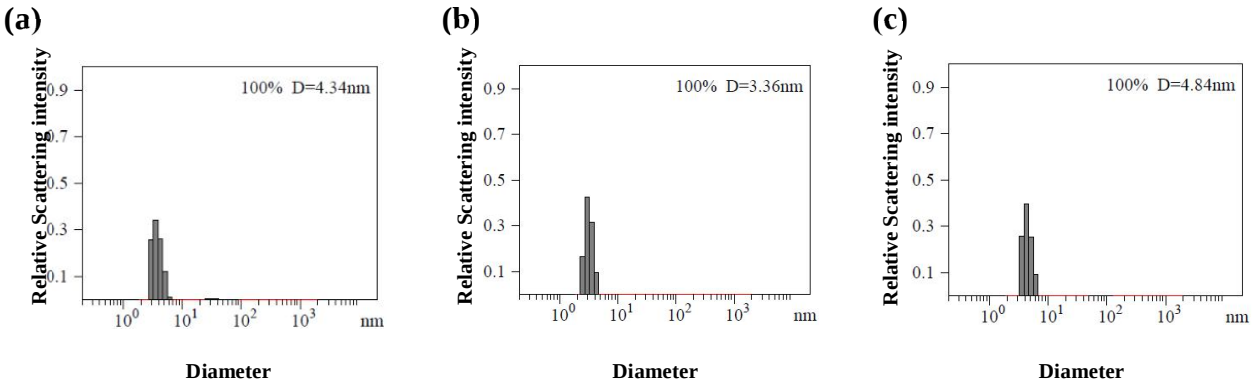

Figure 8S. Distribution of the hydrodynamic diameters of the nanoparticles in water as determined by DLS for the synthesis of MINP(glucose) (a) alkynyl-SCM, (b) core-cross-linked-SCM, and (c) surface-functionalized MINP(glucose) after purification. The data correspond to entry 3 in Table 1S.

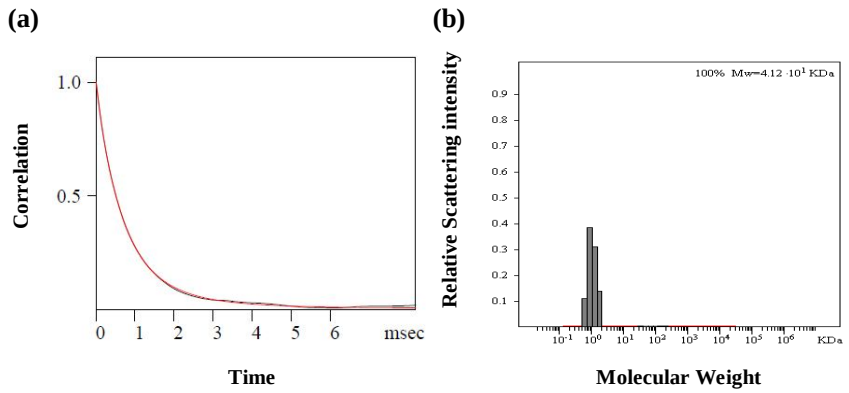

Figure 9S. The correlation curve and the distribution of the molecular weight for MINP(glucose) from the DLS. The data correspond to entry 3 in Table 1S. The PRECISION DECONVOLVE program assumes the intensity of scattering is proportional to the mass of the particle squared. If each unit of building block for the MINP(glucose) is assumed to contain 0.6 molecules of compound **1** (MW = 465 g/mol), 0.4 molecules of compound **2'** (MW = 558 g/mol), 0.6 molecules of compound **3** (MW = 264 g/mol), one molecule of DVB (MW = 130 g/mol), and 0.06 molecules of 6-vinylbenzoxaborole (MW = 160 g/mol), the molecular weight of MINP(glucose) translates to 51 [= 41200 / (0.6×465 +0.4×558 +0.6×264 +130 +0.06×160)] of such units.

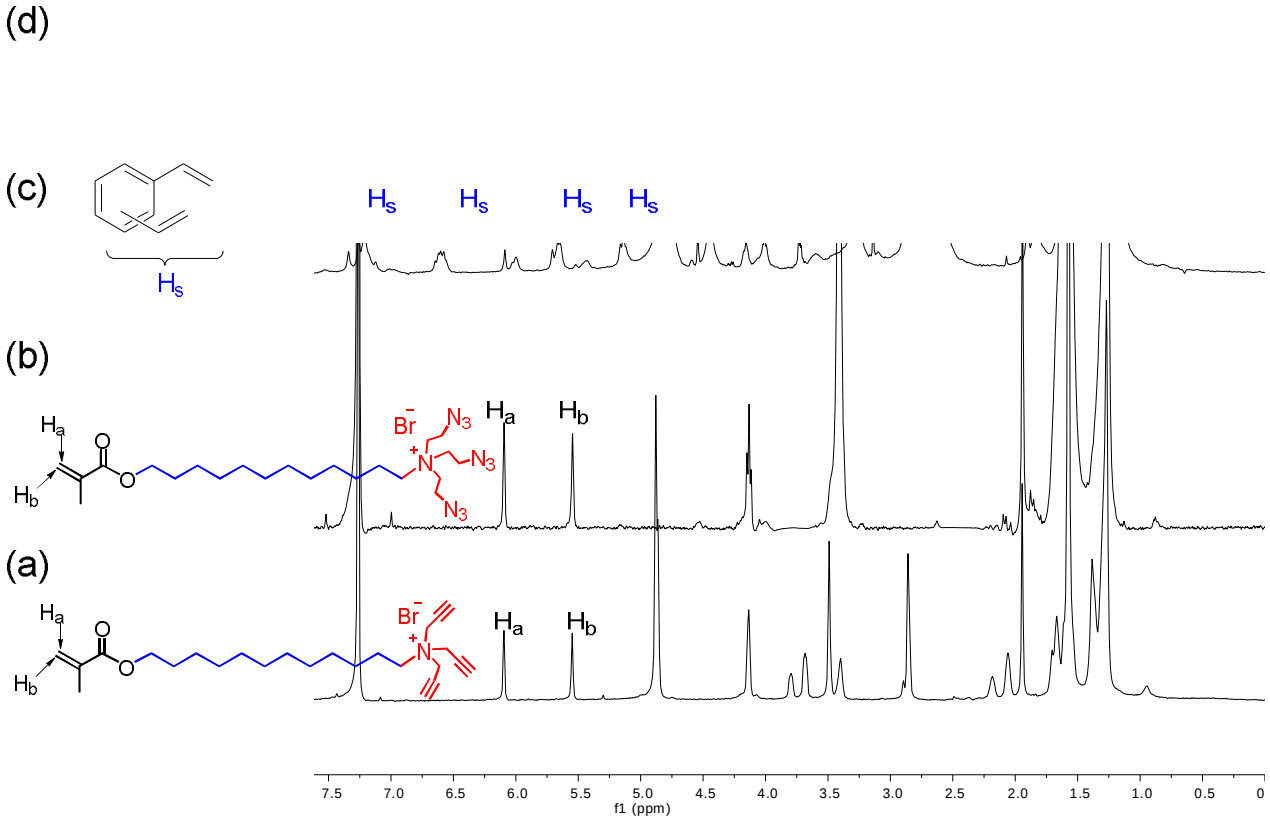

Figure 10S. ^{1}H NMR spectra of (a) Compound **1** in $CDCl_3$, (b) Compound **2'** in $CDCl_3$, (c) alkynyl-SCM in D_2O, and (d) NINP in D_2O at 298 K. The data correspond to entry 4 in Table 1S.

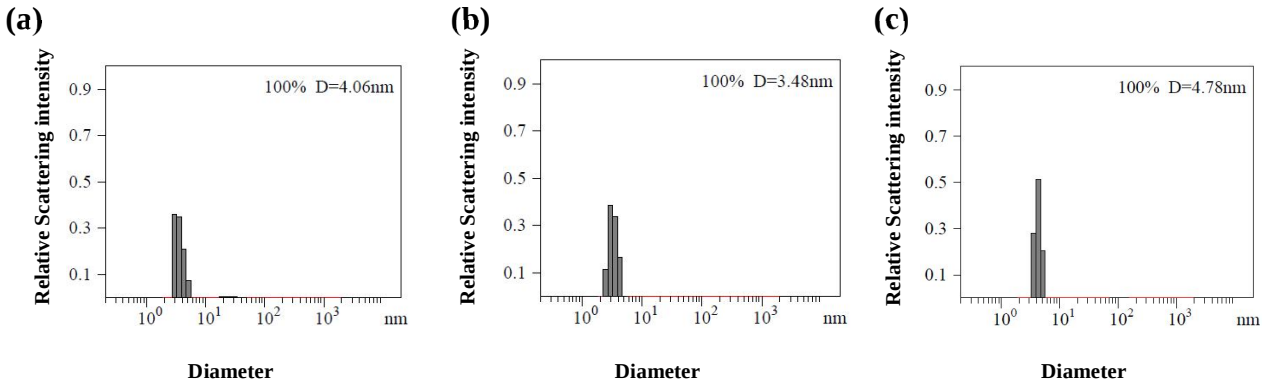

Figure 11S. Distribution of the hydrodynamic diameters of the nanoparticles in water as determined by DLS for the synthesis of NINP (a) alkynyl-SCM, (b) core-cross-linked-SCM, and (c) surface-functionalized NINP after purification. The data correspond to entry 4 in Table 1S.

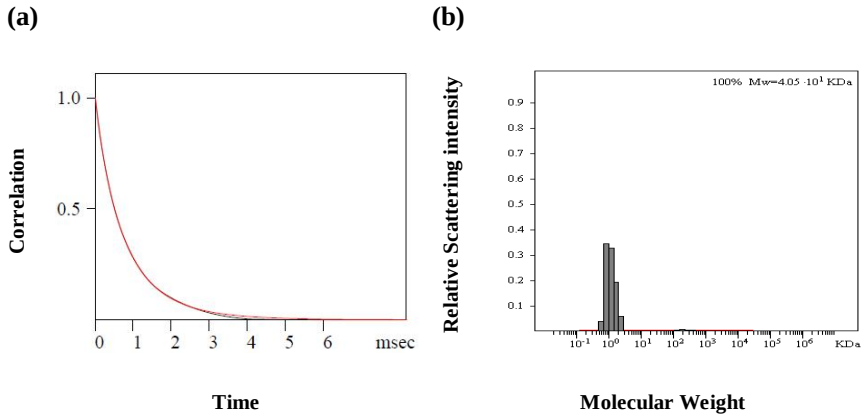

Figure 12S. The correlation curve and the distribution of the molecular weight for NINP from the DLS. The data correspond to entry 4 in Table 1S. The PRECISION DECONVOLVE program assumes the intensity of scattering is proportional to the mass of the particle squared. If each unit of building block for the NINP is assumed to contain 0.6 molecules of compound **1** (MW = 465 g/mol), 0.4 molecules of compound **2'** (MW = 558 g/mol), 0.6 molecules of compound **3** (MW = 264 g/mol), and one molecule of DVB (MW = 130 g/mol), the molecular weight of NINP translates to 51 [= 40500 / (0.6×465 +0.4×558 +0.6×264 +130)] of such units.

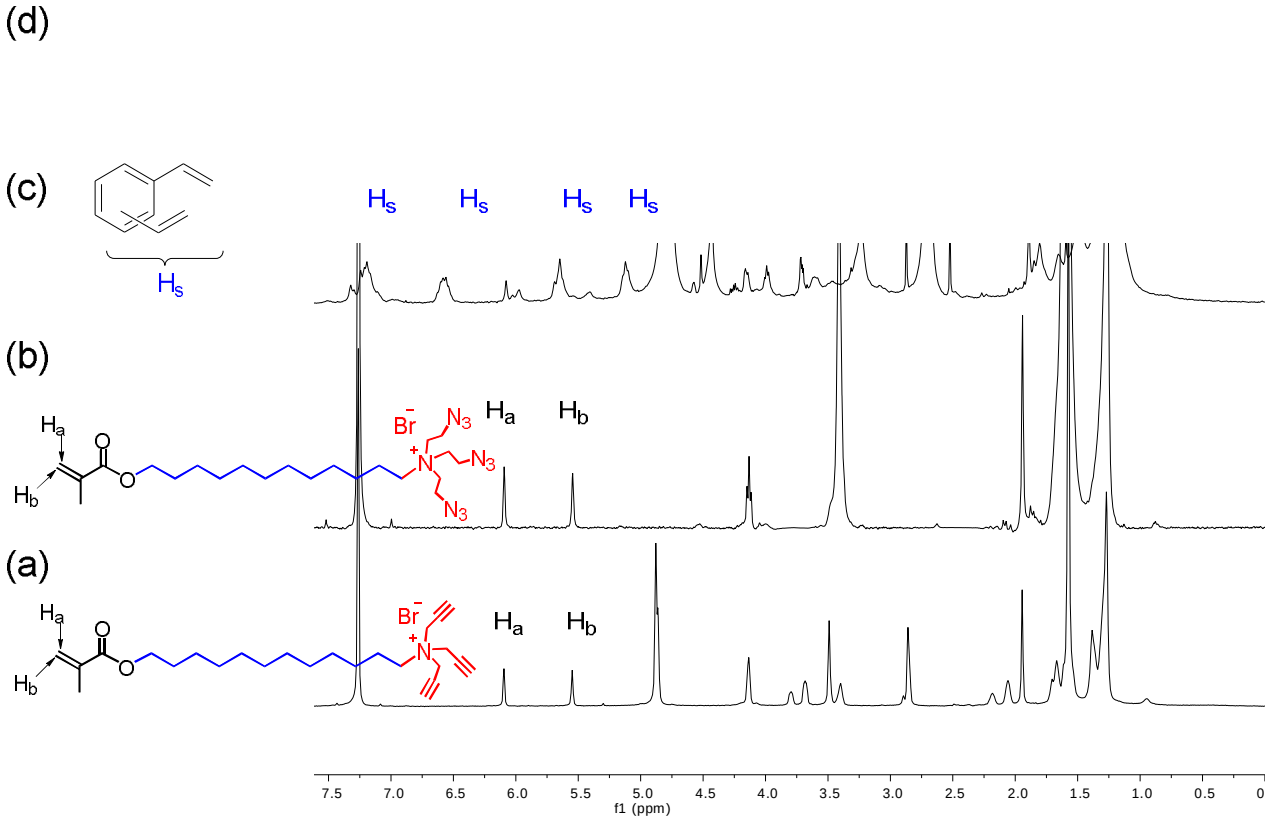

Figure 13S. ^{1}H NMR spectra of (a) Compound **1** in $CDCl_3$, (b) Compound **2'** in $CDCl_3$, (c) alkynyl-SCM in D_2O, and (d) NINP in D_2O at 298 K. The data correspond to entry 5 in Table 1S.

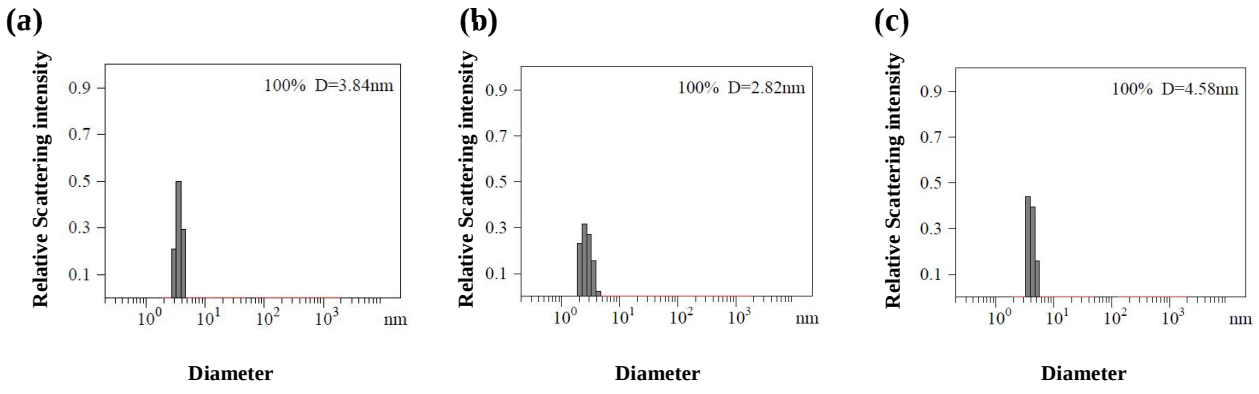

Figure 14S. Distribution of the hydrodynamic diameters of the nanoparticles in water as determined by DLS for the synthesis of NINP (a) alkynyl-SCM, (b) core-cross-linked-SCM, and (c) surface-functionalized NINP after purification. The data correspond to entry 5 in Table 1S.

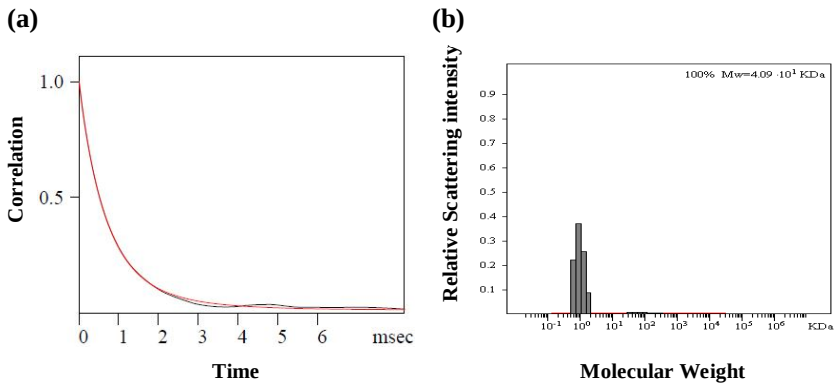

Figure 15S. The correlation curve and the distribution of the molecular weight for NINP from the DLS. The data correspond to entry 5 in Table 1S. The PRECISION DECONVOLVE program assumes the intensity of scattering is proportional to the mass of the particle squared. If each unit of building block for the NINP is assumed to contain 0.6 molecules of compound **1** (MW = 465 g/mol), 0.4 molecules of compound **2'** (MW = 558 g/mol), 0.6 molecules of compound **3** (MW = 264 g/mol), one molecule of DVB (MW = 130 g/mol), and 0.04 molecules of 6-vinylbenzoxaborole (MW = 160 g/mol), the molecular weight of NINP translates to 51 [= 40900 / (0.6×465 +0.4×558 +0.6×264 +130 +0.04×160)] of such units.

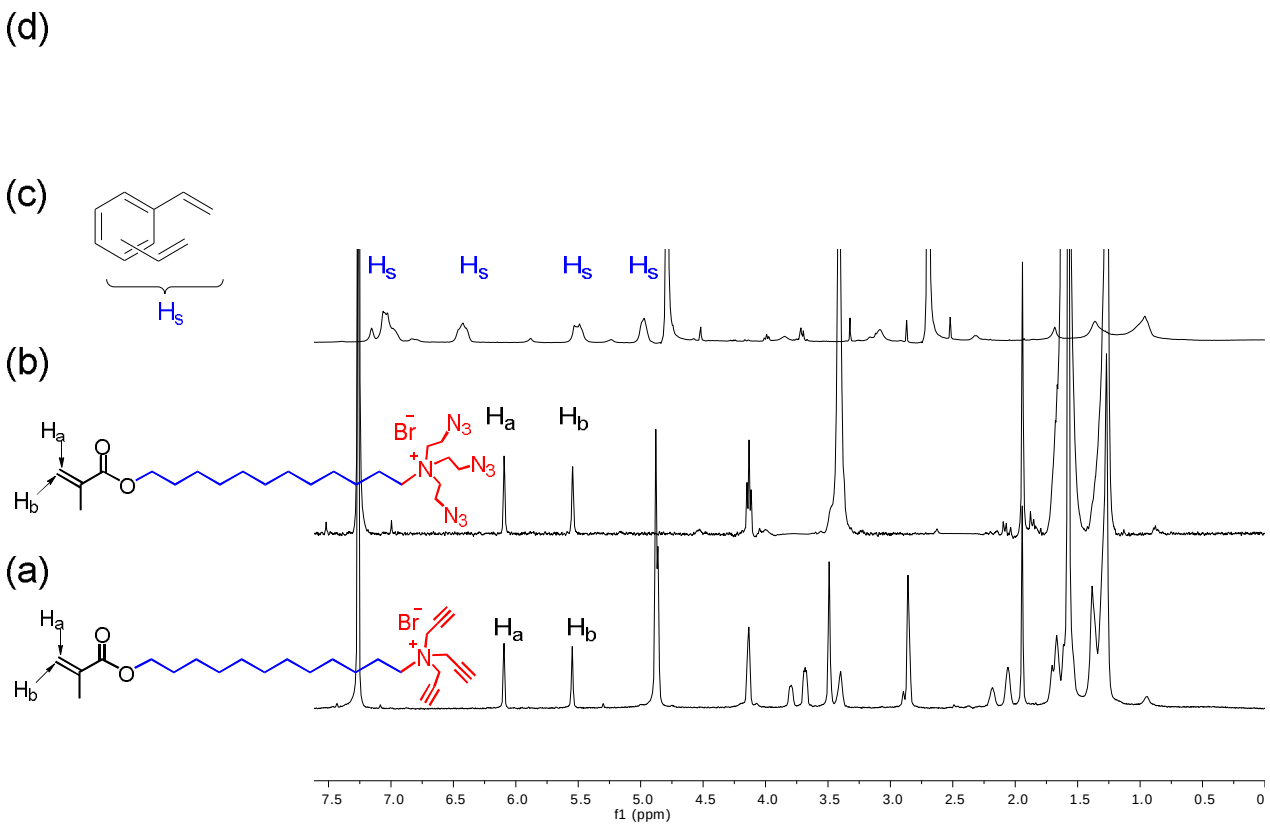

Figure 16S. ^{1}H NMR spectra of (a) Compound **1** in $CDCl_3$, (b) Compound **2'** in $CDCl_3$, (c) alkynyl-SCM in D_2O, and (d) MINP(mannose) in D_2O at 298 K. The data correspond to entry 6 in Table 1S.

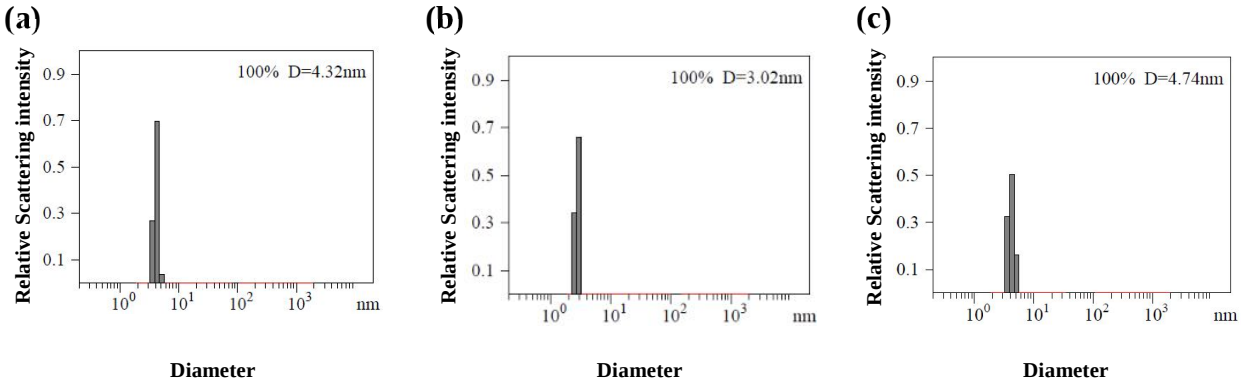

Figure 17S. Distribution of the hydrodynamic diameters of the nanoparticles in water as determined by DLS for the synthesis of MINP(mannose) (a) alkynyl-SCM, (b) core-cross-linked-SCM, and (c) surface-functionalized MINP(mannose) after purification. The data correspond to entry 6 in Table 1S.

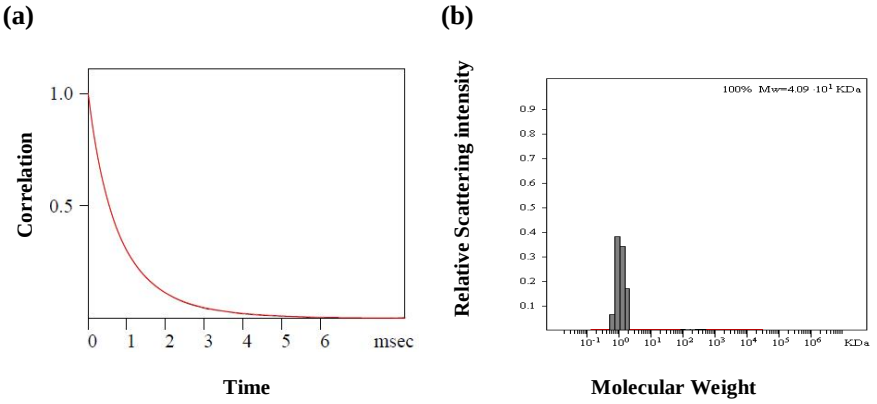

Figure 18S. The correlation curve and the distribution of the molecular weight for MINP(mannose) from the DLS. The data correspond to entry 6 in Table 1S. The PRECISION DECONVOLVE program assumes the intensity of scattering is proportional to the mass of the particle squared. If each unit of building block for the MINP(mannose) is assumed to contain 0.6 molecules of compound **1** (MW = 465 g/mol), 0.4 molecules of compound **2'** (MW = 558 g/mol), 0.6 molecules of compound **3** (MW = 264 g/mol), one molecule of DVB (MW = 130 g/mol), and 0.04 molecules of 6-vinylbenzoxaborole (MW = 160 g/mol), the molecular weight of MINP(mannose) translates to 51 [= 40900 / (0.6×465 +0.4×558 +0.6×264 +130 +0.04×160)] of such units.

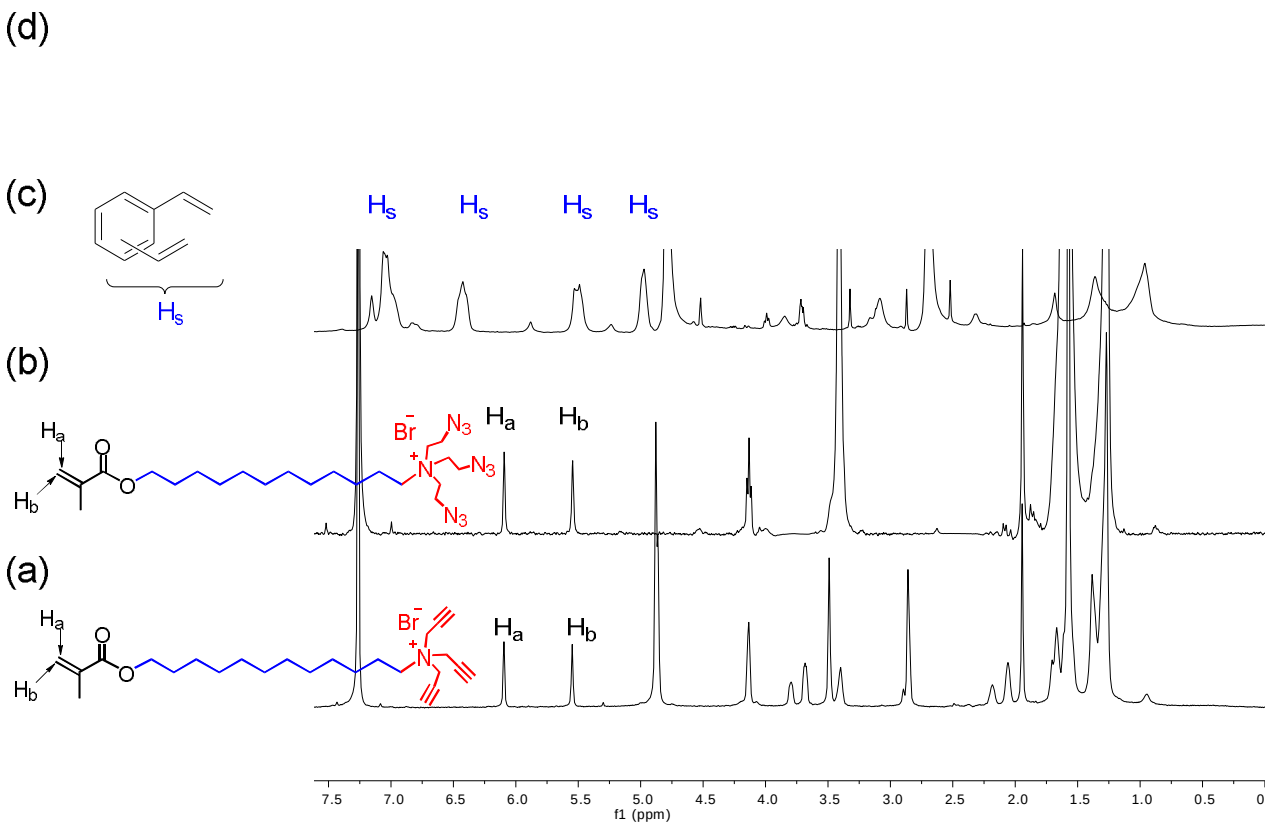

Figure 19S. ^{1}H NMR spectra of (a) Compound **1** in $CDCl_3$, (b) Compound **2'** in $CDCl_3$, (c) alkynyl-SCM in D_2O, and (d) MINP(galactose) in D_2O at 298 K. The data correspond to entry 7 in Table 1S.

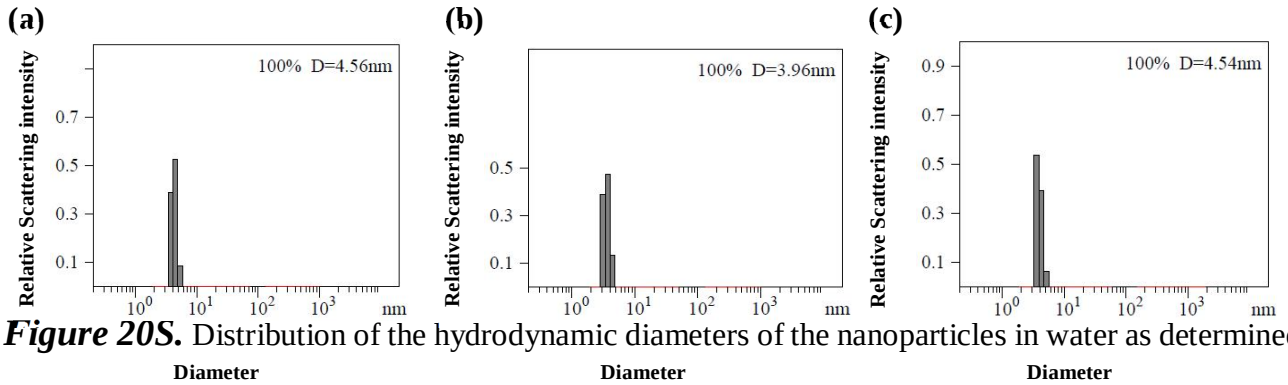

Figure 20S. Distribution of the hydrodynamic diameters of the nanoparticles in water as determined by DLS for the synthesis of MINP(galactose) (a) alkynyl-SCM, (b) core-cross-linked-SCM, and (c) surface-functionalized MINP(galactose) after purification. The data correspond to entry 7 in Table 1S.

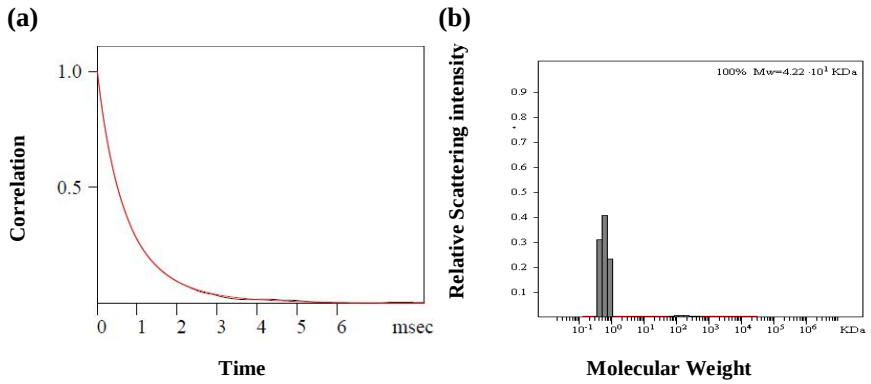

Figure 21S. The correlation curve and the distribution of the molecular weight for MINP(galactose) from the DLS. The data correspond to entry 7 in Table 1S. The PRECISION DECONVOLVE program assumes the intensity of scattering is proportional to the mass of the particle squared. If each unit of building block for the MINP(galactose) is assumed to contain 0.6 molecules of compound **1** (MW = 465 g/mol), 0.4 molecules of compound **2'** (MW = 558 g/mol), 0.6 molecules of compound **3** (MW = 264 g/mol), one molecule of DVB (MW = 130 g/mol), and 0.04 molecules of 6-vinylbenzoxaborole (MW = 160 g/mol), the molecular weight of MINP(galactose) translates to 53 [= 42200 / (0.6×465 +0.4×558 +0.6×264 +130 +0.04×160)] of such units.

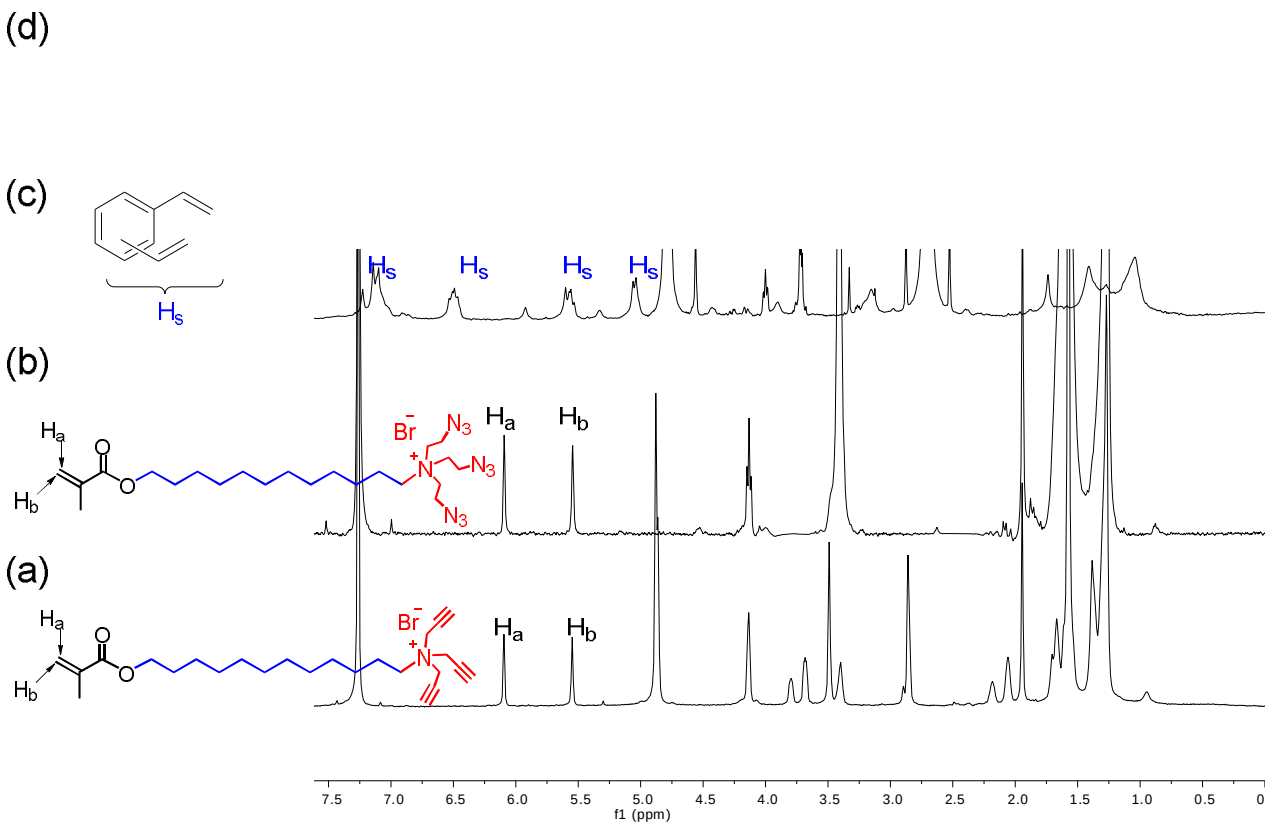

Figure 22S. ^{1}H NMR spectra of (a) Compound **1** in $CDCl_3$, (b) Compound **2'** in $CDCl_3$, (c) alkynyl-SCM in D_2O, and (d) MINP(**5**) in D_2O at 298 K. The data correspond to entry 8 in Table 1S.

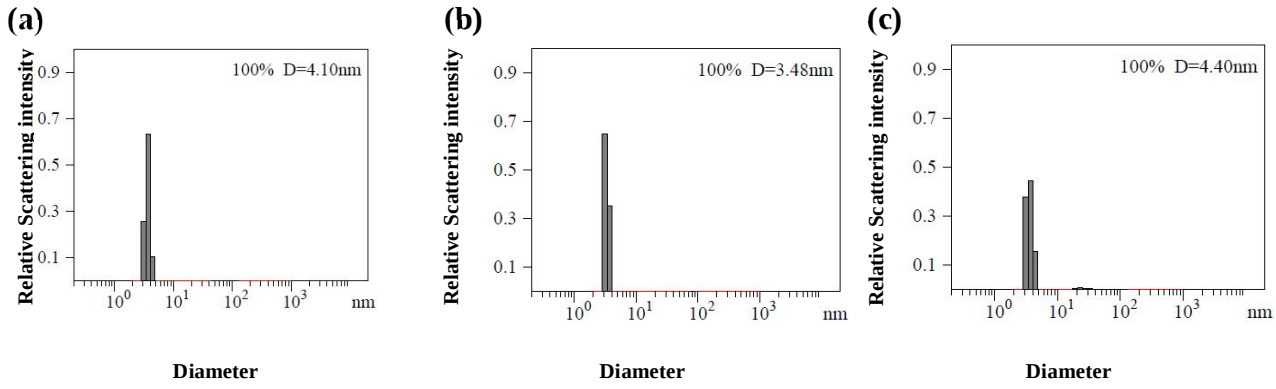

Figure 23S. Distribution of the hydrodynamic diameters of the nanoparticles in water as determined by DLS for the synthesis of MINP(**5**) (a) alkynyl-SCM, (b) core-cross-linked-SCM, and (c) surface-functionalized MINP(**5**) after purification. The data correspond to entry 8 in Table 1S.

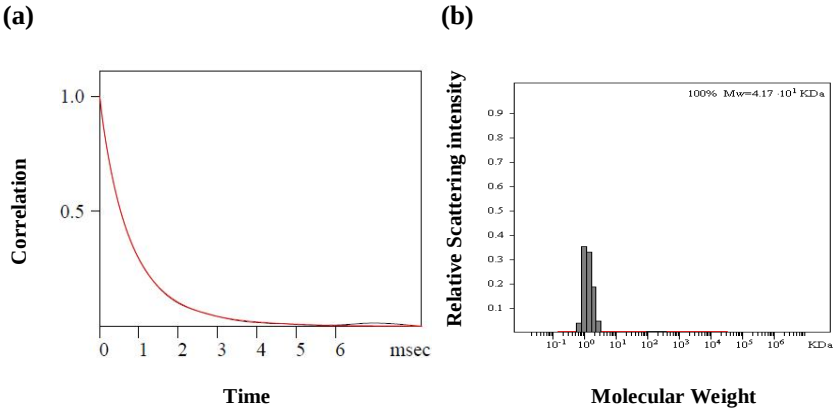

Figure 24S. The correlation curve and the distribution of the molecular weight for MINP(**5**) from the DLS. The data correspond to entry 8 in Table 1S. The PRECISION DECONVOLVE program assumes the intensity of scattering is proportional to the mass of the particle squared. If each unit of building block for the MINP(**5**) is assumed to contain 0.6 molecules of compound **1** (MW = 465 g/mol), 0.4 molecules of compound **2'** (MW = 558 g/mol), 0.6 molecules of compound **3** (MW = 264 g/mol), one molecule of DVB (MW = 130 g/mol), and 0.04 molecules of 6-vinylbenzoxaborole (MW = 160 g/mol), the molecular weight of MINP(**5**) translates to 52 [= 41700 / (0.6×465 +0.4×558 +0.6×264 +130 +0.02×160)] of such units.

Synthesis of oligosaccharide MINPs. A solution of 6-vinylbenzoxaborole (**4**) in methanol (20 µL of a 6.4 mg/mL, 0.0008 mmol) was added to maltose in methanol (10 µL of 13.68 mg/mL, 0.0004 mmol) in a vial containing methanol (5 mL). After the mixture was stirred for 6 h at room temperature, methanol was removed *in vacuo*. A micellar solution of **10** (0.03 mmol), **2'** (0.02 mmol), divinylbenzene (DVB, 2.8 µL, 0.02 mmol), and 2,2-dimethoxy-2-phenylacetophenone (DMPA,10 µL of a 12.8 mg/mL solution in DMSO, 0.0005 mmol) in D_2O (2.0 mL) was added to the sugar–boronate complex. (D_2O instead of H_2O was used to allow the reaction progress to be monitored by ^1H NMR spectroscopy.) The mixture was subjected to ultrasonication for 10 min before $CuCl_2$ (10 µL of a 6.7 mg/mL solution in D_2O, 0.0005 mmol) and sodium ascorbate (10 µL of a 99 mg/mL solution in D_2O, 0.005 mmol) were added. After the reaction mixture was stirred slowly at room temperature for 12 h,

the reaction mixture was transferred into a glass vial, purged with nitrogen for 15 min, sealed with a rubber stopper, and irradiated in a Rayonet reactor for 8 h. Compound **3** (10.6 mg, 0.04 mmol), $CuCl_2$ (10 μL of a 6.7 mg/mL solution in D_2O, 0.0005 mmol), and sodium ascorbate (10 μL of a 99 mg/mL solution in D_2O, 0.005 mmol) were added. After being stirred for another 6 h at room temperature, the reaction mixture was poured into acetone (8 mL). The precipitate collected by centrifugation was washed with a mixture of acetone/water (5 mL/1 mL), and methanol/acetic acid (5 mL/0.1 mL) for three times and finally with acetone (1×5 mL) to neutral before being dried in air to afford the final MINPs.

Table 2S. Oligosaccharide formulation

Entry	MINP	Amount of 0.04 M Sugar / μL	Amount of 0.04 M 6-vinylBenzoxoborole / μL	Ratio (Sugar:benzoxoborole)
1	MINP(maltose)[a]	10	10	1:1
2	MINP(maltose)[a]	10	20	1:2
3	MINP(maltose)[a]	10	30	1:3
4	MINP(maltose)[b]	10	20	1:2
5	MINP(cellobiose)[a]	10	20	1:2
6	MINP(gentiobiose)[a]	10	20	1:2
7	MINP(maltulose)[a]	10	20	1:2
8	MINP(lactose)[a]	10	20	1:2
9	MINP(maltotriose)[a]	10	20	1:2
10	MINP(H)[a]	10	30	1:3
11	MINP(A)[a]	10	30	1:3
12	MINP(B)[a]	10	30	1:3

[a] The micellar solution was prepared with compound **10**/compound **2'**. [b] The micellar solution was prepared with compound **1**/compound **2'**.

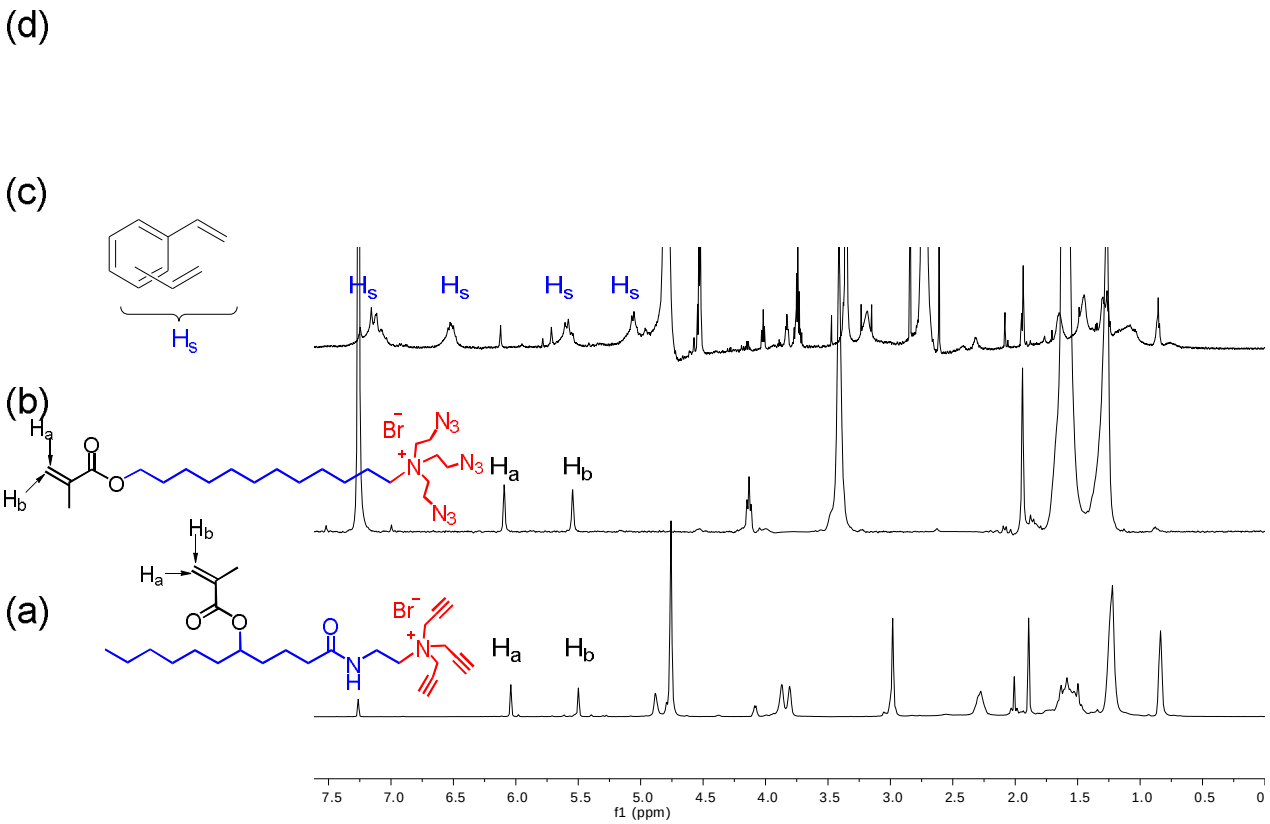

Figure 25S. ^{1}H NMR spectra of (a) Compound **10** in $CDCl_3$, (b) Compound **2'** in $CDCl_3$, (c) alkynyl-SCM in D_2O, and (d) MINP(maltose) in D_2O at 298 K. The data correspond to entry 1 in Table 2S.

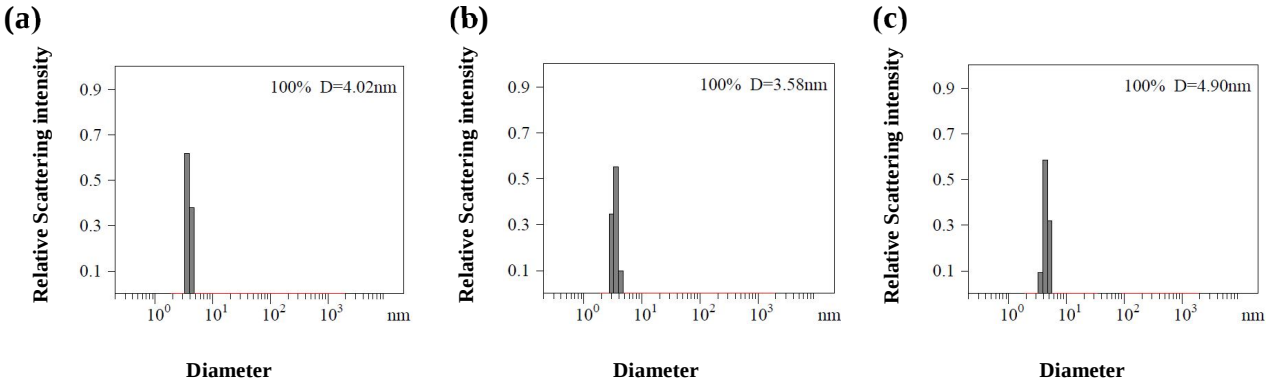

Figure 26S. Distribution of the hydrodynamic diameters of the nanoparticles in water as determined by DLS for the synthesis of MINP(maltose) (a) alkynyl-SCM, (b) core-cross-linked-SCM, and (c) surface-functionalized MINP(maltose) after purification. The data correspond to entry 1 in Table 2S.

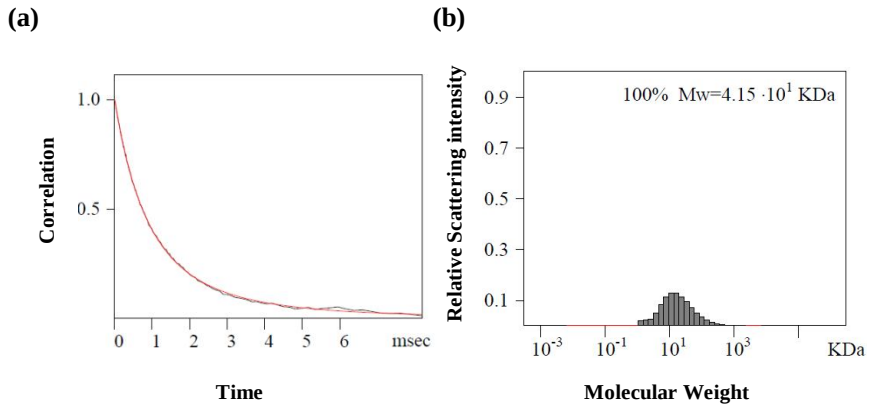

Figure 27S. The correlation curve and the distribution of the molecular weight for MINP(maltose) from the DLS. The data correspond to entry 1 in Table 2S. The PRECISION DECONVOLVE program assumes the intensity of scattering is proportional to the mass of the particle squared. If each unit of building block for the MINP(maltose) is assumed to contain 0.4 molecules of compound **2'** (MW = 558 g/mol), 0.6 molecules of Compound **10** (MW = 508 g/mol), 0.6 molecules of compound **3** (MW = 264 g/mol), one molecule of DVB (MW = 130 g/mol), and 0.02 molecules of 6-vinylbenzoxaborole (MW = 160 g/mol), the molecular weight of MINP(maltose) translates to 51 [= 41500 / (0.4×558 +0.6×508 +0.6×264 +130 +0.02×160)] of such units.

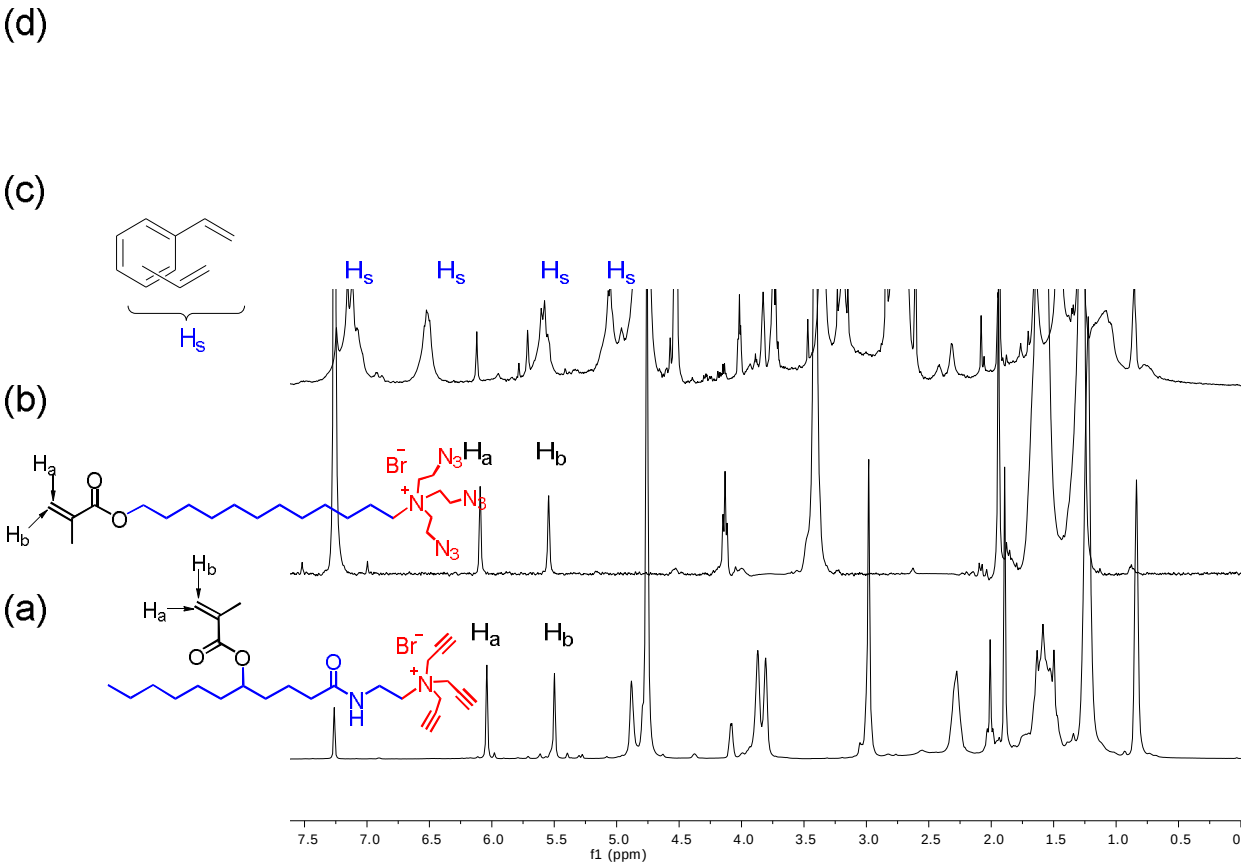

Figure 28S. ^{1}H NMR spectra of (a) Compound **10** in $CDCl_3$, (b) Compound **2'** in $CDCl_3$, (c) alkynyl-SCM in D_2O, and (d) MINP(maltose) in D_2O at 298 K. The data correspond to entry 2 in Table 2S.

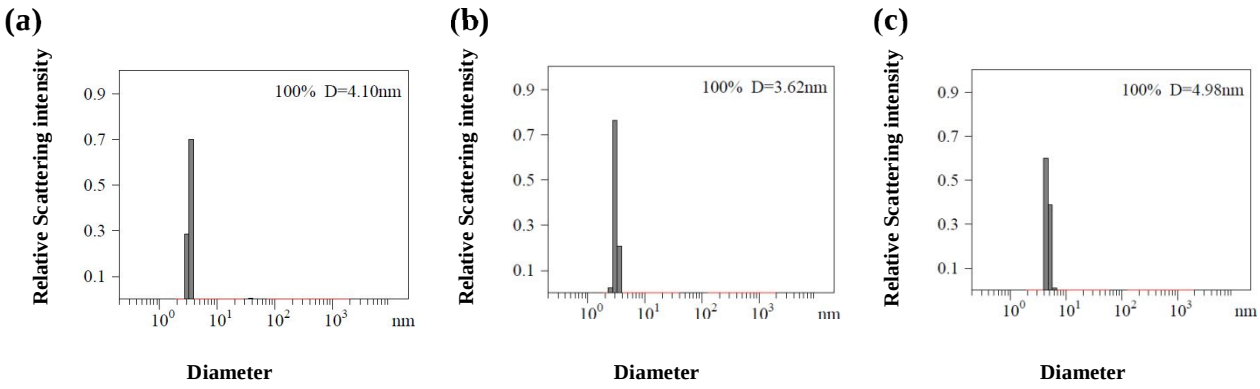

Figure 29S. Distribution of the hydrodynamic diameters of the nanoparticles in water as determined by DLS for the synthesis of MINP(maltose) (a) alkynyl-SCM, (b) core-cross-linked-SCM, and (c) surface-functionalized MINP(maltose) after purification. The data correspond to entry 2 in Table 2S.

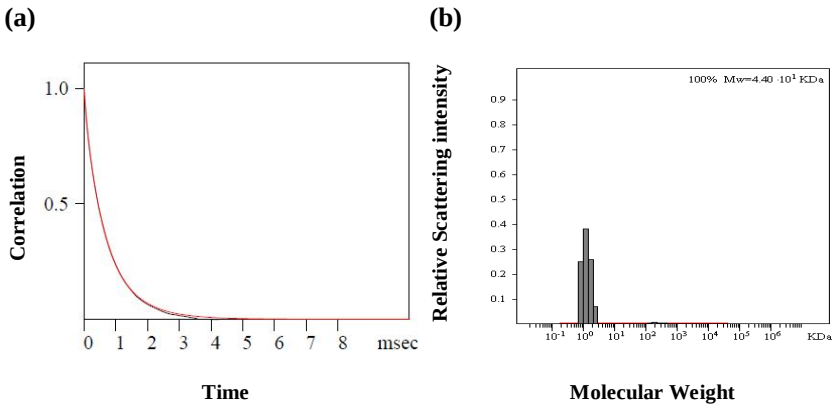

Figure 30S. The correlation curve and the distribution of the molecular weight for MINP(maltose) from the DLS. The data correspond to entry 2 in Table 2S. The PRECISION DECONVOLVE program assumes the intensity of scattering is proportional to the mass of the particle squared. If each unit of building block for the MINP(maltose) is assumed to contain 0.6 molecules of Compound **10** (MW = 508 g/mol), 0.4 molecules of compound **2'** (MW = 558 g/mol), 0.6 molecules of compound **3** (MW = 264 g/mol), one molecule of DVB (MW = 130 g/mol), and 0.04 molecules of 6-vinylbenzoxaborole (MW = 160 g/mol), the molecular weight of MINP(maltose) translates to 53 [= 44000 / (0.6×508 +0.4×558 +0.6×264 +130 +0.04×160)] of such units.

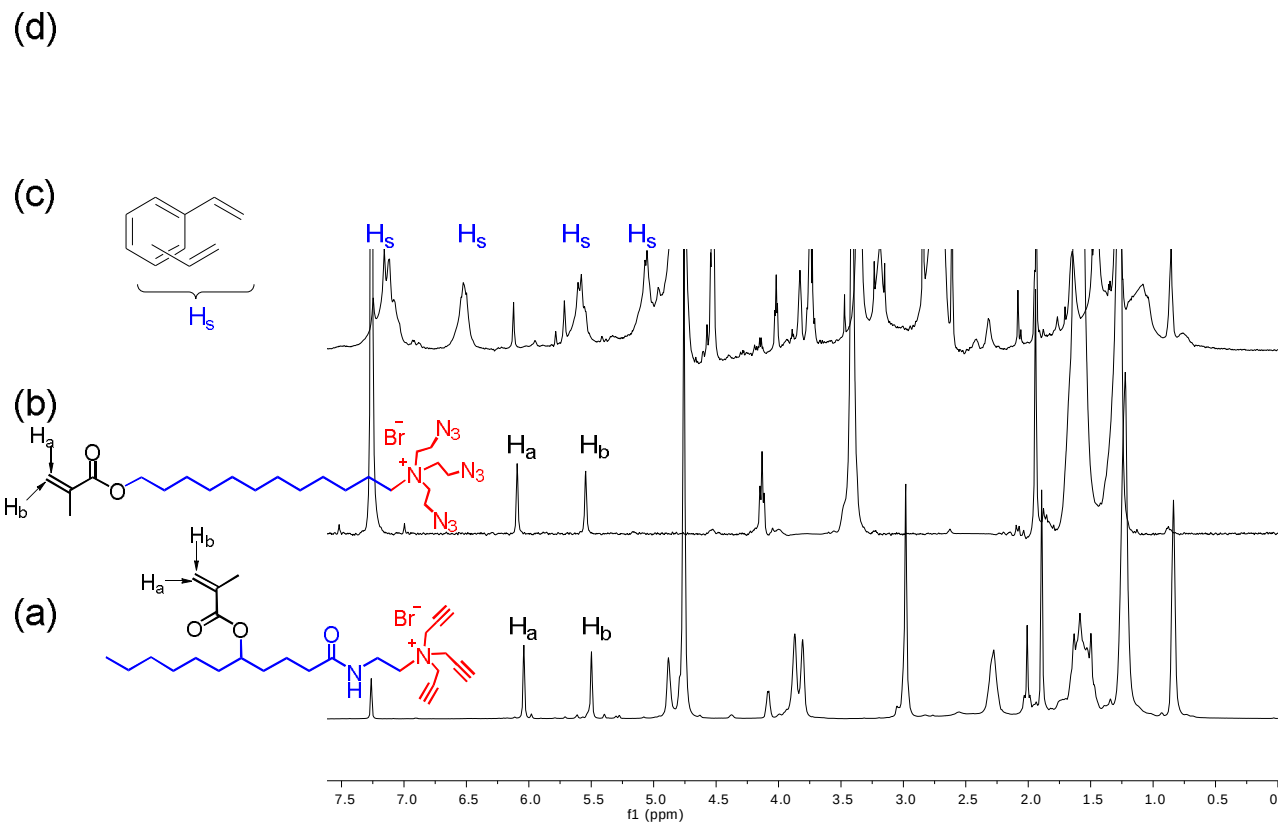

Figure 31S. ^{1}H NMR spectra of (a) Compound **10** in $CDCl_3$, (b) Compound **2'** in $CDCl_3$, (c) alkynyl-SCM in D_2O, and (d) MINP(maltose) in D_2O at 298 K. The data correspond to entry 3 in Table 2S.

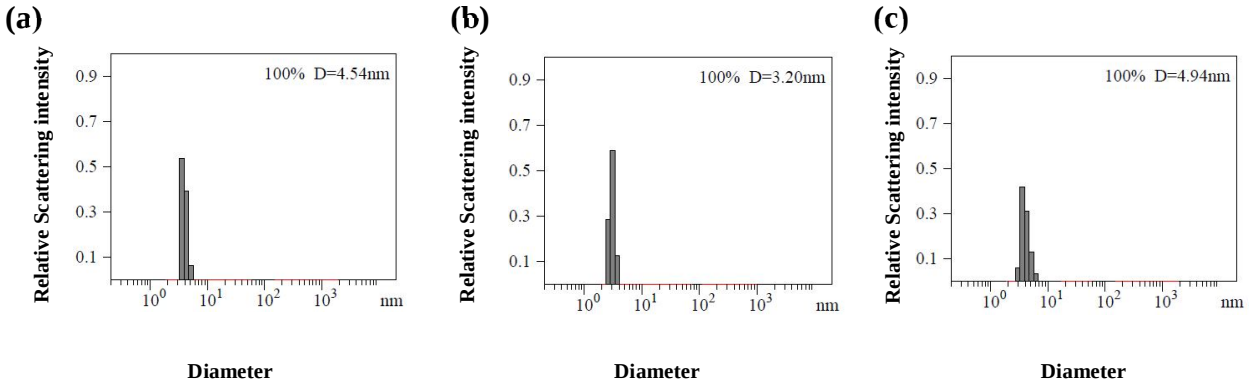

Figure 32S. Distribution of the hydrodynamic diameters of the nanoparticles in water as determined by DLS for the synthesis of MINP(maltose) (a) alkynyl-SCM, (b) core-cross-linked-SCM, and (c) surface-functionalized MINP(maltose) after purification. The data correspond to entry 3 in Table 2S.

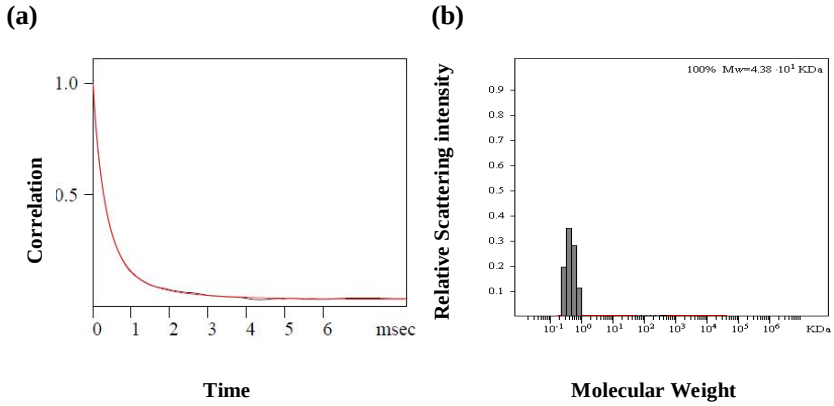

Figure 33S. The correlation curve and the distribution of the molecular weight for MINP(maltose) from the DLS The data correspond to entry 3 in Table 2S. The PRECISION DECONVOLVE program assumes the intensity of scattering is proportional to the mass of the particle squared. If each unit of building block for the MINP(maltose) is assumed to contain 0.4 molecules of compound **2'** (MW = 558 g/mol), 0.6 molecules of Compound **10** (MW = 508 g/mol), 0.6 molecules of compound **3** (MW = 264 g/mol), one molecule of DVB (MW = 130 g/mol), and 0.06 molecules of 6-vinylbenzoxaborole (MW = 160 g/mol), the molecular weight of MINP(maltose) translates to 53 [= 43800 / (0.4×558 +0.6×508 +0.6×264 +130 +0.06×160)] of such units.

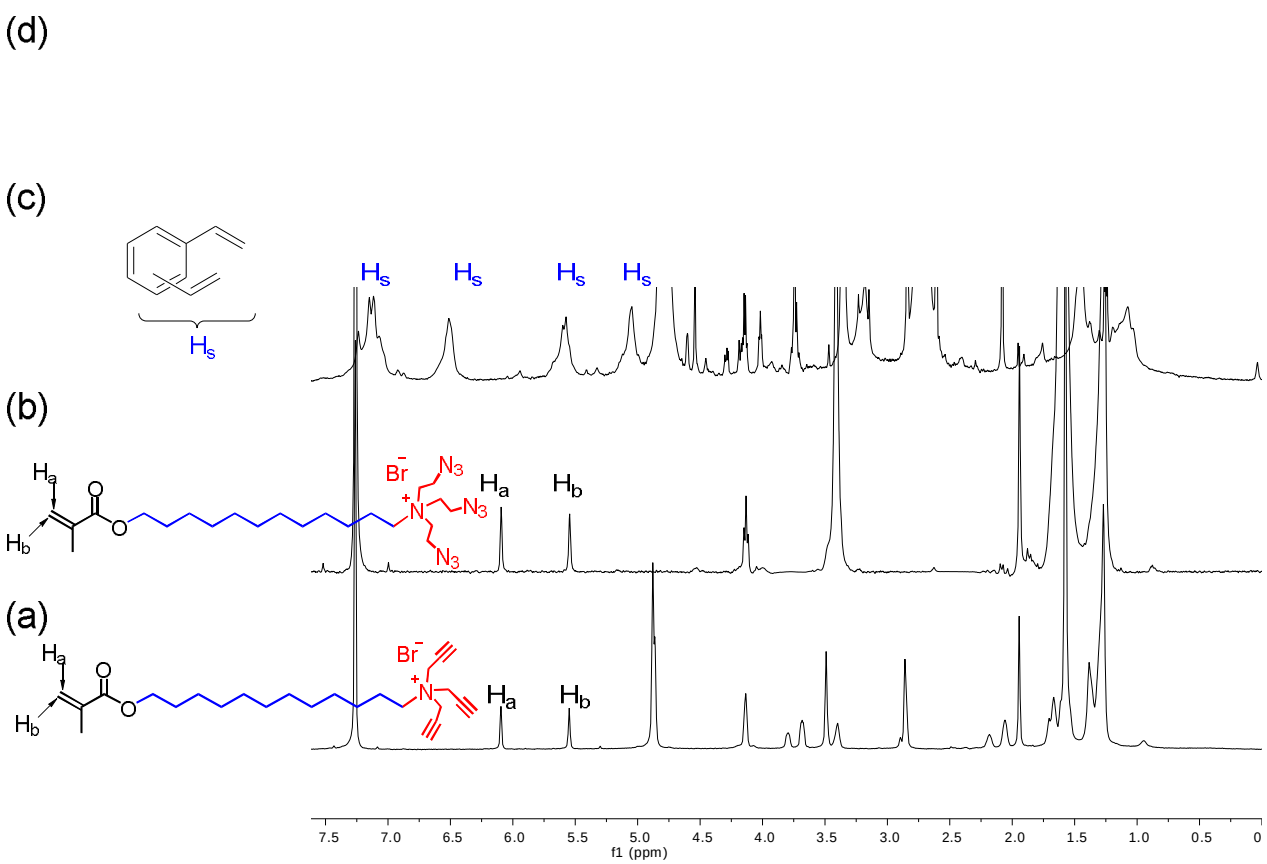

Figure 34S. ^{1}H NMR spectra of (a) Compound **1** in $CDCl_3$, (b) Compound **2'** in $CDCl_3$, (c) alkynyl-SCM in D_2O, and (d) MINP(maltose) in D_2O at 298 K. The data correspond to entry 4 in Table 2S.

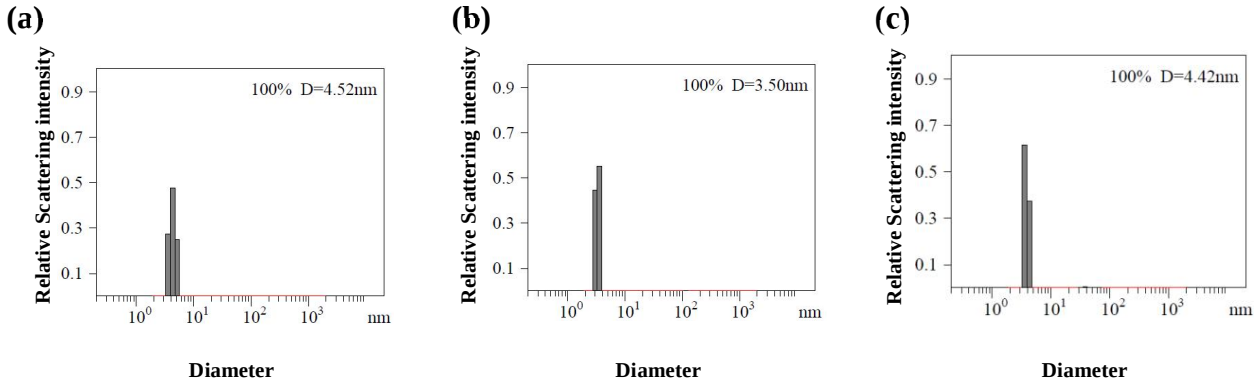

Figure 35S. Distribution of the hydrodynamic diameters of the nanoparticles in water as determined by DLS for the synthesis of MINP(maltose) (a) alkynyl-SCM, (b) core-cross-linked-SCM, and (c) surface-functionalized MINP(maltose) after purification. The data correspond to entry 4 in Table 2S.

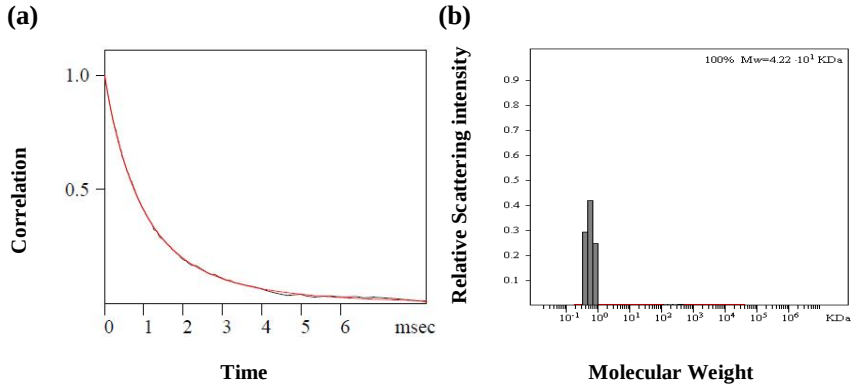

Figure 36S. The correlation curve and the distribution of the molecular weight for MINP(maltose) from the DLS. The data correspond to entry 4 in Table 2S. The PRECISION DECONVOLVE program assumes the intensity of scattering is proportional to the mass of the particle squared. If each unit of building block for the MINP(maltose) is assumed to contain 0.6 molecules of compound **1** (MW = 465 g/mol), 0.4 molecules of compound **2'** (MW = 558 g/mol), 0.6 molecules of compound **3** (MW = 264 g/mol), one molecule of DVB (MW = 130 g/mol), and 0.04 molecules of 6-vinylbenzoxaborole (MW = 160 g/mol), the molecular weight of MINP(maltose) translates to 53 [= 42200 / (0.6×465 +0.4×558 +0.6×264 +130 +0.04×160)] of such units.

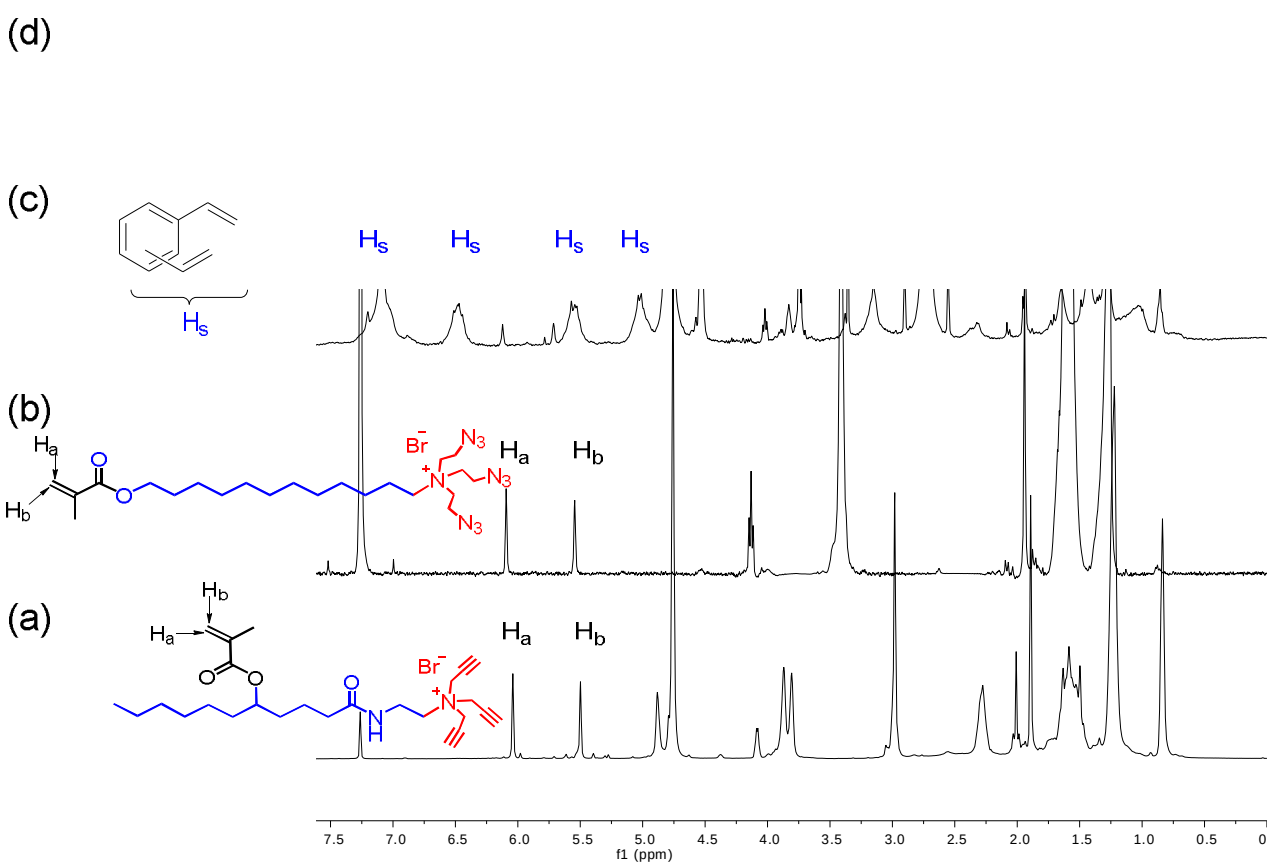

Figure 37S. ^{1}H NMR spectra of (a) Compound **10** in $CDCl_3$, (b) Compound **2'** in $CDCl_3$, (c) alkynyl-SCM in D_2O, and (d) MINP(cellobiose) in D_2O at 298 K. The data correspond to entry 5 in Table 2S.

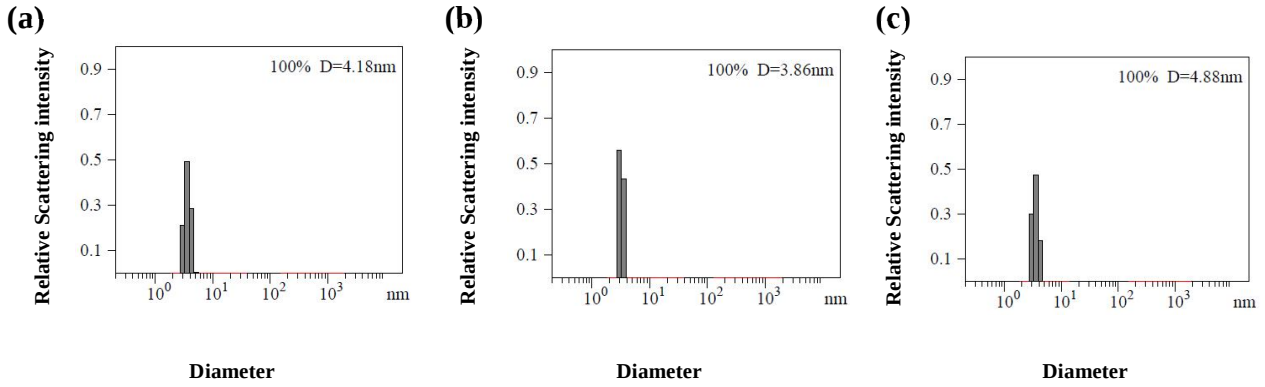

Figure 38S. Distribution of the hydrodynamic diameters of the nanoparticles in water as determined by DLS for the synthesis of MINP(cellobiose) (a) alkynyl-SCM, (b) core-cross-linked-SCM, and (c) surface-functionalized MINP(cellobiose) after purification. The data correspond to entry 5 in Table 2S.

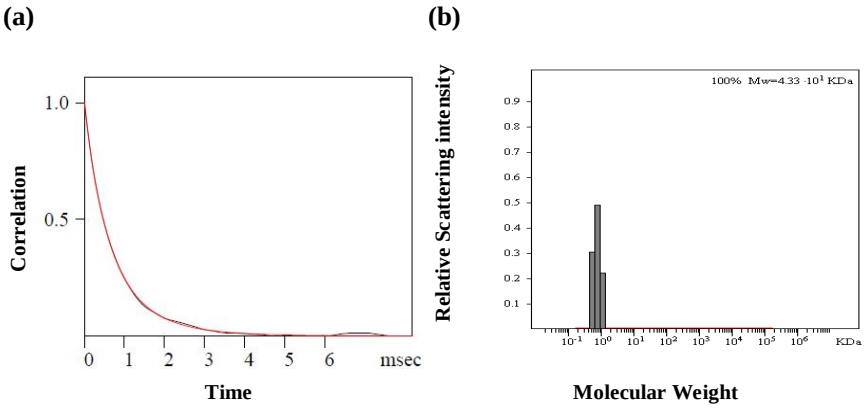

Figure 39S. The correlation curve and the distribution of the molecular weight for MINP(cellobiose) from the DLS The data correspond to entry 5 in Table 2S. The PRECISION DECONVOLVE program assumes the intensity of scattering is proportional to the mass of the particle squared. If each unit of building block for the MINP(cellobiose) is assumed to contain 0.4 molecules of compound **2'** (MW = 558 g/mol), 0.6 molecules of Compound **10** (MW = 508 g/mol), 0.6 molecules of compound **3** (MW = 264 g/mol), one molecule of DVB (MW = 130 g/mol), and 0.04 molecules of 6-vinylbenzoxaborole (MW = 160 g/mol), the molecular weight of MINP(cellobiose) translates to 53 [= 43300 / (0.4×558 +0.6×508 +0.6×264 +130 +0.04×160)] of such units.

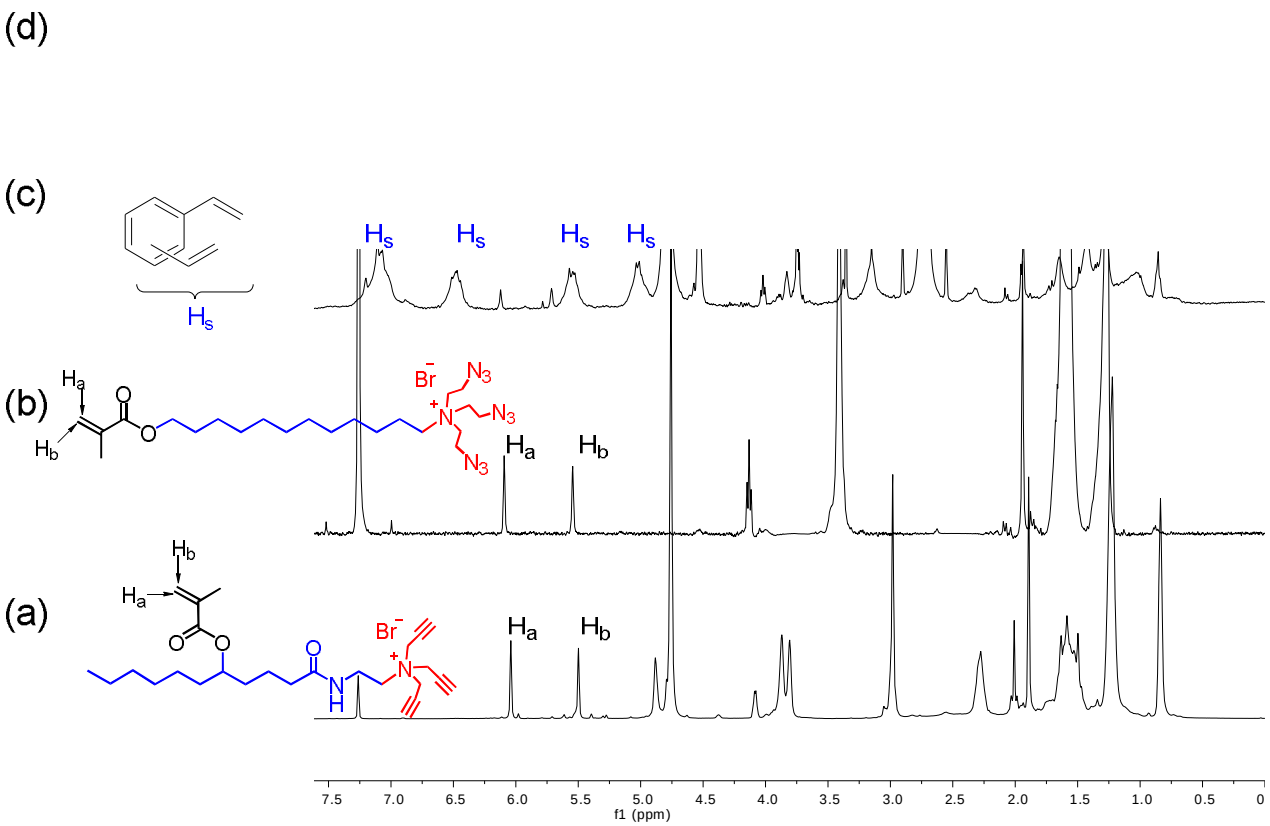

Figure 40S. ^{1}H NMR spectra of (a) Compound **10** in $CDCl_3$, (b) Compound **2'** in $CDCl_3$, (c) alkynyl-SCM in D_2O, and (d) MINP(gentiobiose) in D_2O at 298 K. The data correspond to entry 6 in Table 2S.

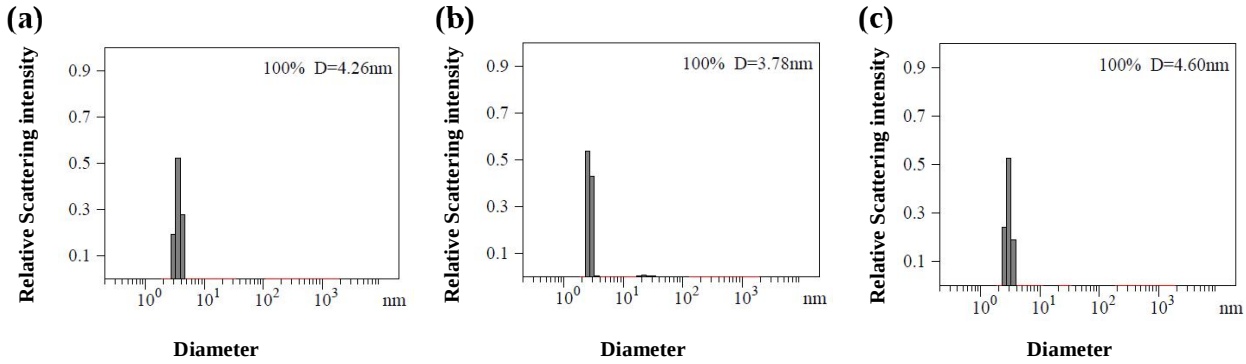

Figure 41S. Distribution of the hydrodynamic diameters of the nanoparticles in water as determined by DLS for the synthesis of MINP(gentiobiose) (a) alkynyl-SCM, (b) core-cross-linked-SCM, and (c) surface-functionalized MINP(gentiobiose) after purification. The data correspond to entry 6 in Table 2S.

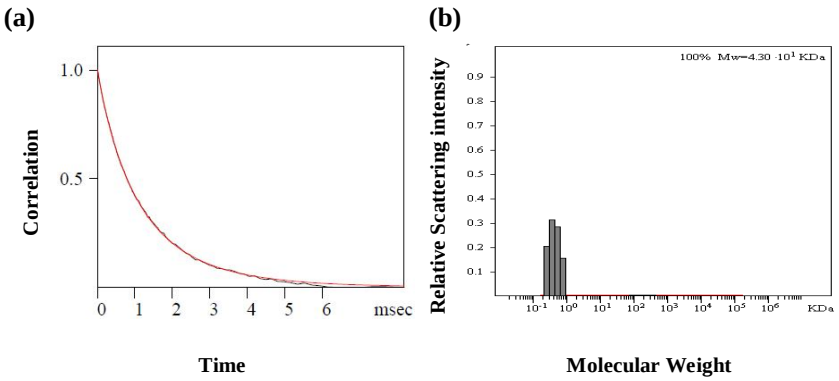

Figure 42S. The correlation curve and the distribution of the molecular weight for MINP(gentiobiose) from the DLS The data correspond to entry 6 in Table 2S. The PRECISION DECONVOLVE program assumes the intensity of scattering is proportional to the mass of the particle squared. If each unit of building block for the MINP(gentiobiose) is assumed to contain 0.4 molecules of compound **2'** (MW = 558 g/mol), 0.6 molecules of Compound **10** (MW = 508 g/mol), 0.6 molecules of compound **3** (MW = 264 g/mol), one molecule of DVB (MW = 130 g/mol), and 0.04 molecules of 6-vinylbenzoxaborole (MW = 160 g/mol), the molecular weight of MINP(gentiobiose) translates to 52 [= 43000 / (0.4×558 +0.6×508 +0.6×264 +130 +0.04×160)] of such units.

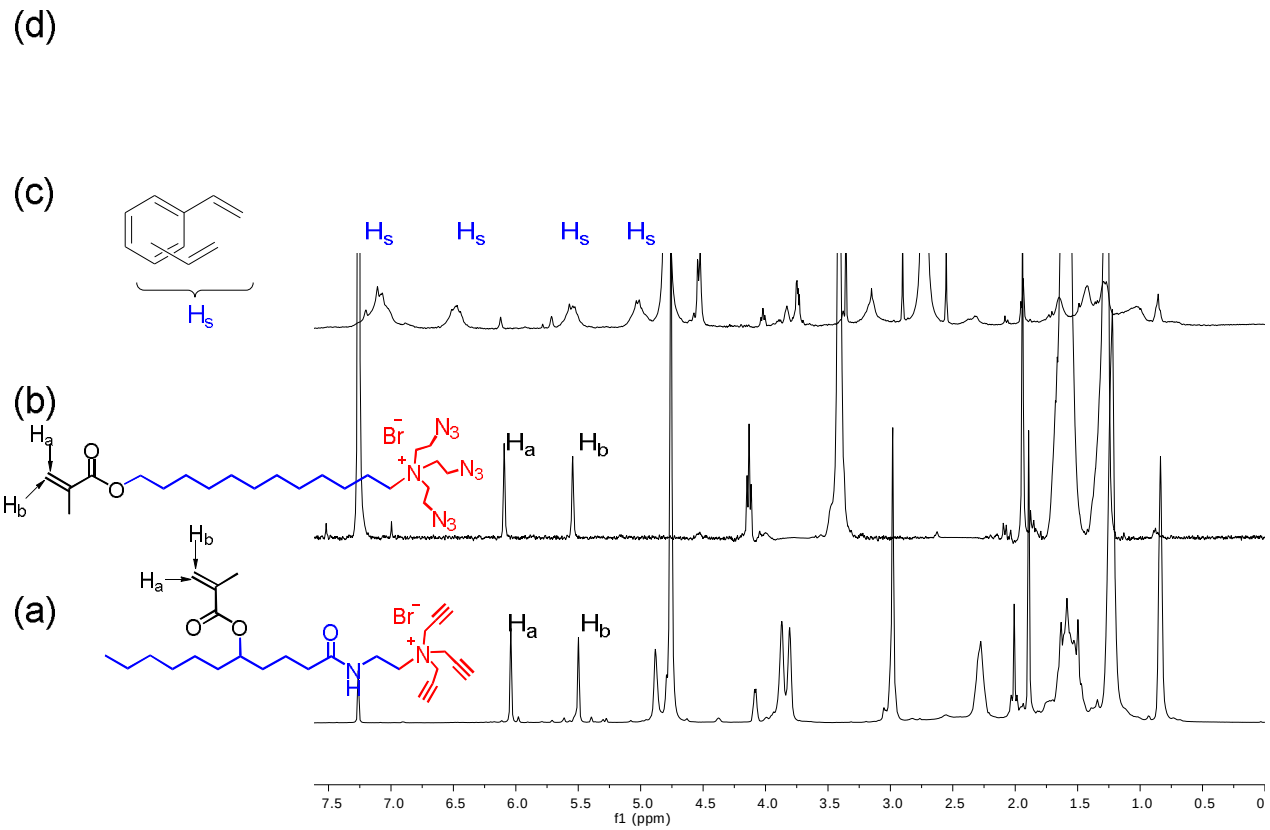

Figure 43S. ^{1}H NMR spectra of (a) Compound **10** in $CDCl_3$, (b) Compound **2'** in $CDCl_3$, (c) alkynyl-SCM in D_2O, and (d) MINP(maltulose) in D_2O at 298 K. The data correspond to entry 7 in Table 2S.

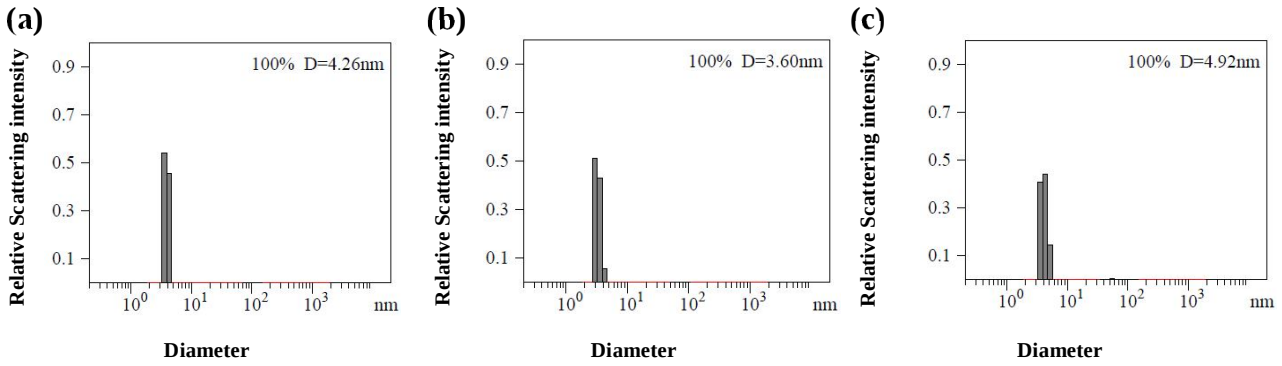

Figure 44S. Distribution of the hydrodynamic diameters of the nanoparticles in water as determined by DLS for the synthesis of MINP(maltulose) (a) alkynyl-SCM, (b) core-cross-linked-SCM, and (c) surface-functionalized MINP(maltulose) after purification. The data correspond to entry 7 in Table 2S.

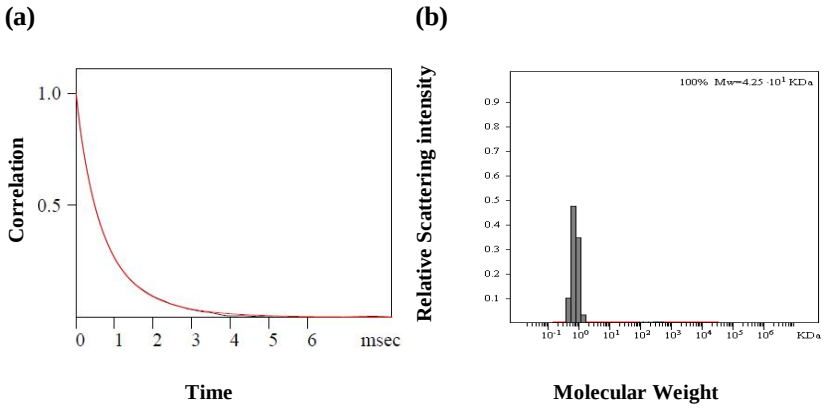

Figure 45S. The correlation curve and the distribution of the molecular weight for MINP(maltulose) from the DLS The data correspond to entry 7 in Table 2S. The PRECISION DECONVOLVE program assumes the intensity of scattering is proportional to the mass of the particle squared. If each unit of building block for the MINP(maltulose) is assumed to contain 0.4 molecules of compound **2'** (MW = 558 g/mol), 0.6 molecules of Compound **10** (MW = 508 g/mol), 0.6 molecules of compound **3** (MW = 264 g/mol), one molecule of DVB (MW = 130 g/mol), and 0.04 molecules of 6-vinylbenzoxaborole (MW = 160 g/mol), the molecular weight of MINP(maltulose) translates to 52 [= 42500 / (0.4×558 +0.6×508 +0.6×264 +130 +0.04×160)] of such units.

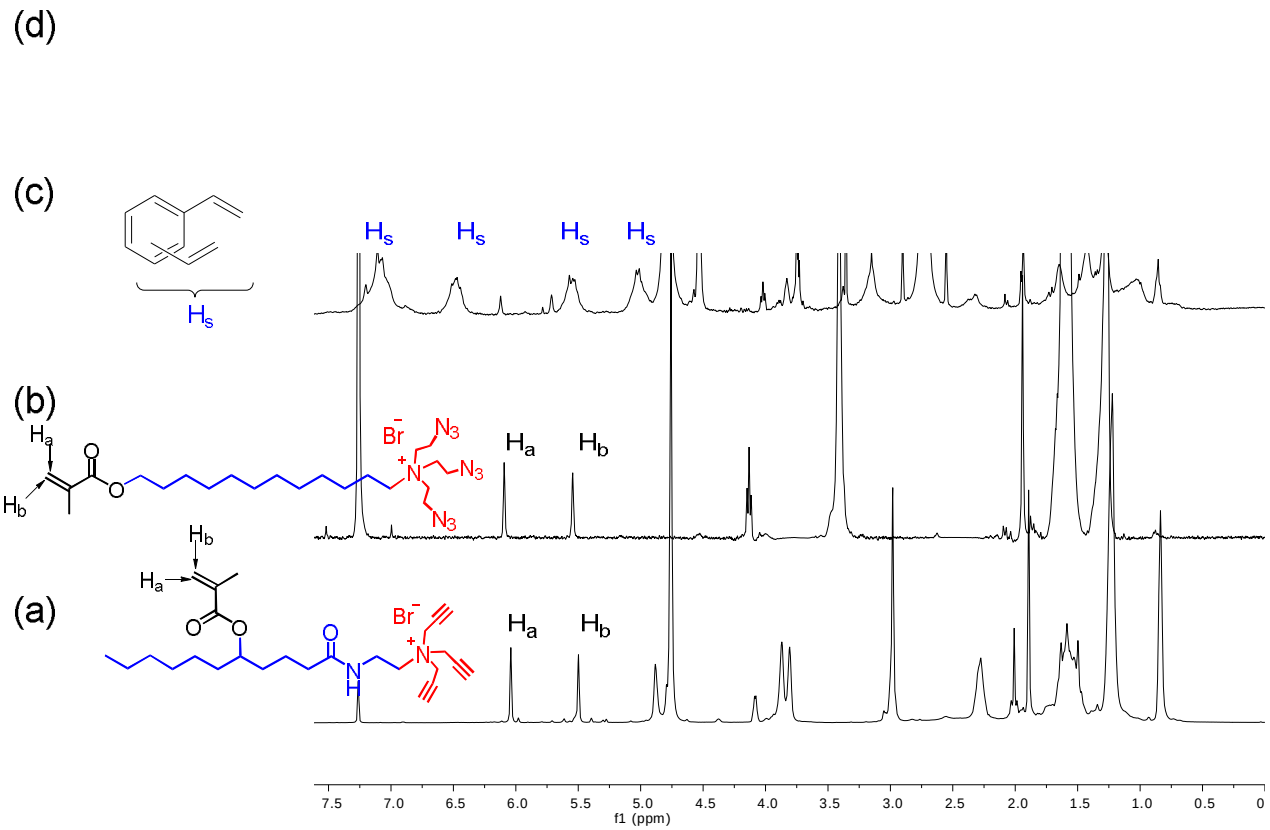

Figure 46S. ^{1}H NMR spectra of (a) Compound **10** in $CDCl_3$, (b) Compound **2'** in $CDCl_3$, (c) alkynyl-SCM in D_2O, and (d) MINP(lactose) in D_2O at 298 K. The data correspond to entry 8 in Table 2S.

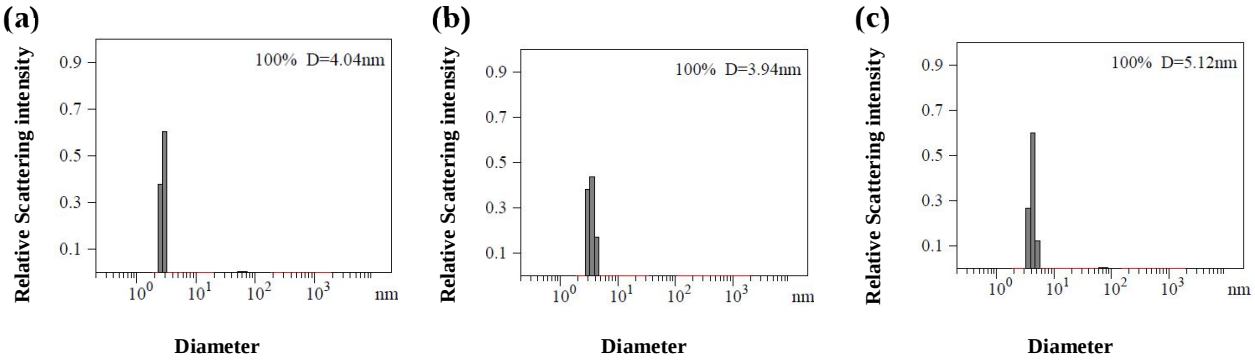

Figure 47S. Distribution of the hydrodynamic diameters of the nanoparticles in water as determined by DLS for the synthesis of MINP(lactose) (a) alkynyl-SCM, (b) core-cross-linked-SCM, and (c) surface-functionalized MINP(lactose) after purification. The data correspond to entry 8 in Table 2S.

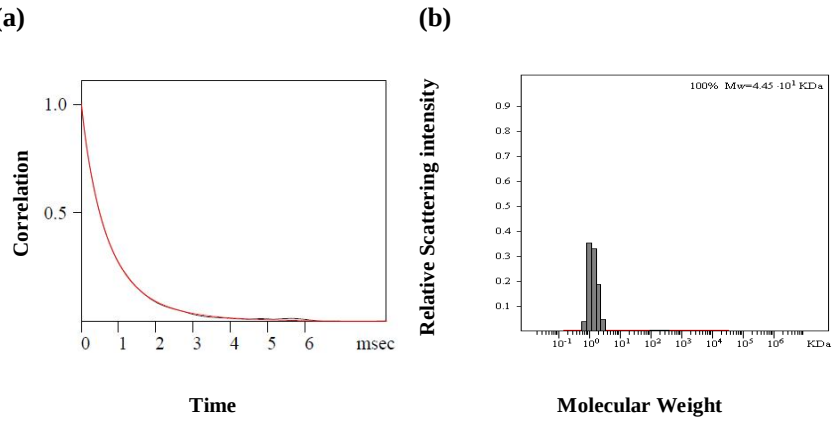

Figure 48S. The correlation curve and the distribution of the molecular weight for MINP(lactose) from the DLS The data correspond to entry 8 in Table 2S. The PRECISION DECONVOLVE program assumes the intensity of scattering is proportional to the mass of the particle squared. If each unit of building block for the MINP(lactose) is assumed to contain 0.4 molecules of compound **2'** (MW = 558 g/mol), 0.6 molecules of Compound **10** (MW = 508 g/mol), 0.6 molecules of compound **3** (MW = 264 g/mol), one molecule of DVB (MW = 130 g/mol), and 0.04 molecules of 6-vinylbenzoxaborole (MW = 160 g/mol), the molecular weight of MINP(lactose) translates to 54 [= 44500 / (0.4×558 +0.6×508 +0.6×264 +130 +0.04×160)] of such units.

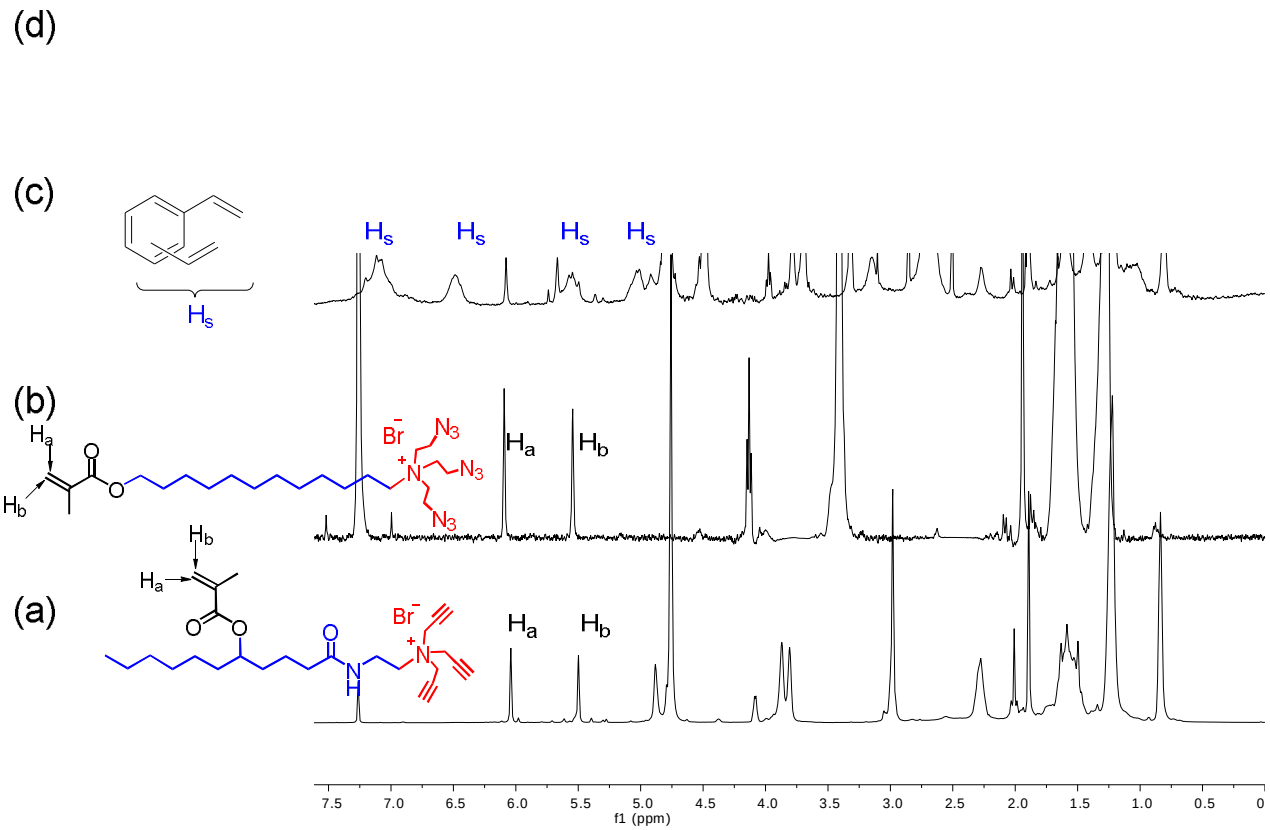

Figure 49S. ^{1}H NMR spectra of (a) Compound **10** in $CDCl_3$, (b) Compound **2'** in $CDCl_3$, (c) alkynyl-SCM in D_2O, and (d) MINP(maltotriose) in D_2O at 298 K. The data correspond to entry 9 in Table 2S.

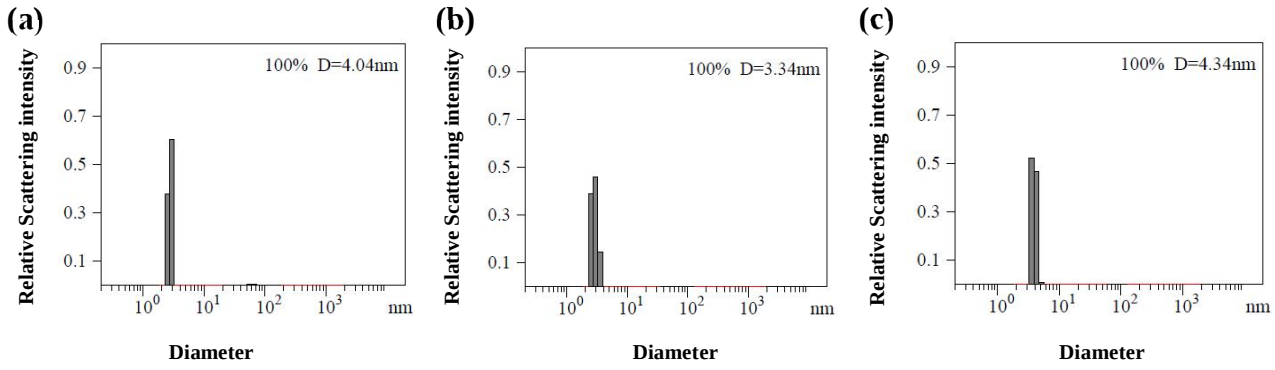

Figure 50S. Distribution of the hydrodynamic diameters of the nanoparticles in water as determined by DLS for the synthesis of MINP(maltotriose) (a) alkynyl-SCM, (b) core-cross-linked-SCM, and (c) surface-functionalized MINP(maltotriose) after purification. The data correspond to entry 9 in Table 2S.

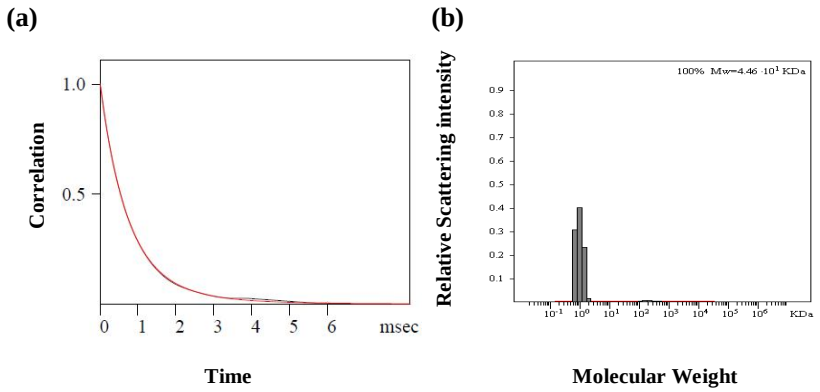

Figure 51S. The correlation curve and the distribution of the molecular weight for MINP(maltotriose) from the DLS The data correspond to entry 9 in Table 2S. The PRECISION DECONVOLVE program assumes the intensity of scattering is proportional to the mass of the particle squared. If each unit of building block for the MINP(maltotriose) is assumed to contain 0.4 molecules of compound **2'** (MW = 558 g/mol), 0.6 molecules of Compound **10** (MW = 508 g/mol), 0.6 molecules of compound **3** (MW = 264 g/mol), one molecule of DVB (MW = 130 g/mol), and 0.04 molecules of 6-vinylbenzoxaborole (MW = 160 g/mol), the molecular weight of MINP(maltotriose) translates to 54 [= 44600 / (0.4×558 +0.6×508 +0.6×264 +130 +0.04×160)] of such units.

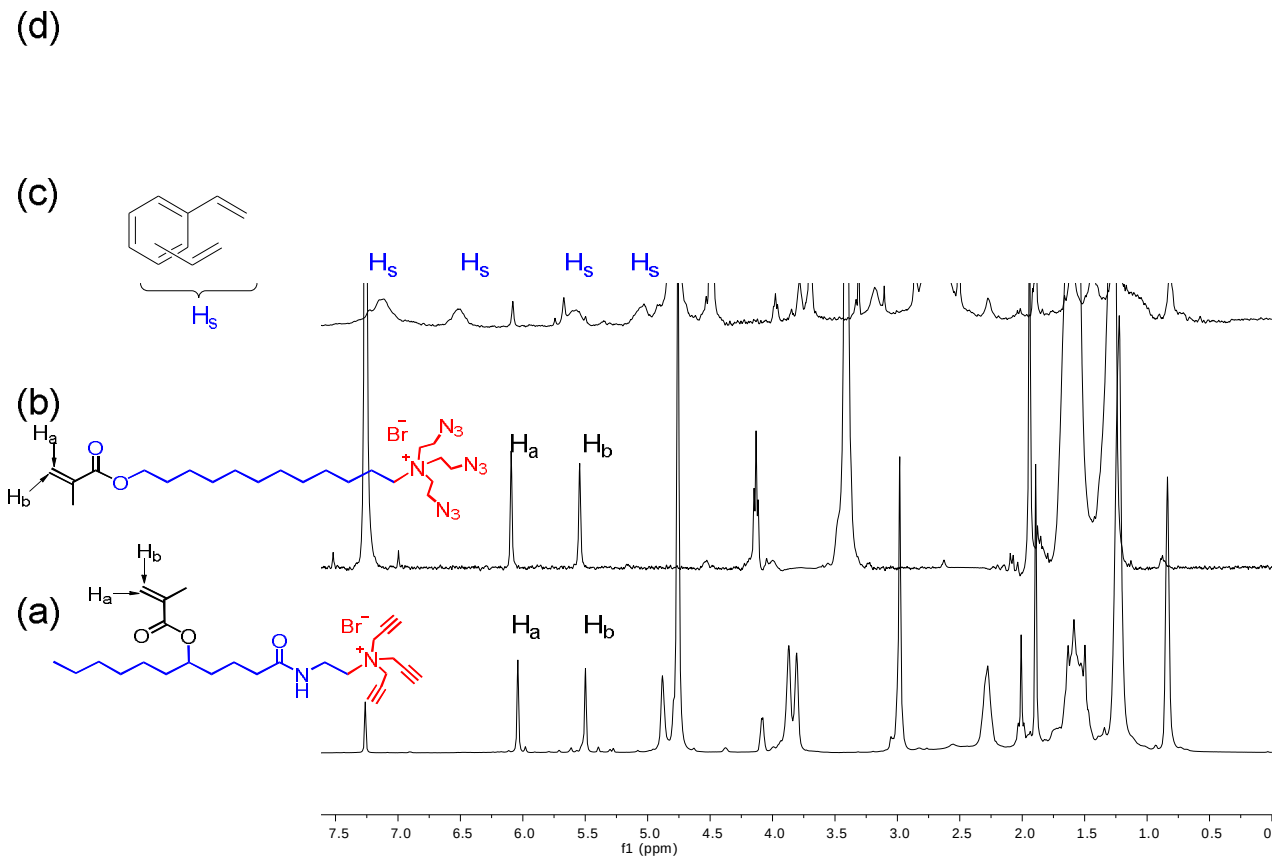

Figure 52S. ^{1}H NMR spectra of (a) Compound **10** in $CDCl_3$, (b) Compound **2'** in $CDCl_3$, (c) alkynyl-SCM in D_2O, and (d) MINP(sugar H) in D_2O at 298 K. The data correspond to entry 10 in Table 2S.

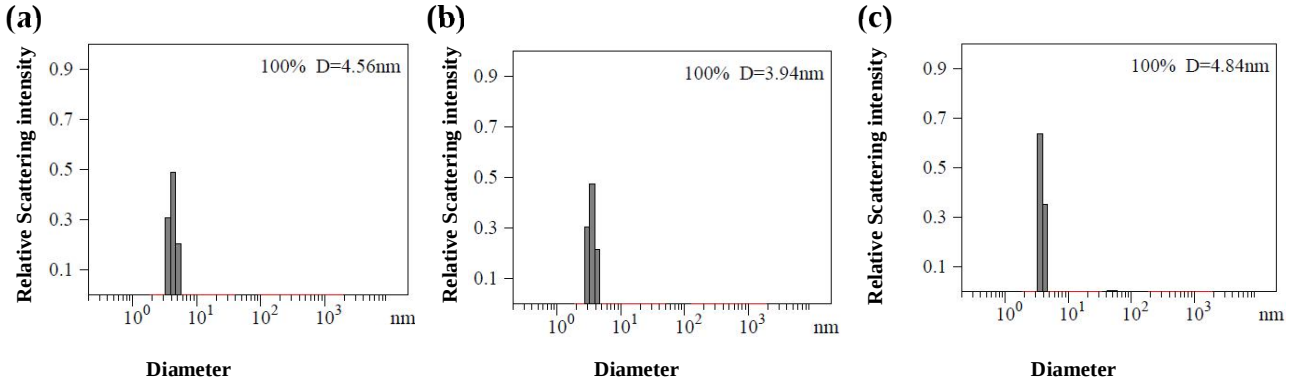

Figure 53S. Distribution of the hydrodynamic diameters of the nanoparticles in water as determined by DLS for the synthesis of MINP(sugar H) (a) alkynyl-SCM, (b) core-cross-linked-SCM, and (c) surface-functionalized MINP(sugar H) after purification. The data correspond to entry 10 in Table 2S.

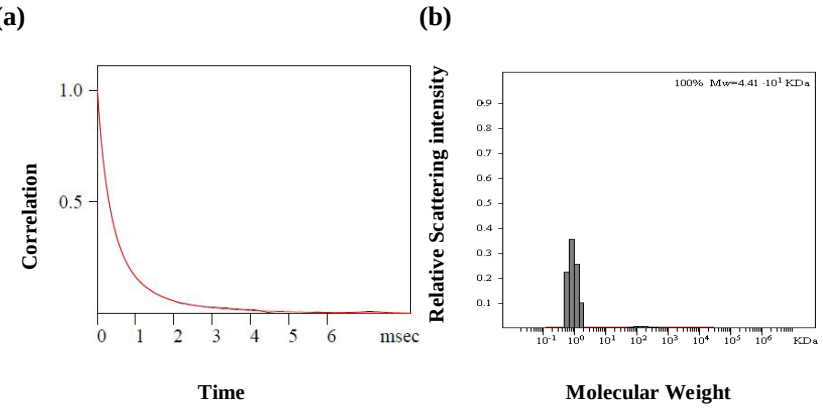

Figure 54S. The correlation curve and the distribution of the molecular weight for MINP(sugar H) from the DLS. The data correspond to entry 10 in Table 2S. The PRECISION DECONVOLVE program assumes the intensity of scattering is proportional to the mass of the particle squared. If each unit of building block for the MINP(sugar H) is assumed to contain 0.4 molecules of compound **2'** (MW = 558 g/mol), 0.6 molecules of Compound **10** (MW = 508 g/mol), 0.6 molecules of compound **3** (MW = 264 g/mol), one molecule of DVB (MW = 130 g/mol), and 0.06 molecules of 6-vinylbenzoxaborole (MW = 160 g/mol), the molecular weight of MINP(sugar H) translates to 53 [= 44100 / (0.4×558 +0.6×508 +0.6×264 +130 +0.06×160)] of such units.

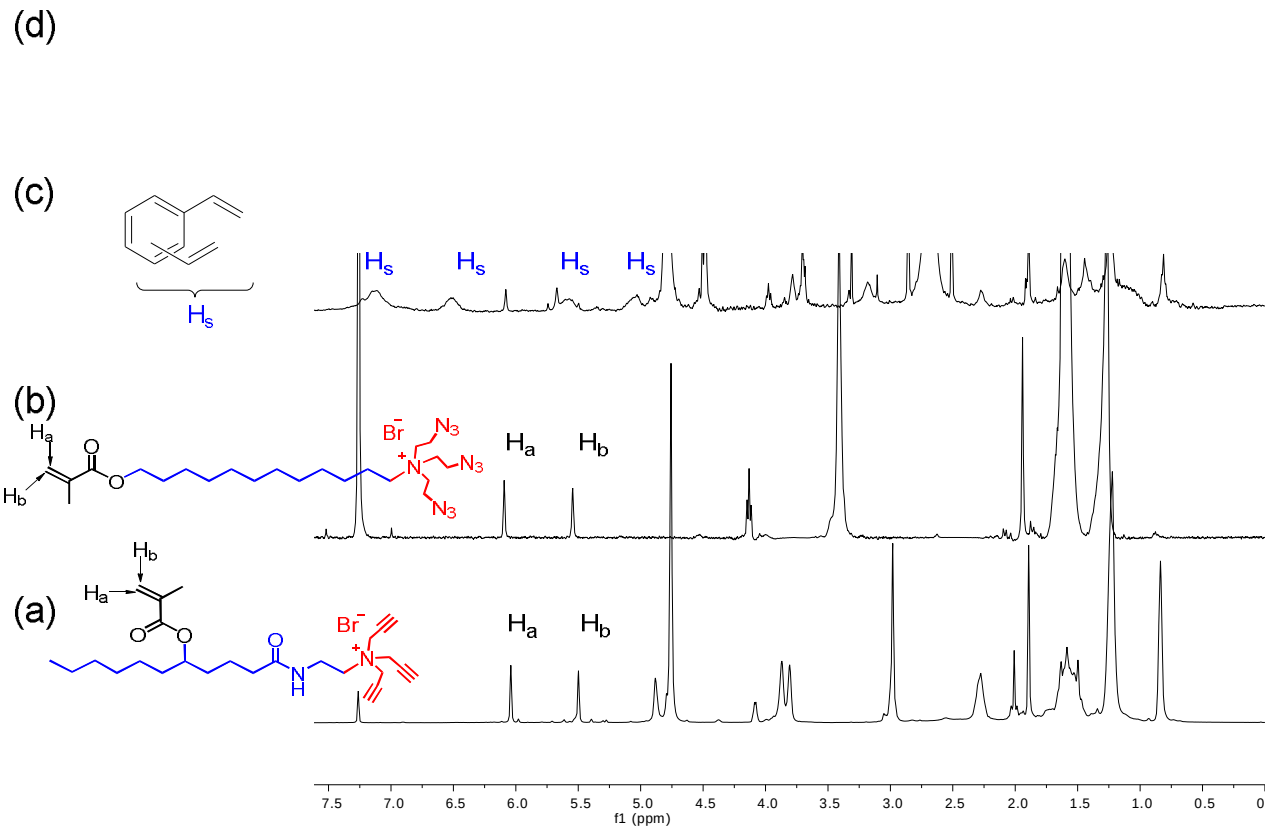

Figure 55S. ^{1}H NMR spectra of (a) Compound **10** in $CDCl_3$, (b) Compound **2'** in $CDCl_3$, (c) alkynyl-SCM in D_2O, and (d) MINP(sugar A) in D_2O at 298 K. The data correspond to entry 11 in Table 2S.

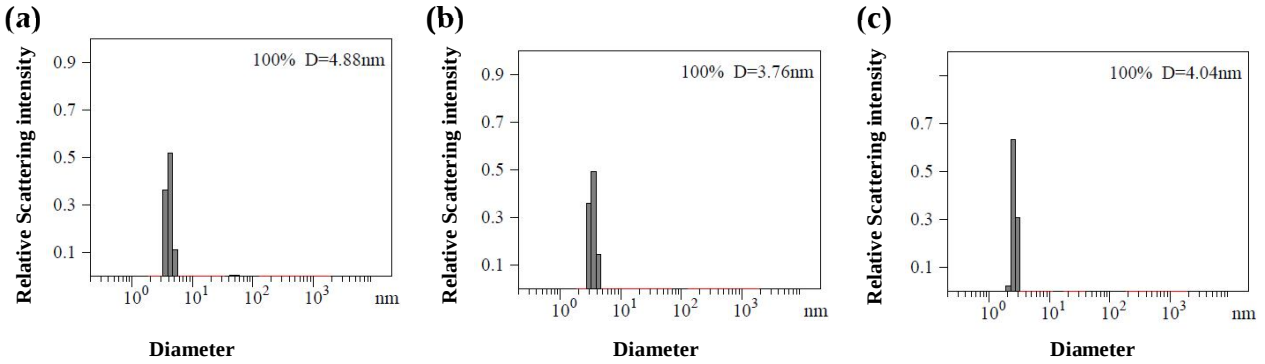

Figure 56S. Distribution of the hydrodynamic diameters of the nanoparticles in water as determined by DLS for the synthesis of MINP(sugar A) (a) alkynyl-SCM, (b) core-cross-linked-SCM, and (c) surface-functionalized MINP(sugar A) after purification. The data correspond to entry 11 in Table 2S.

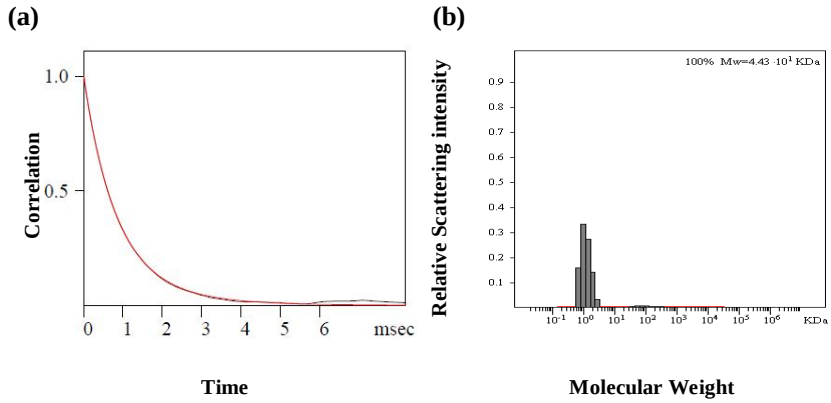

Figure 57S. The correlation curve and the distribution of the molecular weight for MINP(sugar A) from the DLS. The data correspond to entry 11 in Table 2S. The PRECISION DECONVOLVE program assumes the intensity of scattering is proportional to the mass of the particle squared. If each unit of building block for the MINP(sugar A) is assumed to contain 0.4 molecules of compound **2'** (MW = 558 g/mol), 0.6 molecules of Compound **10** (MW = 508 g/mol), 0.6 molecules of compound **3** (MW = 264 g/mol), one molecule of DVB (MW = 130 g/mol), and 0.06 molecules of 6-vinylbenzoxaborole (MW = 160 g/mol), the molecular weight of MINP(sugar A) translates to 54 [= 44300 / (0.4×558 +0.6×508 +0.6×264 +130 +0.06×160)] of such units.

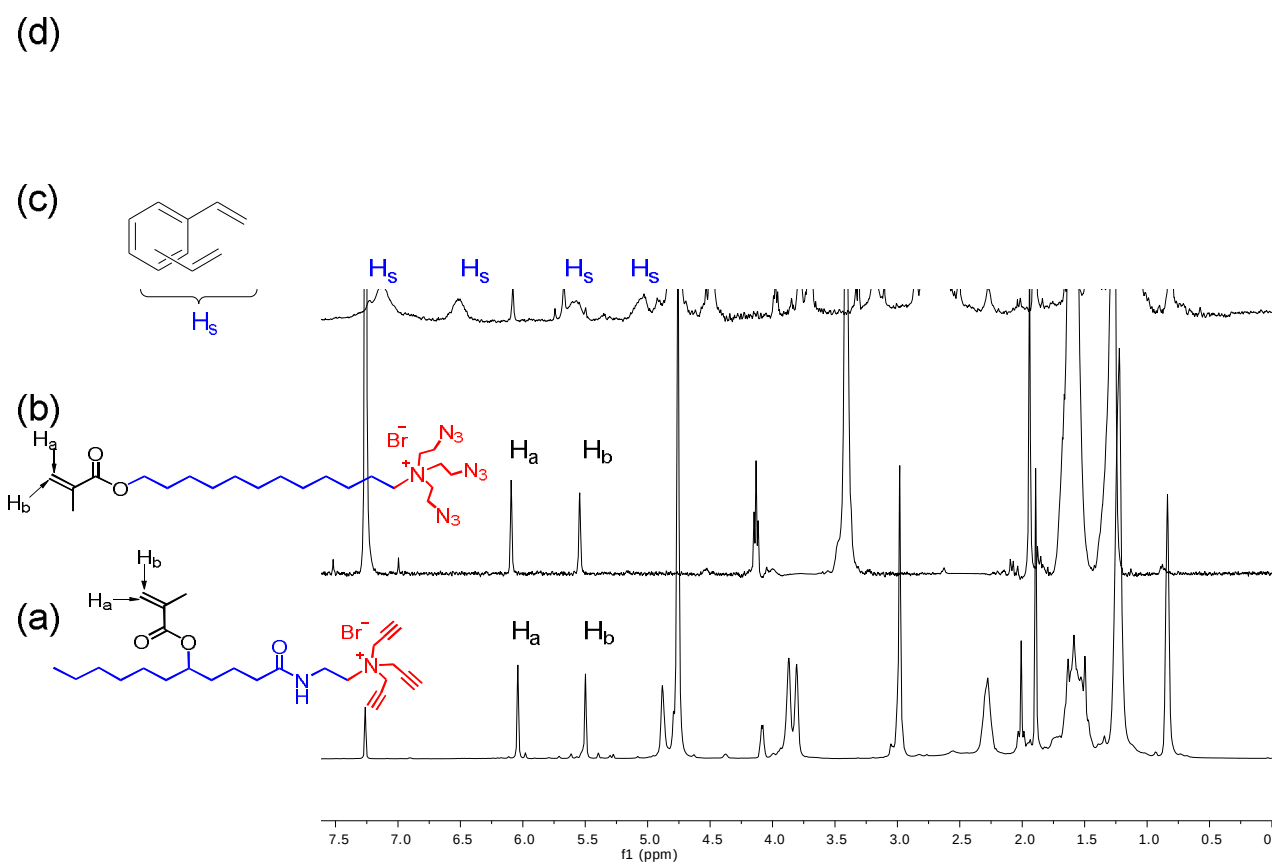

Figure 58S. ^{1}H NMR spectra of (a) Compound **10** in $CDCl_3$, (b) Compound **2'** in $CDCl_3$, (c) alkynyl-SCM in D_2O, and (d) MINP(sugar B) in D_2O at 298 K. The data correspond to entry 12 in Table 2S.

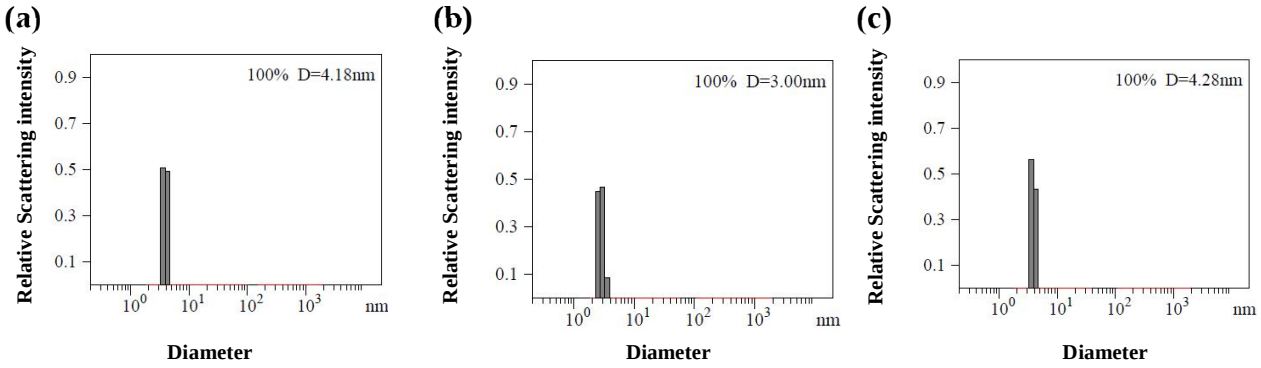

Figure 59S. Distribution of the hydrodynamic diameters of the nanoparticles in water as determined by DLS for the synthesis of MINP(sugar B) (a) alkynyl-SCM, (b) core-cross-linked-SCM, and (c) surface-functionalized MINP(sugar B) after purification. The data correspond to entry 12 in Table 2S.

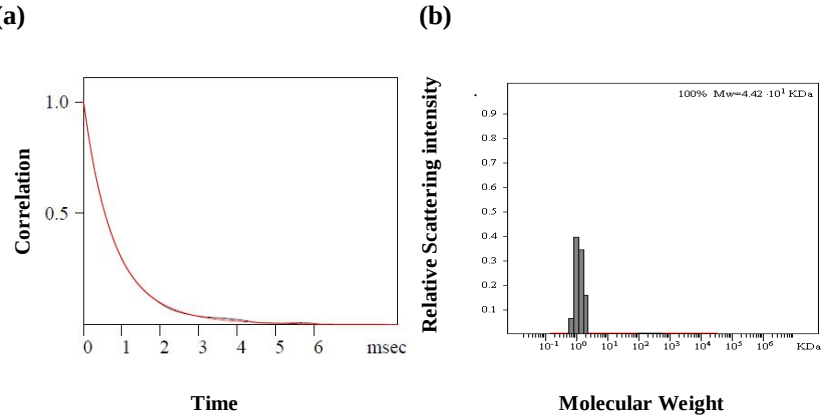

Figure 60S. The correlation curve and the distribution of the molecular weight for MINP(sugar B) from the DLS. The data correspond to entry 12 in Table 2S. The PRECISION DECONVOLVE program assumes the intensity of scattering is proportional to the mass of the particle squared. If each unit of building block for the MINP(sugar B) is assumed to contain 0.4 molecules of compound **2'** (MW = 558 g/mol), 0.6 molecules of Compound **10** (MW = 508 g/mol), 0.6 molecules of compound **3** (MW = 264 g/mol), one molecule of DVB (MW = 130 g/mol), and 0.06 molecules of 6-vinylbenzoxaborole (MW = 160 g/mol), the molecular weight of MINP(sugar B) translates to 53 [= 44200 / (0.4×558 +0.6×508 +0.6×264 +130 +0.06×160)] of such units.

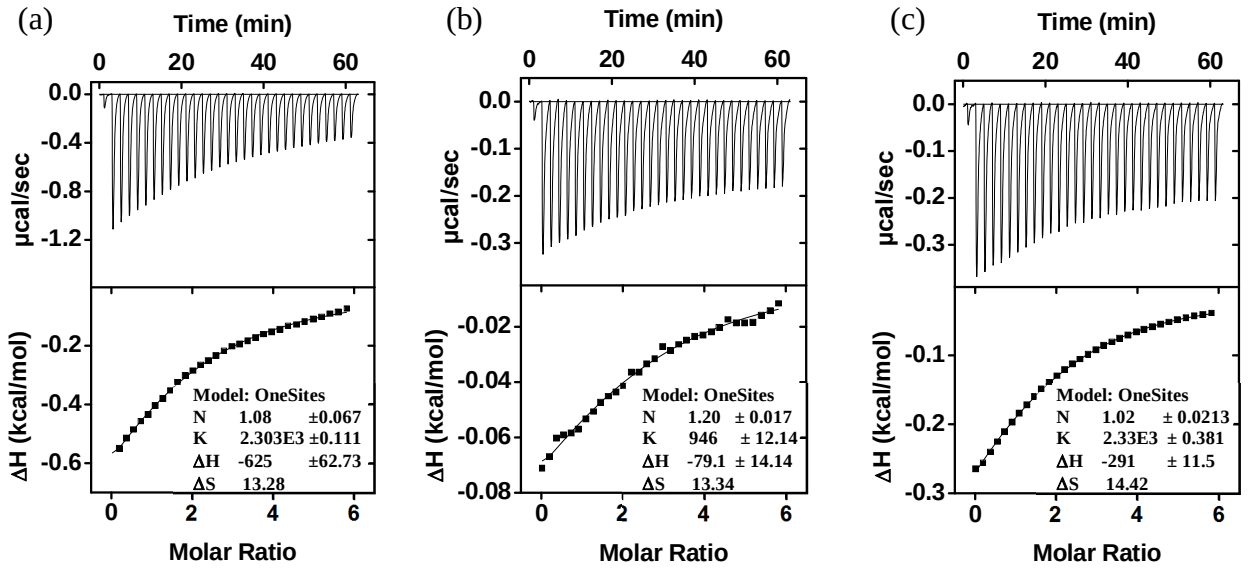

Figure 61S. ITC titration curves obtained at 298 K for the titration of MINP(glucose) with (a) glucose/FM **4** = 1:2, (b) glucose/FM **4 =** 1:1, and (c) glucose/FM **4** = 1:3 in 10 mM HEPES buffer (pH 7.4). The data correspond to entries 1–3, respectively, in Table 1. The top panel shows the raw calorimetric data. The area under each peak represents the amount of heat generated at each ejection and is plotted against the molar ratio of MINP to the substrate. The solid line is the best fit of the experimental data to the sequential binding of N equal and independent binding sites on the MINP. The heat of dilution for the substrate, obtained by adding the substrate to the buffer, was subtracted from the heat released during the binding. Binding parameters were auto-generated after curve fitting using Microcal Origin 7.

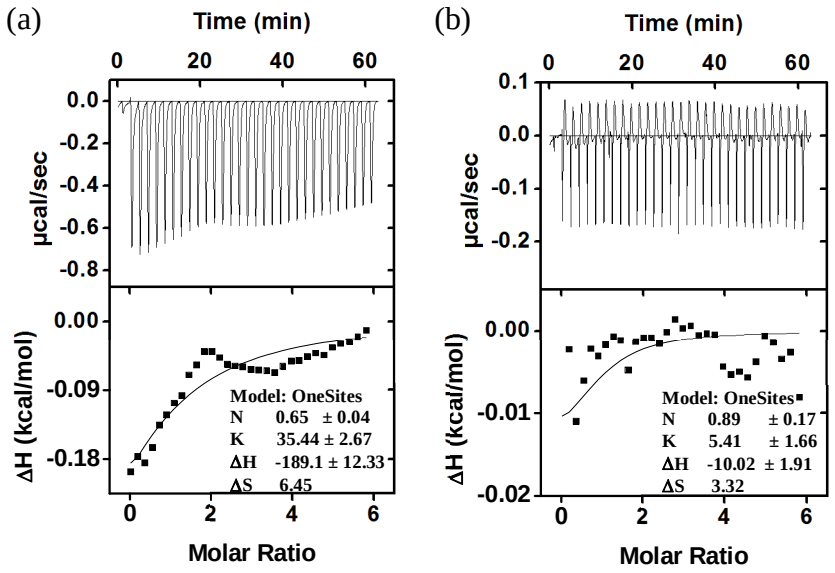

Figure 62S. ITC titration curves obtained at 298 K for the titration of (a) NINP without FM **4** and the glucose template and (b) NINP with FM **4** but without the glucose template in 10 mM HEPES buffer (pH 7.4). The data correspond to entries 4–5, respectively, in Table 1. The top panel shows the raw calorimetric data. The area under each peak represents the amount of heat generated at each ejection and is plotted against the molar ratio of MINP to the substrate. The solid line is the best fit of the experimental data to the sequential binding of N equal and independent binding sites on the MINP. The heat of dilution for the substrate, obtained by adding the substrate to the buffer, was subtracted from the heat released during the binding. Binding parameters were auto-generated after curve fitting using Microcal Origin 7.

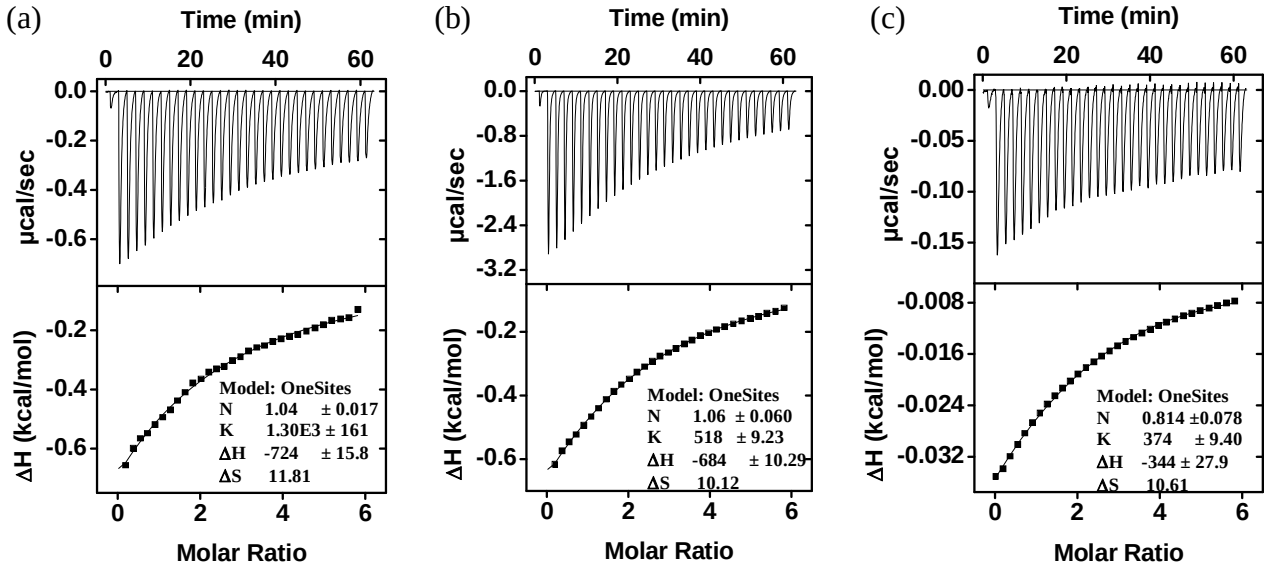

Figure 63S. ITC titration curves obtained at 298 K for the titration of MINP(glucose) with glucose at pH 8.5 (a), glucose at pH 6.5 (b), and allose at pH 7.4 (c) in 10 mM HEPES buffer (template/FM **4** = 1:2). The data correspond to entries 6–8, respectively, in Table 1. The top panel shows the raw calorimetric data. The area under each peak represents the amount of heat generated at each ejection and is plotted against the molar ratio of MINP to the substrate. The solid line is the best fit of the experimental data to the sequential binding of N equal and independent binding sites on the MINP. The heat of dilution for the substrate, obtained by adding the substrate to the buffer, was subtracted from the heat released during the binding. Binding parameters were auto-generated after curve fitting using Microcal Origin 7.

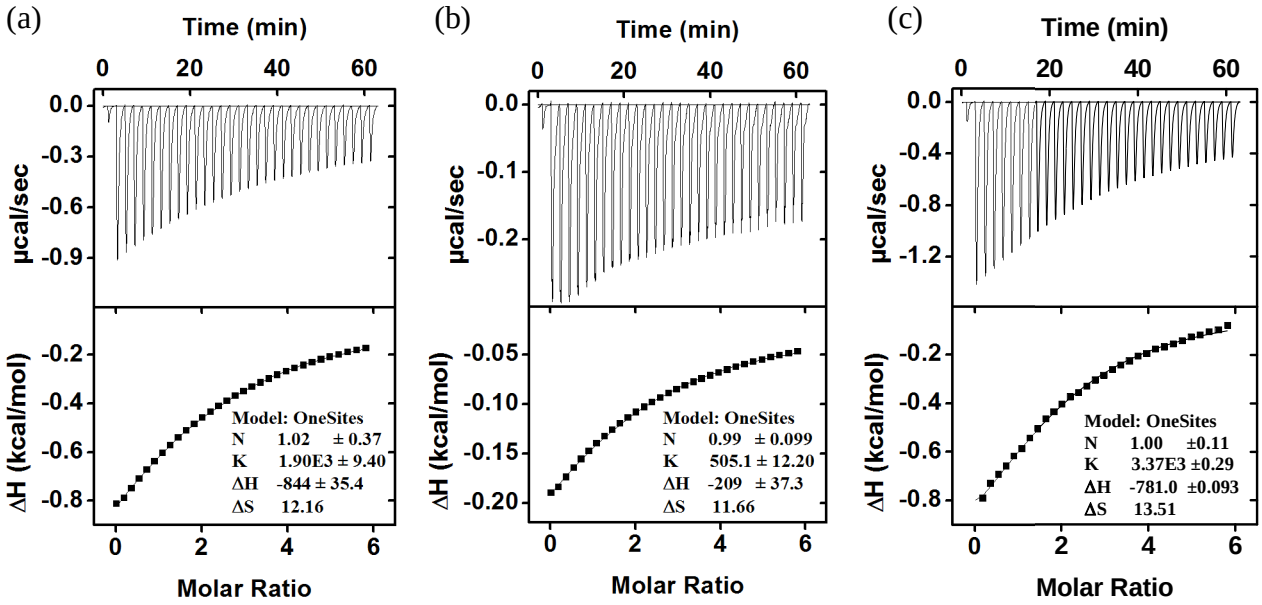

Figure 64S. ITC titration curves obtained at 298 K for the titration of (a) MINP(mannose) with mannose, (b) MINP(mannose) with altrose, and (c) MINP(galactose) with galactose in 10 mM HEPES buffer (pH 7.4, template/FM **4** = 1:2). The data correspond to entries 9–11, respectively, in Table 1. The top panel shows the raw calorimetric data. The area under each peak represents the amount of heat generated at each ejection and is plotted against the molar ratio of MINP to the substrate. The solid line is the best fit of the experimental data to the sequential binding of N equal and independent binding sites on the MINP. The heat of dilution for the substrate, obtained by adding the substrate to the buffer, was subtracted from the heat released during the binding. Binding parameters were auto-generated after curve fitting using Microcal Origin 7.

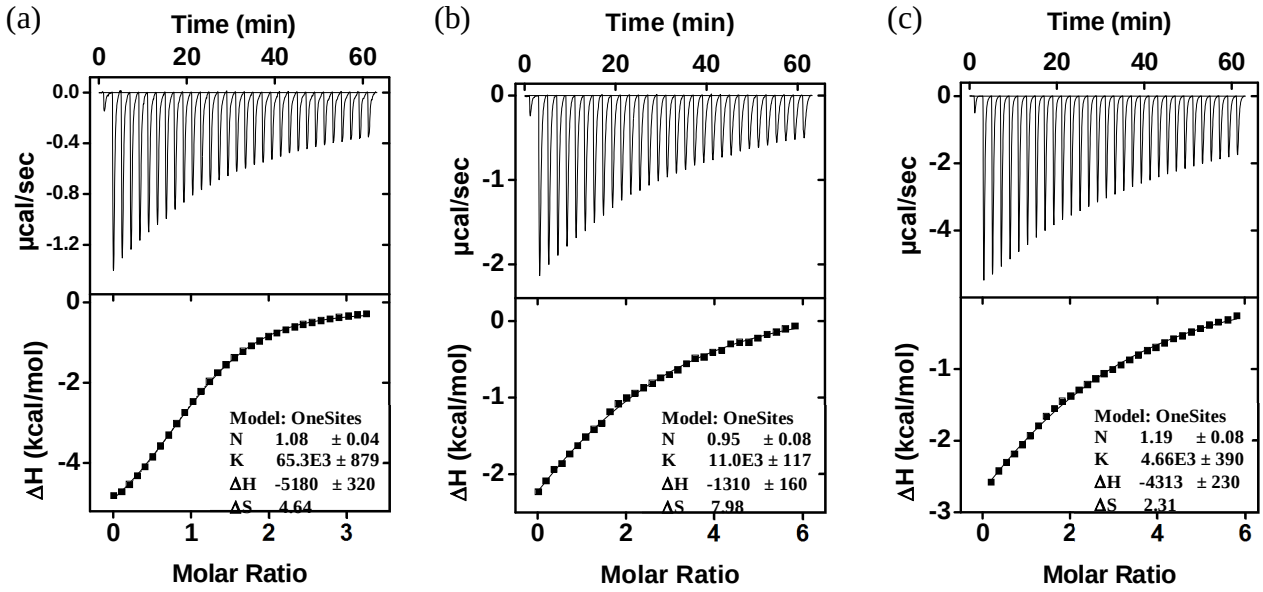

Figure 65S. ITC titration curves obtained at 298 K for the titration of MINP(**6**) with **6** (a), **7** (b), and **8** (c) in 10 mM HEPES buffer (pH 7.4, template/FM **4** = 1:1). The data correspond to entries 12–14, respectively, in Table 1. The top panel shows the raw calorimetric data. The area under each peak represents the amount of heat generated at each ejection and is plotted against the molar ratio of MINP to the substrate. The solid line is the best fit of the experimental data to the sequential binding of N equal and independent binding sites on the MINP. The heat of dilution for the substrate, obtained by adding the substrate to the buffer, was subtracted from the heat released during the binding. Binding parameters were auto-generated after curve fitting using Microcal Origin 7.

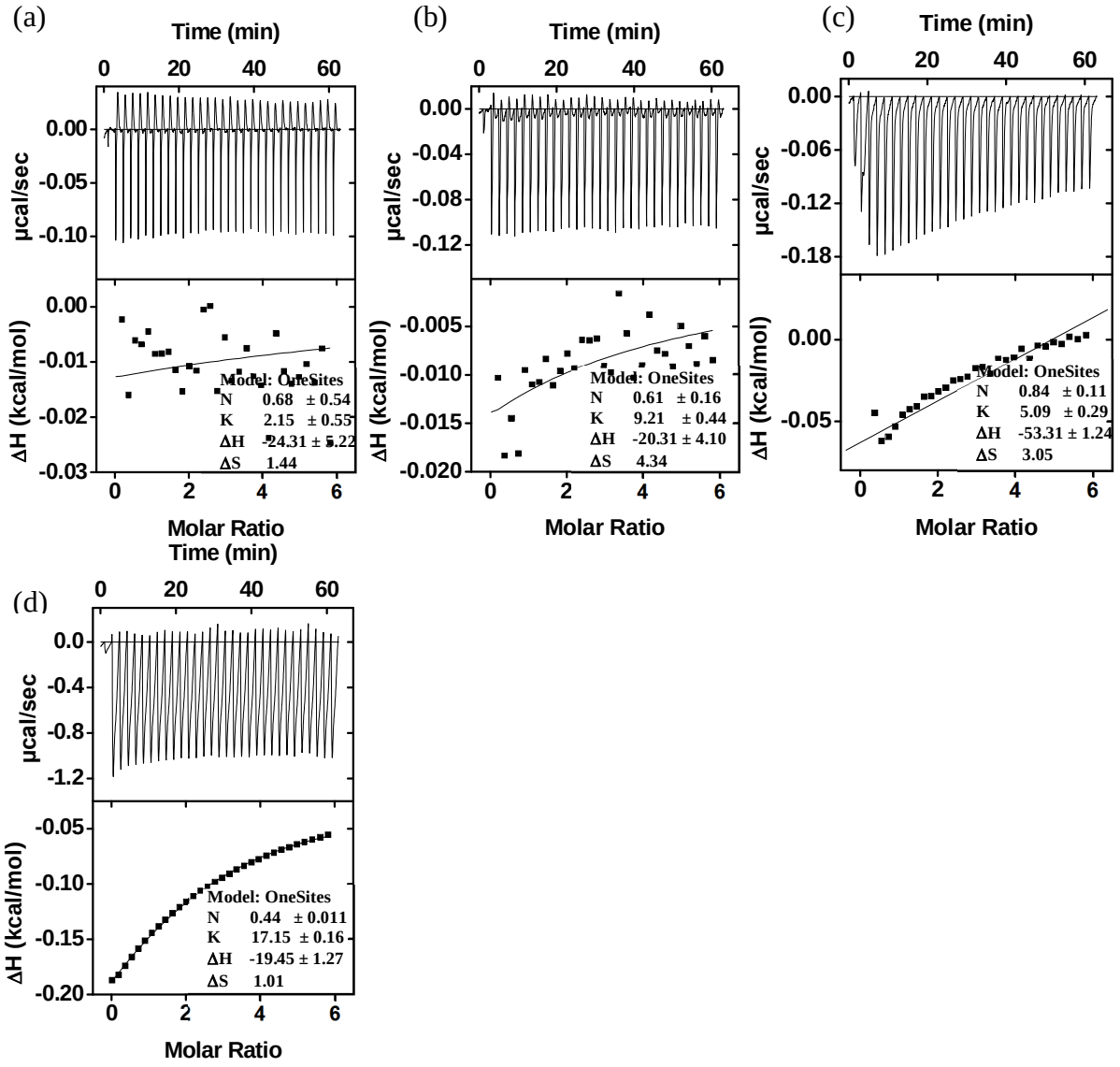

Figure 66S. ITC titration curves obtained at 298 K for the titration of MINP(glucose) with mannose (a), galactose (b), altrose (c), and gulose (d) in 10 mM HEPES buffer (pH 7.4, glucose/FM **4** = 1:2). The top panel shows the raw calorimetric data. The area under each peak represents the amount of heat generated at each ejection and is plotted against the molar ratio of MINP to the substrate. The solid line is the best fit of the experimental data to the sequential binding of N equal and independent binding sites on the MINP. The heat of dilution for the substrate, obtained by adding the substrate to the buffer, was subtracted from the heat released during the binding. Binding parameters were auto-generated after curve fitting using Microcal Origin 7.

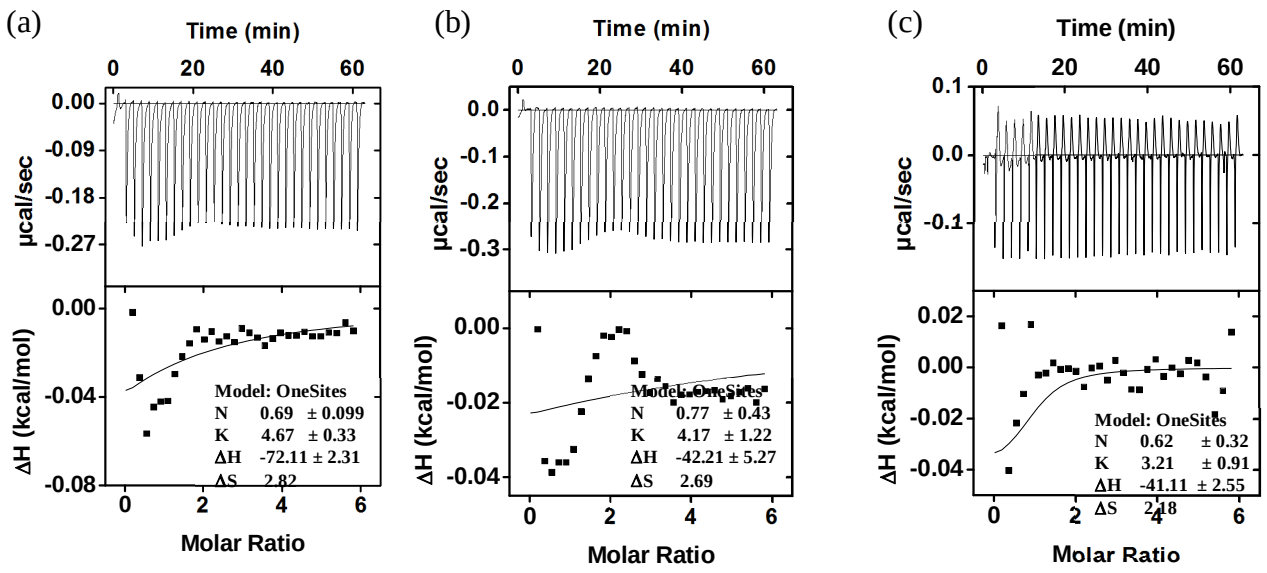

Figure 67S. ITC titration curves obtained at 298 K for the titration of MINP(glucose) with talose (a), idose (b), and xylose (c) in 10 mM HEPES buffer (pH 7.4, glucose/FM **4** = 1:2). The top panel shows the raw calorimetric data. The area under each peak represents the amount of heat generated at each ejection and is plotted against the molar ratio of MINP to the substrate. The solid line is the best fit of the experimental data to the sequential binding of N equal and independent binding sites on the MINP. The heat of dilution for the substrate, obtained by adding the substrate to the buffer, was subtracted from the heat released during the binding. Binding parameters were auto-generated after curve fitting using Microcal Origin 7.

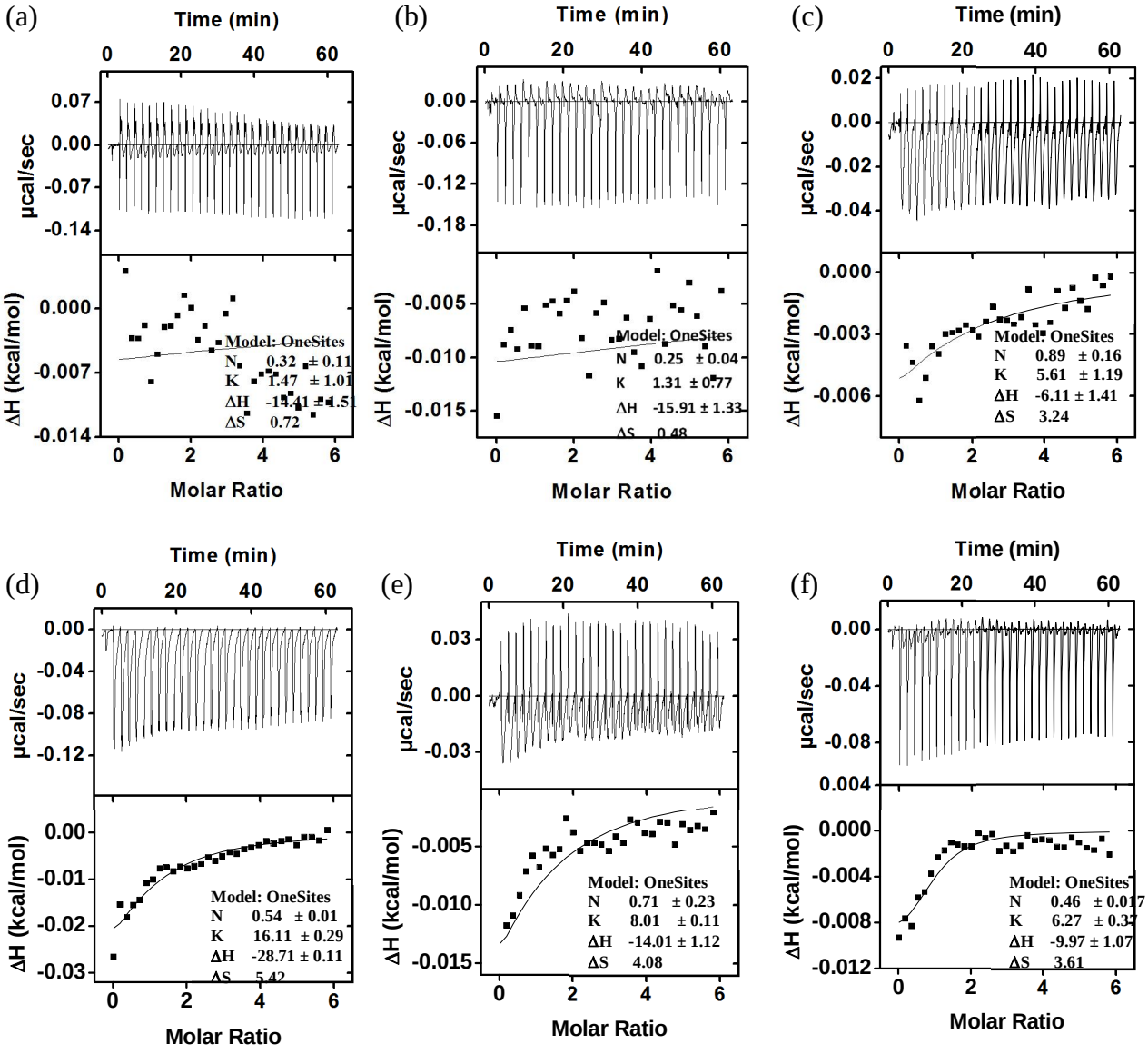

Figure 68S. ITC titration curves obtained at 298 K for the titration of MINP(mannose) with glucose (a), allose (b), galactose (c), gulose (d), talose (e), and idose (f) in 10 mM HEPES buffer (pH 7.4, mannose/FM **4** =1:2). The top panel shows the raw calorimetric data. The area under each peak represents the amount of heat generated at each ejection and is plotted against the molar ratio of MINP to the substrate. The solid line is the best fit of the experimental data to the sequential binding of N equal and independent binding sites on the MINP. The heat of dilution for the substrate, obtained by adding the substrate to the buffer, was subtracted from the heat released during the binding. Binding parameters were auto-generated after curve fitting using Microcal Origin 7.

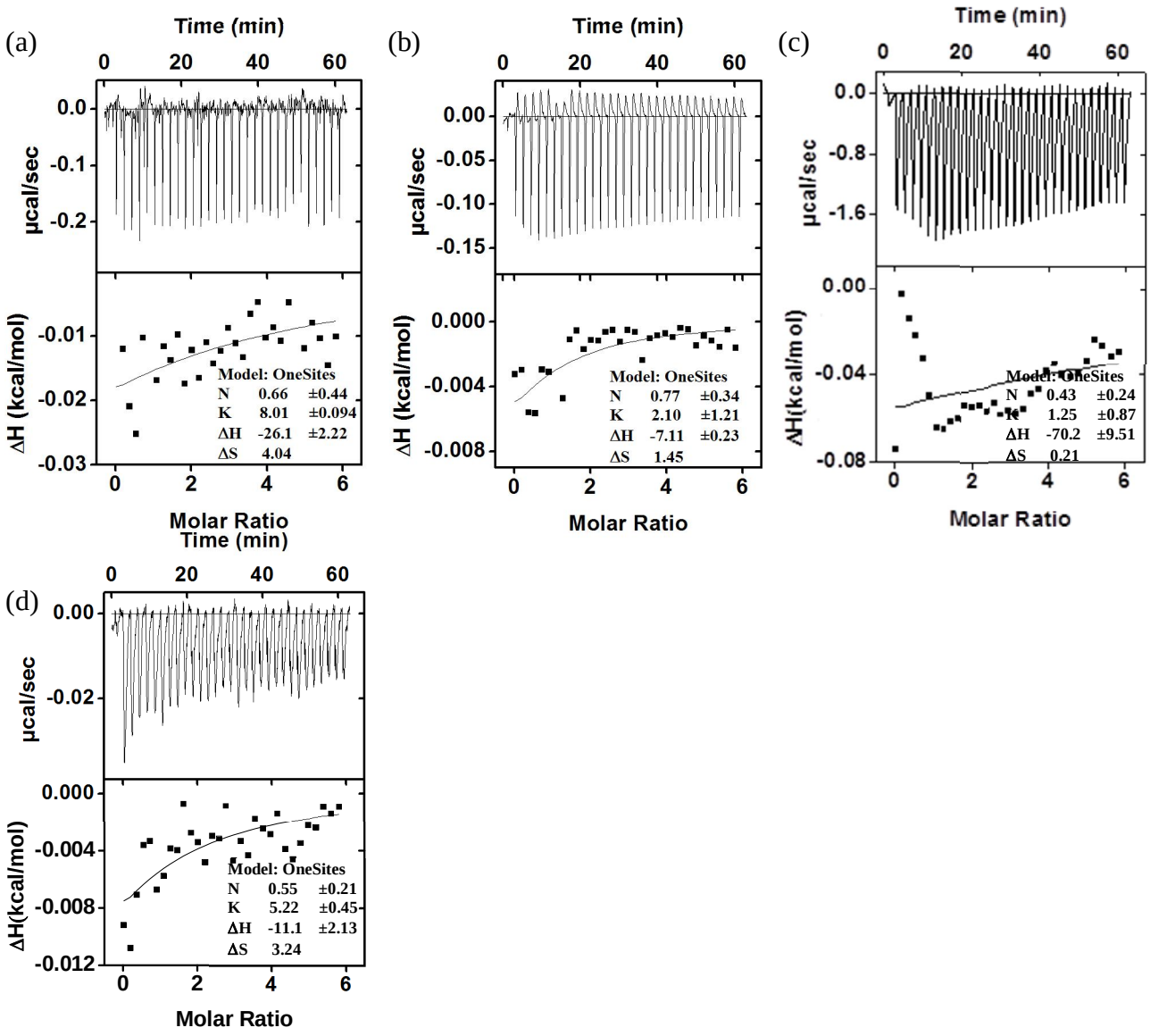

Figure 69S. ITC titration curves obtained at 298 K for the titration of MINP(galactose) with glucose (a), mannose (b), allose (c), and altrose (d) in 10 mM HEPES buffer (pH 7.4, galactose/FM **4** = 1:2). The top panel shows the raw calorimetric data. The area under each peak represents the amount of heat generated at each ejection and is plotted against the molar ratio of MINP to the substrate. The solid line is the best fit of the experimental data to the sequential binding of N equal and independent binding sites on the MINP. The heat of dilution for the substrate, obtained by adding the substrate to the buffer, was subtracted from the heat released during the binding. Binding parameters were auto-generated after curve fitting using Microcal Origin 7.

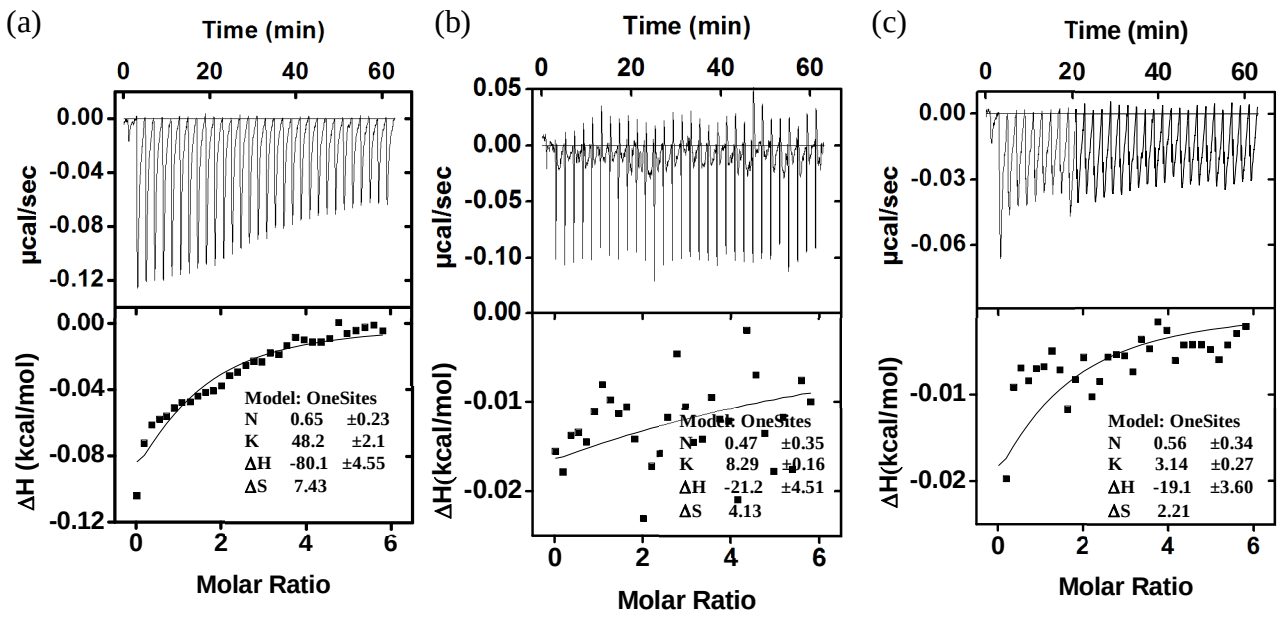

Figure 70S. ITC titration curves obtained at 298 K for the titration of MINP(galactose) with gulose (a), talose (b), and idose (c) in 10 mM HEPES buffer (pH 7.4, galactose/FM **4** = 1:2). The top panel shows the raw calorimetric data. The area under each peak represents the amount of heat generated at each ejection and is plotted against the molar ratio of MINP to the substrate. The solid line is the best fit of the experimental data to the sequential binding of N equal and independent binding sites on the MINP. The heat of dilution for the substrate, obtained by adding the substrate to the buffer, was subtracted from the heat released during the binding. Binding parameters were auto-generated after curve fitting using Microcal Origin 7.

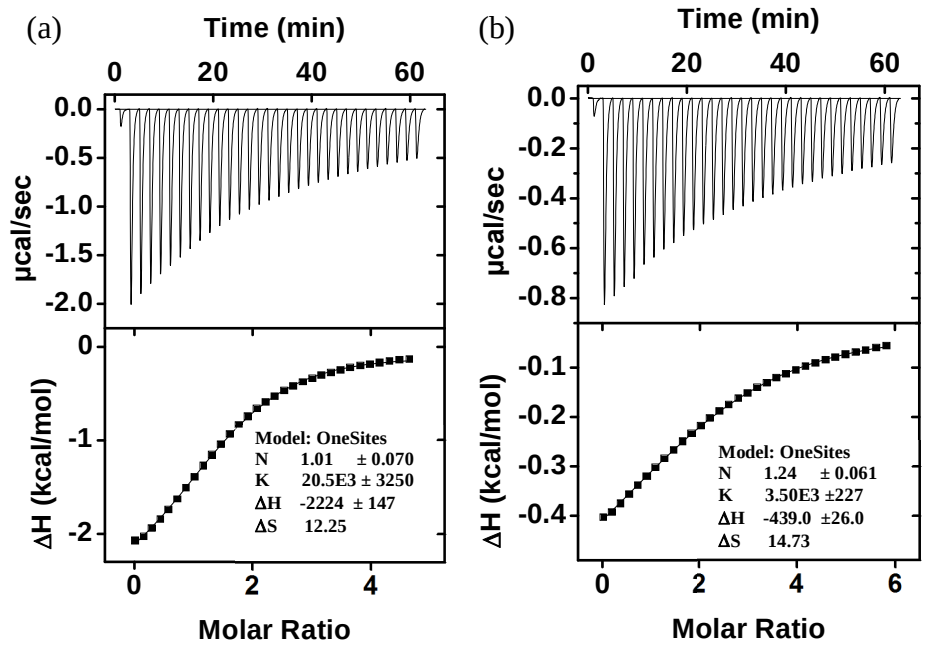

Figure 71S. ITC titration curves obtained at 298 K for the titration of (a) MINP(maltose) prepared with cross-linkable surfactants compound **10**/compound **2'** and (b) MINP(maltose) prepared with cross-linkable surfactants compound **1**/compound **2'** by maltose in 10 mM HEPES buffer (pH 7.4, maltose/FM **4** = 1:2). The data correspond to entries 1–2, respectively, in Table 2. The top panel shows the raw calorimetric data. The area under each peak represents the amount of heat generated at each ejection and is plotted against the molar ratio of MINP to the substrate. The solid line is the best fit of the experimental data to the sequential binding of N equal and independent binding sites on the MINP. The heat of dilution for the substrate, obtained by adding the substrate to the buffer, was subtracted from the heat released during the binding. Binding parameters were auto-generated after curve fitting using Microcal Origin 7.

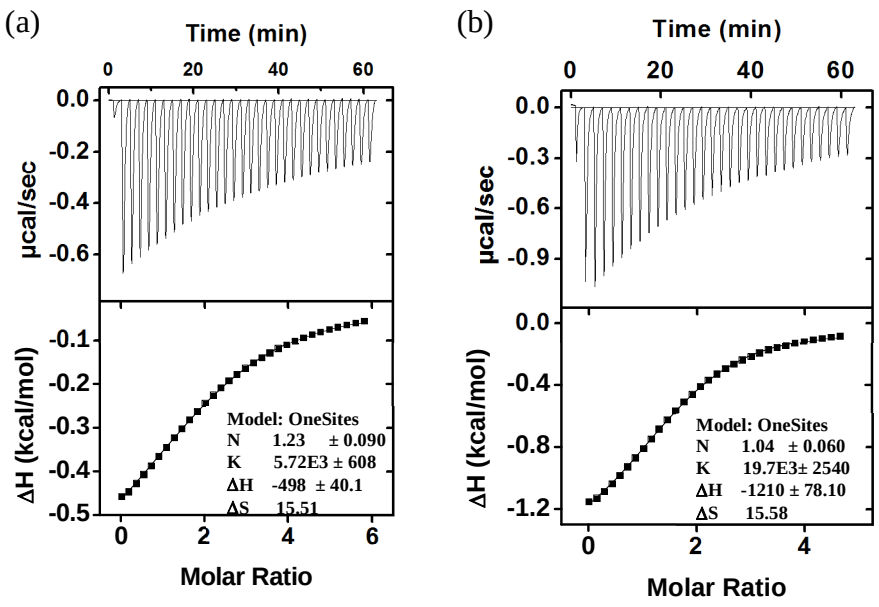

Figure 72S. ITC titration curves obtained at 298 K for the titration of MINP(maltose) with (a) maltose/FM **4** = 1:1 and (b) maltose/FM **4** = 1:3 in 10 mM HEPES buffer (pH 7.4). The data correspond to entries 3–4, respectively, in Table 2. The top panel shows the raw calorimetric data. The area under each peak represents the amount of heat generated at each ejection and is plotted against the molar ratio of MINP to the substrate. The solid line is the best fit of the experimental data to the sequential binding of N equal and independent binding sites on the MINP. The heat of dilution for the substrate, obtained by adding the substrate to the buffer, was subtracted from the heat released during the binding. Binding parameters were auto-generated after curve fitting using Microcal Origin 7.

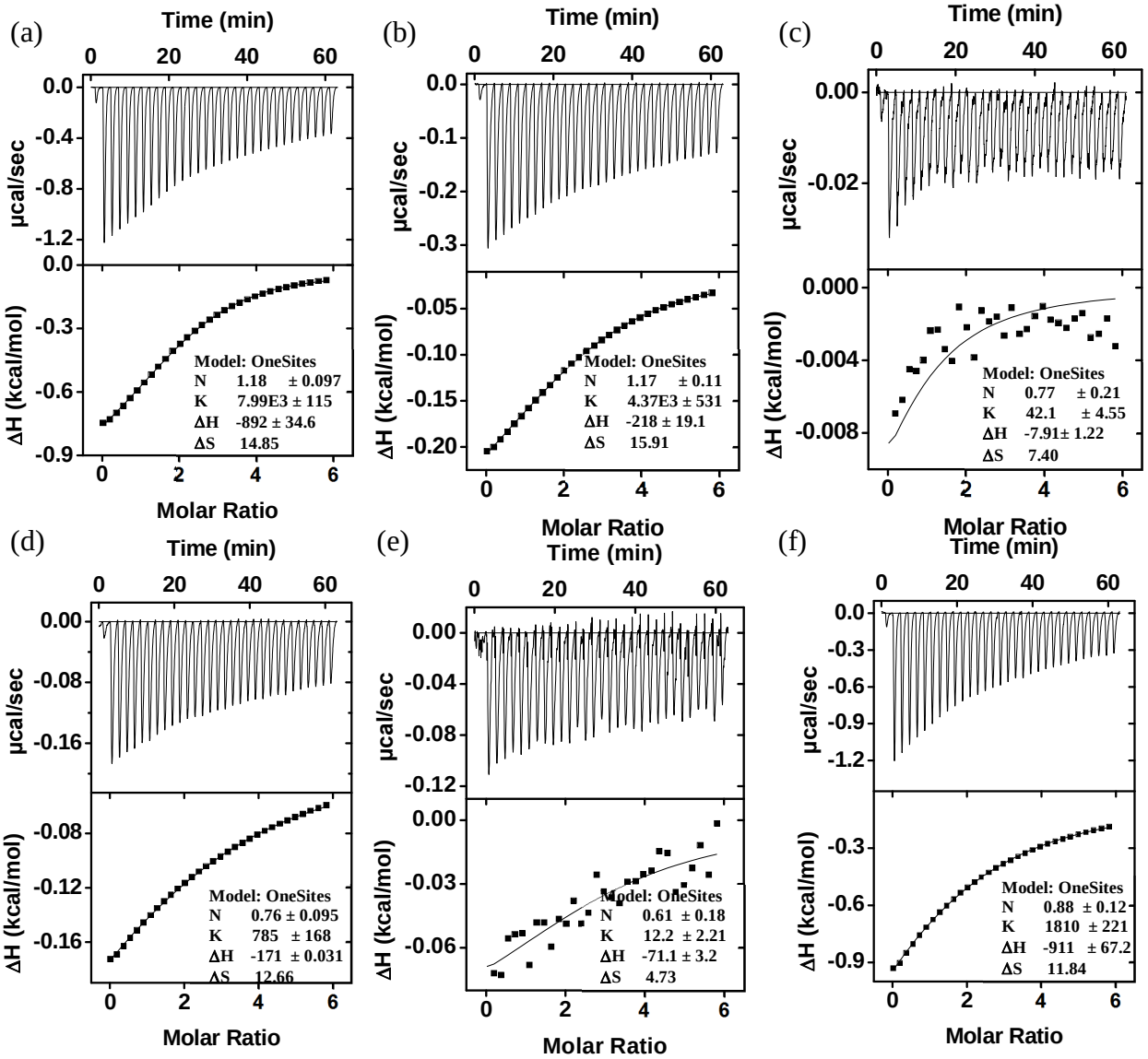

Figure 73S. ITC titration curves obtained at 298 K for the titration of MINP(maltose) with cellobiose (a), gentiobiose (b), maltulose (c), lactose (d), maltotriose (e), and glucose (f) in 10 mM HEPES buffer (pH 7.4, maltose/FM **4** = 1:2). The data correspond to entries 5–10, respectively, in Table 2. The top panel shows the raw calorimetric data. The area under each peak represents the amount of heat generated at each ejection and is plotted against the molar ratio of MINP to the substrate. The solid line is the best fit of the experimental data to the sequential binding of N equal and independent binding sites on the MINP. The heat of dilution for the substrate, obtained by adding the substrate to the buffer, was subtracted from the heat released during the binding. Binding parameters were auto-generated after curve fitting using Microcal Origin 7.

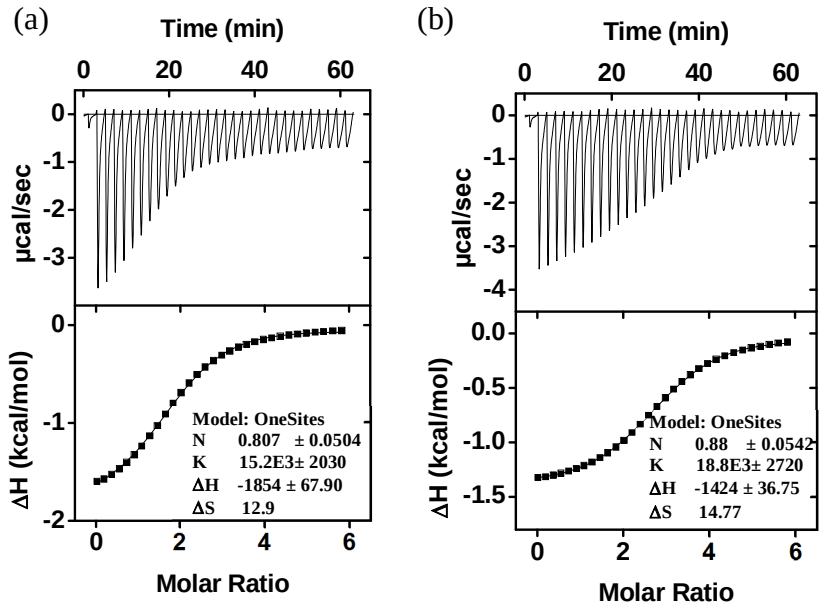

Figure 74S. ITC titration curves obtained at 298 K for the titration of MINP(maltose) with maltose in the presence of cellobiose (a) and lactose (b) in 10 mM HEPES buffer (pH 7.4, maltose/FM **3** = 1:2). [MINP] = 15 µM. [Cellobiose] = [lactose] = 75 µM. The data correspond to entries 11–12, respectively, in Table 2. The top panel shows the raw calorimetric data. The area under each peak represents the amount of heat generated at each ejection and is plotted against the molar ratio of MINP to the substrate. The solid line is the best fit of the experimental data to the sequential binding of N equal and independent binding sites on the MINP. The heat of dilution for the substrate, obtained by adding the substrate to the buffer, was subtracted from the heat released during the binding. Binding parameters were auto-generated after curve fitting using Microcal Origin 7.

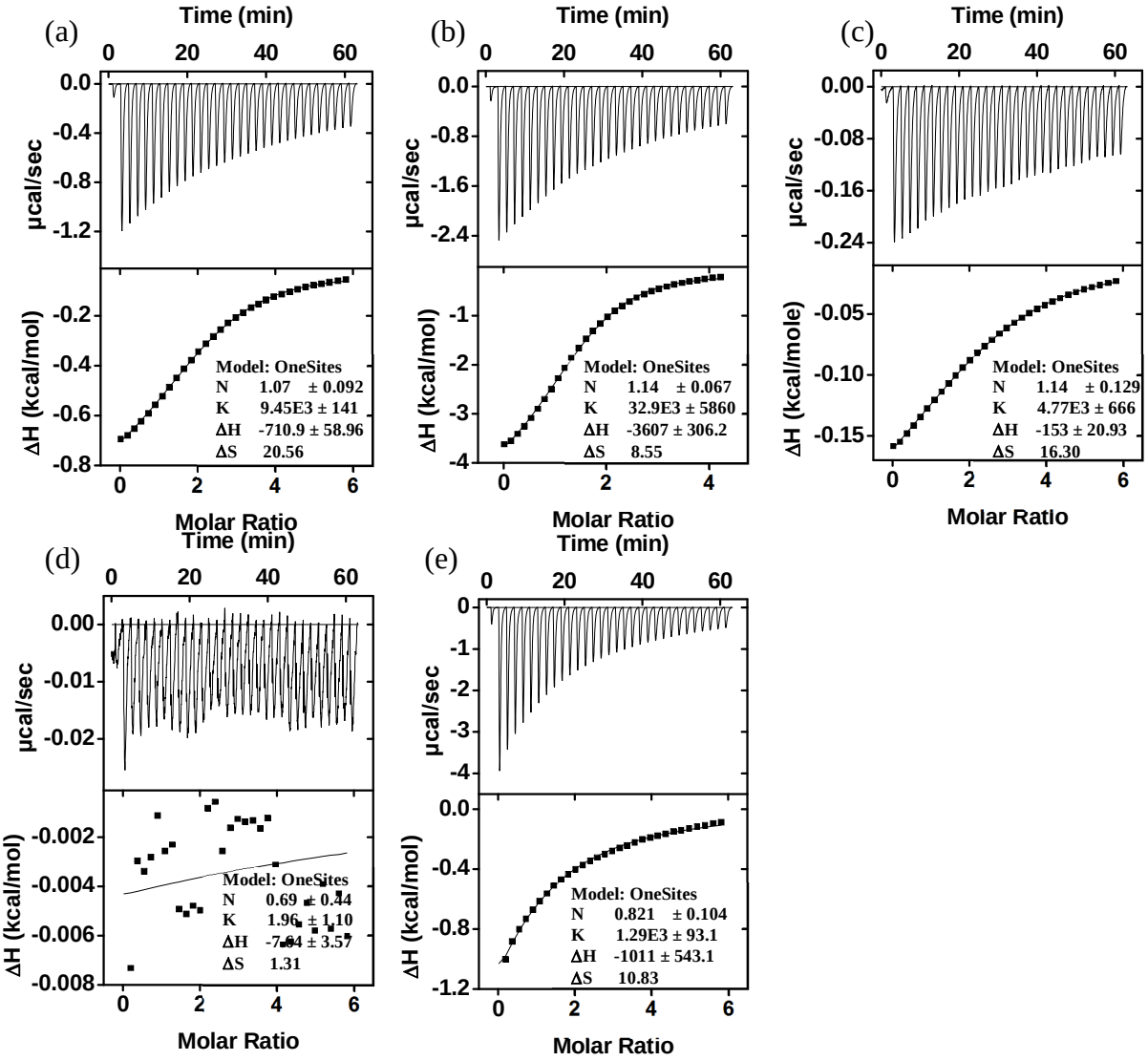

Figure 75S. ITC titration curves obtained at 298 K for the titration of MINP(cellobiose) with maltose (a), cellobiose (b), gentiobiose (c), maltulose (d), and lactose (e) in 10 mM HEPES buffer (pH 7.4, cellobiose/FM **3** = 1:2). The data correspond to entries 13–17, respectively, in Table 2. The top panel shows the raw calorimetric data. The area under each peak represents the amount of heat generated at each ejection and is plotted against the molar ratio of MINP to the substrate. The solid line is the best fit of the experimental data to the sequential binding of N equal and independent binding sites on the MINP. The heat of dilution for the substrate, obtained by adding the substrate to the buffer, was subtracted from the heat released during the binding. Binding parameters were auto-generated after curve fitting using Microcal Origin 7.

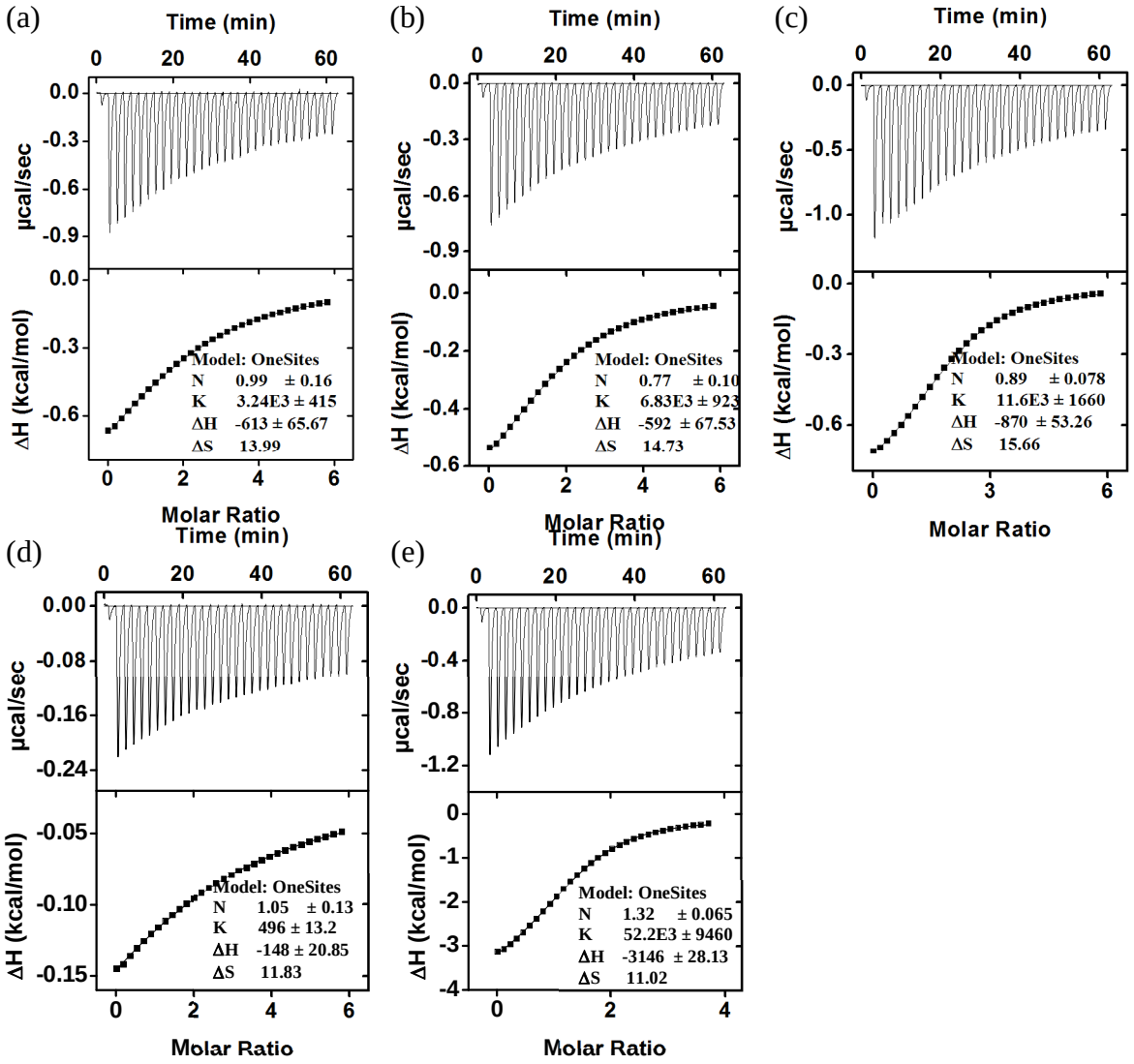

Figure 76S. ITC titration curves obtained at 298 K for the titration of MINP(lactose) with maltose (a), cellobiose (b), gentiobiose (c), maltulose (d), and lactose (e) in 10 mM HEPES buffer (pH 7.4, lactose/FM **3** = 1:2). The data correspond to entries 18–22, respectively, in Table 2. The top panel shows the raw calorimetric data. The area under each peak represents the amount of heat generated at each ejection and is plotted against the molar ratio of MINP to the substrate. The solid line is the best fit of the experimental data to the sequential binding of N equal and independent binding sites on the MINP. The heat of dilution for the substrate, obtained by adding the substrate to the buffer, was subtracted from the heat released during the binding. Binding parameters were auto-generated after curve fitting using Microcal Origin 7.

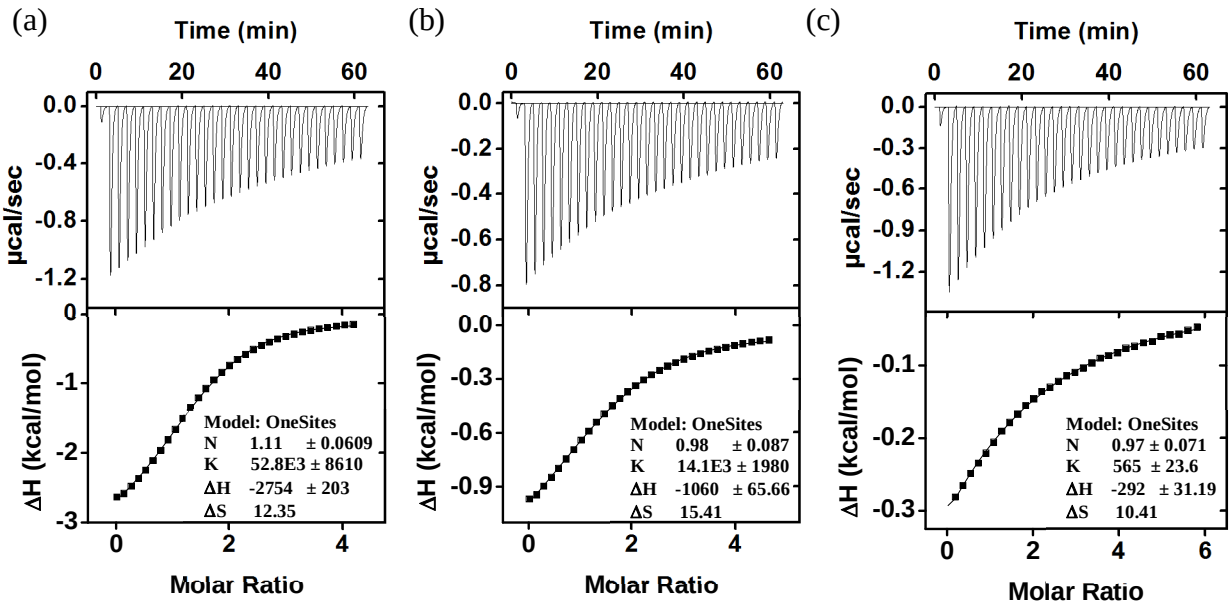

Figure 77S. ITC titration curves obtained at 298 K for the titration of MINP(maltotriose) with maltotriose (a), maltose (b), and glucose (c) in 10 mM HEPES buffer (pH 7.4, maltotriose/FM **3** = 1:2). The data correspond to entries 23–25, respectively, in Table 2. The top panel shows the raw calorimetric data. The area under each peak represents the amount of heat generated at each ejection and is plotted against the molar ratio of MINP to the substrate. The solid line is the best fit of the experimental data to the sequential binding of N equal and independent binding sites on the MINP. The heat of dilution for the substrate, obtained by adding the substrate to the buffer, was subtracted from the heat released during the binding. Binding parameters were auto-generated after curve fitting using Microcal Origin 7.

Table 3S. ITC binding data for oligosaccharide guests.[a]

Entry	Host	Guest	K_a (10^3 M^{-1})	K_{rel}	-Δ*G* (kcal/mol)	N
1	MINP(maltose)[b]	maltose	9.20 ± 0.11	-	-5.40	1.2±0.1
2	MINP(maltose)[c]	maltose	4.03 ± 0.51	-	-4.91	1.0±0.1
3	MINP(maltulose)	maltose	0.005±0.001	0.005	--[d]	--[d]
4	MINP(maltulose)	cellobiose	0.002±0.001	0.0002	--[d]	--[d]
5	MINP(maltulose)	gentiobiose	5.46 ± 0.63	0.57	-5.09	1.1±0.1
6	MINP(maltulose)	maltulose	9.56 ± 0.14	1	-5.43	0.9±0.1
7	MINP(maltulose)	lactose	1.79 ± 0.22	0.19	-4.43	1.0±0.1
8	MINP(gentiobiose)	maltose	2.95 ± 0.56	0.04	-4.73	1.1±0.1
9	MINP(gentiobiose)	cellobiose	6.31 ± 0.61	0.09	-5.18	1.0 ± 0.1
10	MINP(gentiobiose)	gentiobiose	73.2 ± 1.7	1	-6.63	1.1 ± 0.1
11	MINP(gentiobiose)	maltulose	0.55 ± 0.01	0.008	-3.73	1.0 ± 0.1
12	MINP(gentiobiose)	lactose	10.1 ± 1.6	0.14	-5.46	0.9 ± 0.1

[a]The titrations were performed in 10 mM HEPES buffer at pH 7.4 with template/FM **3** = 1:2. [b] pH 8.5. [c] pH 6.5. [d] Binding was extremely weak. Because the binding constant was estimated from ITC, -Δ*G* and *N* are not listed.

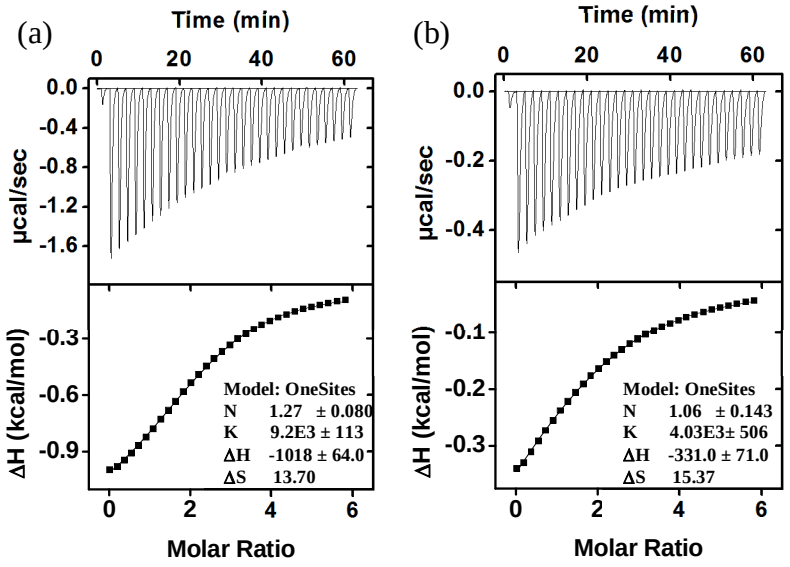

Figure 78S. ITC titration curves obtained at 298 K for the titration of MINP(maltose) with maltose at pH 8.5 (a), and pH 6.5 (b) in 10 mM HEPES buffer (maltose/FM **3** = 1:2). The data correspond to entries 1–2, respectively, in Table 3S. The top panel shows the raw calorimetric data. The area under each peak represents the amount of heat generated at each ejection and is plotted against the molar ratio of MINP to the substrate. The solid line is the best fit of the experimental data to the sequential binding of N equal and independent binding sites on the MINP. The heat of dilution for the substrate, obtained by adding the substrate to the buffer, was subtracted from the heat released during the binding. Binding parameters were auto-generated after curve fitting using Microcal Origin 7.

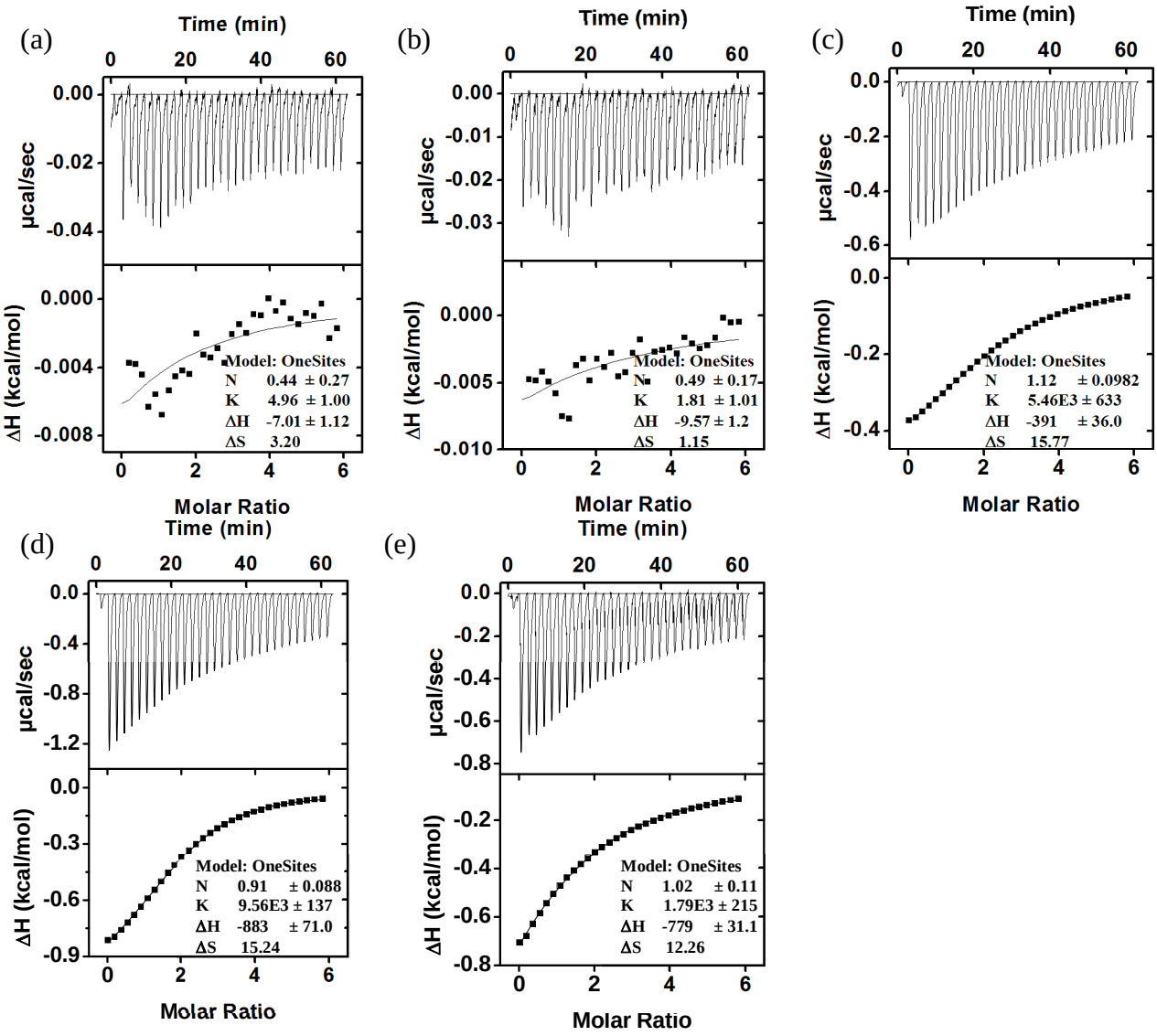

Figure 79S. ITC titration curves obtained at 298 K for the titration of MINP(maltulose) with maltose (a), cellobiose (b), gentiobiose (c), maltulose (d), and lactose (e) in 10 mM HEPES buffer (pH 7.4, maltulose/FM **3** = 1:2). The data correspond to entries 3–7, respectively, in Table 3S. The top panel shows the raw calorimetric data. The area under each peak represents the amount of heat generated at each ejection and is plotted against the molar ratio of MINP to the substrate. The solid line is the best fit of the experimental data to the sequential binding of N equal and independent binding sites on the MINP. The heat of dilution for the substrate, obtained by adding the substrate to the buffer, was subtracted from the heat released during the binding. Binding parameters were auto-generated after curve fitting using Microcal Origin 7.

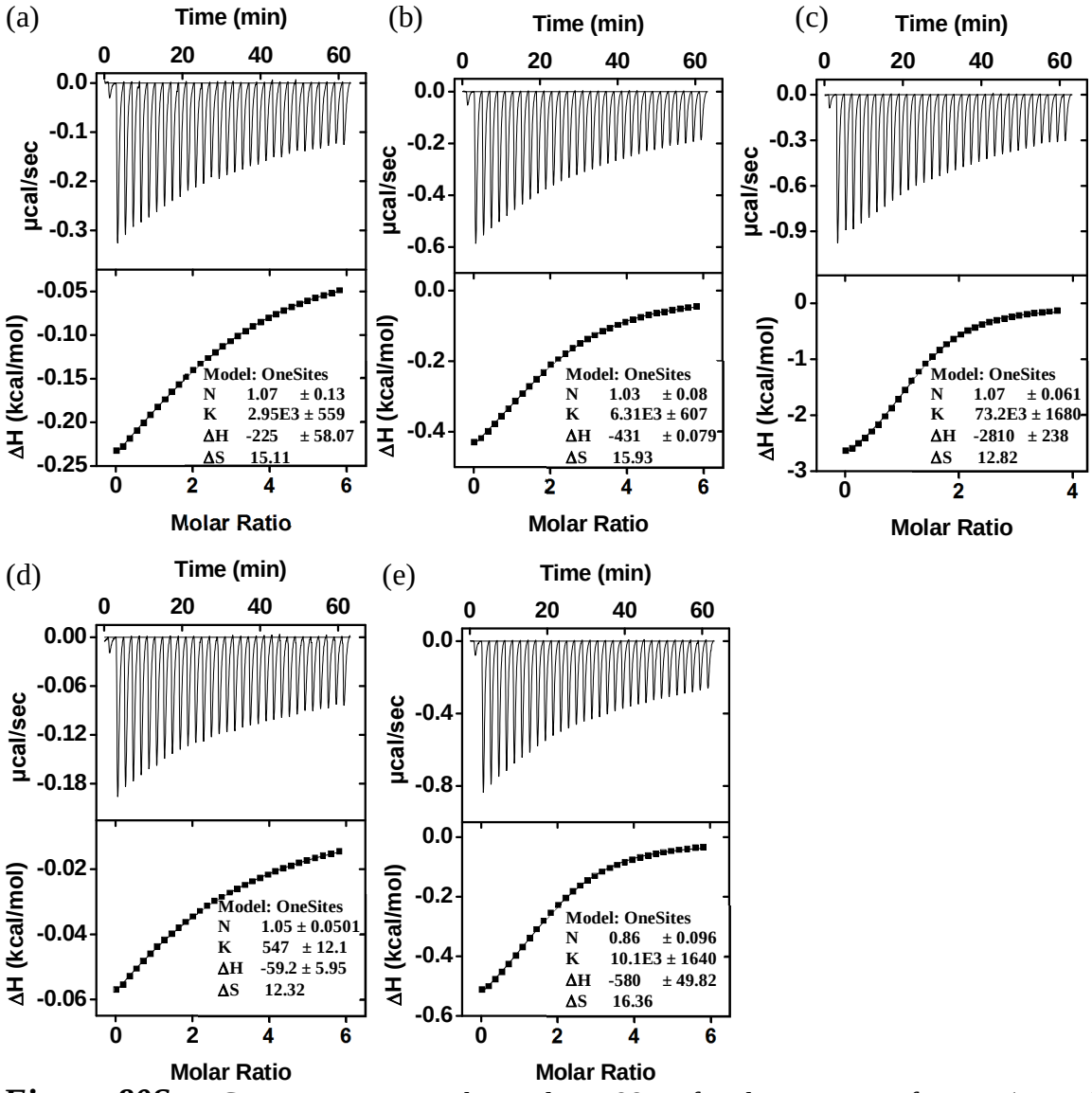

Figure 80S. ITC titration curves obtained at 298 K for the titration of MINP(gentiobiose) with maltose (a), cellobiose (b), gentiobiose (c), maltulose (d), and lactose (e) in 10 mM HEPES buffer (pH 7.4, gentiobiose/FM **3** = 1:2). The data correspond to entries 8–12, respectively, in Table 3S. The top panel shows the raw calorimetric data. The area under each peak represents the amount of heat generated at each ejection and is plotted against the molar ratio of MINP to the substrate. The solid line is the best fit of the experimental data to the sequential binding of N equal and independent binding sites on the MINP. The heat of dilution for the substrate, obtained by adding the substrate to the buffer, was subtracted from the heat released during the binding. Binding parameters were auto-generated after curve fitting using Microcal Origin 7.

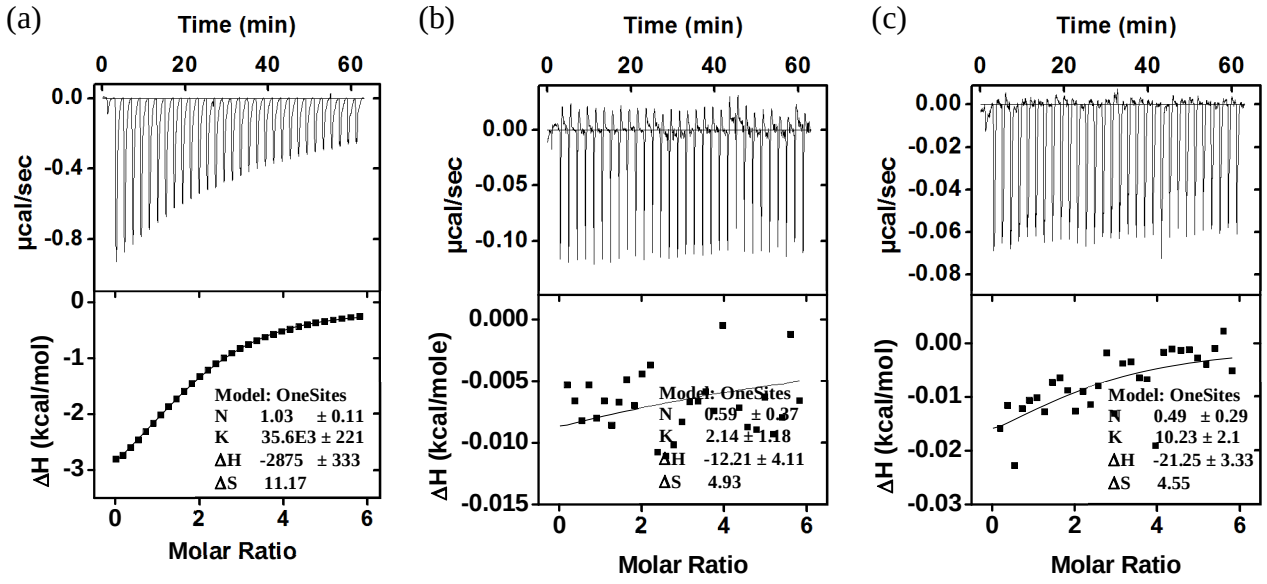

Figure 81S. ITC titration curves obtained at 298 K for the titration of MINP(H) with sugar H (a), sugar A (b), and sugar B (c) in 10 mM HEPES buffer (pH 7.4, sugar H/FM **3** = 1:2). The data correspond to entries 1–3, respectively, in Table 3. The top panel shows the raw calorimetric data. The area under each peak represents the amount of heat generated at each ejection and is plotted against the molar ratio of MINP to the substrate. The solid line is the best fit of the experimental data to the sequential binding of N equal and independent binding sites on the MINP. The heat of dilution for the substrate, obtained by adding the substrate to the buffer, was subtracted from the heat released during the binding. Binding parameters were auto-generated after curve fitting using Microcal Origin 7.

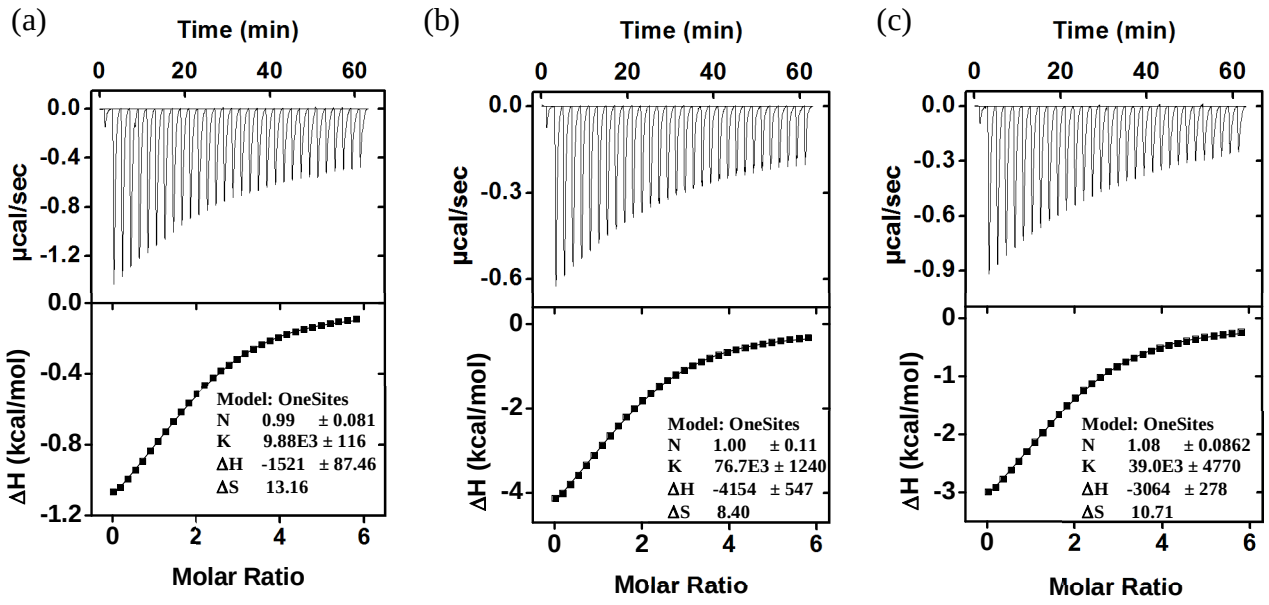

Figure 82S. ITC titration curves obtained at 298 K for the titration of MINP(A) with sugar H (a), sugar A (b), and sugar B (c) in 10 mM HEPES buffer (pH 7.4, sugar A/FM **3** = 1:3). The data correspond to entries 4–6, respectively, in Table 3. The top panel shows the raw calorimetric data. The area under each peak represents the amount of heat generated at each ejection and is plotted against the molar ratio of MINP to the substrate. The solid line is the best fit of the experimental data to the sequential binding of N equal and independent binding sites on the MINP. The heat of dilution for the substrate, obtained by adding the substrate to the buffer, was subtracted from the heat released during the binding. Binding parameters were auto-generated after curve fitting using Microcal Origin 7.

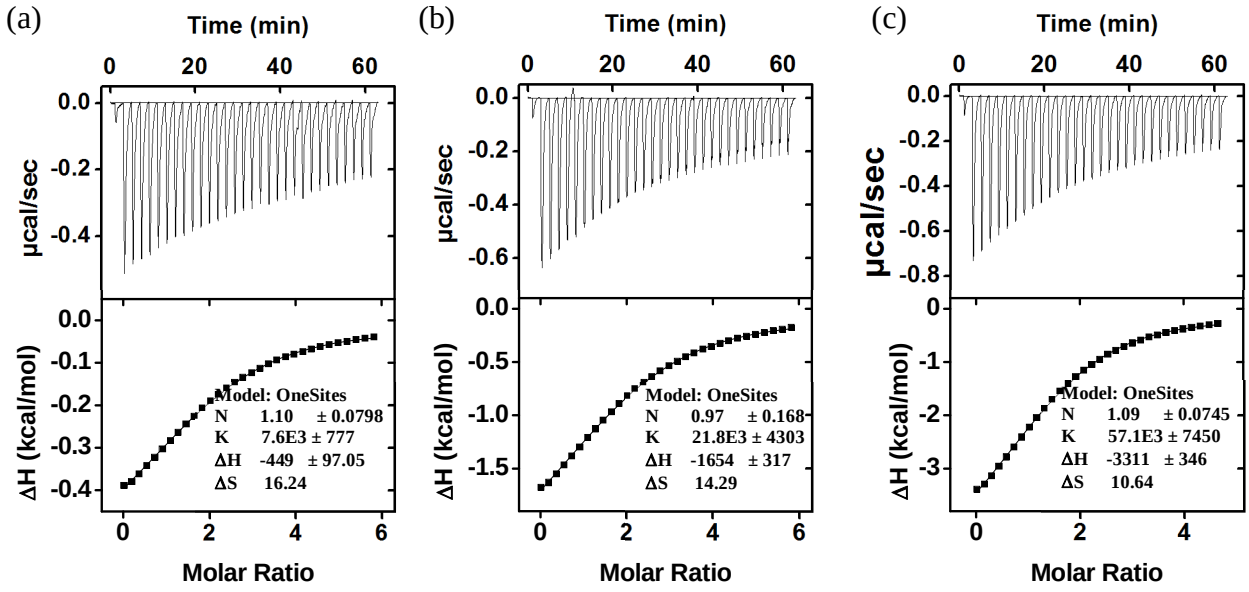

Figure 83S. ITC titration curves obtained at 298 K for the titration of MINP(B) with sugar H (a), sugar A (b), and sugar B (c) in 10 mM HEPES buffer (pH 7.4, sugar B/FM **3** = 1:3). The data correspond to entries 7–9, respectively, in Table 3. The top panel shows the raw calorimetric data. The area under each peak represents the amount of heat generated at each ejection and is plotted against the molar ratio of MINP to the substrate. The solid line is the best fit of the experimental data to the sequential binding of N equal and independent binding sites on the MINP. The heat of dilution for the substrate, obtained by adding the substrate to the buffer, was subtracted from the heat released during the binding. Binding parameters were auto-generated after curve fitting using Microcal Origin 7.

[1]H and [13]C NMR spectra

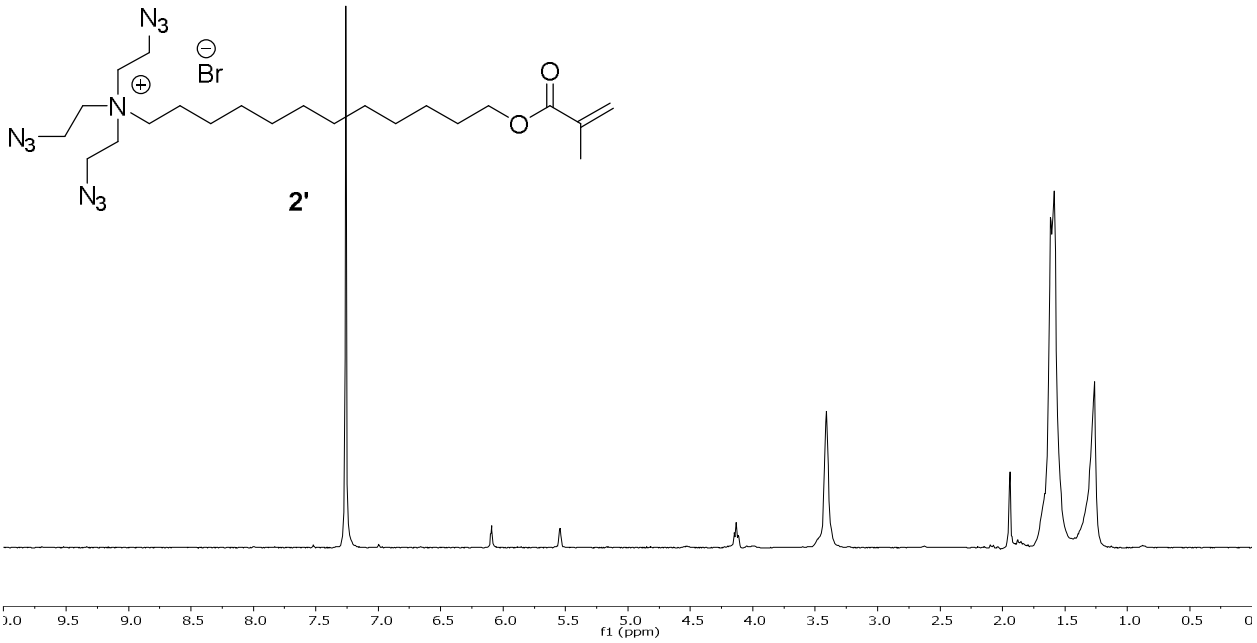

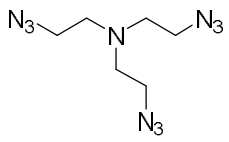
N3
N
N3
N3

13

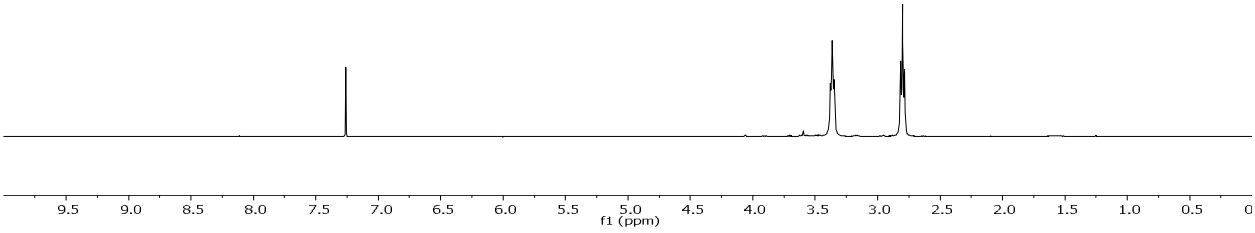
9.5 9.0 8.5 8.0 7.5 7.0 6.5 6.0 5.5 5.0 4.5 4.0 3.5 3.0 2.5 2.0 1.5 1.0 0.5 0
f1 (ppm)

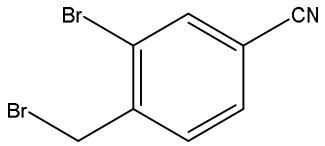
Br
CN
Br

14

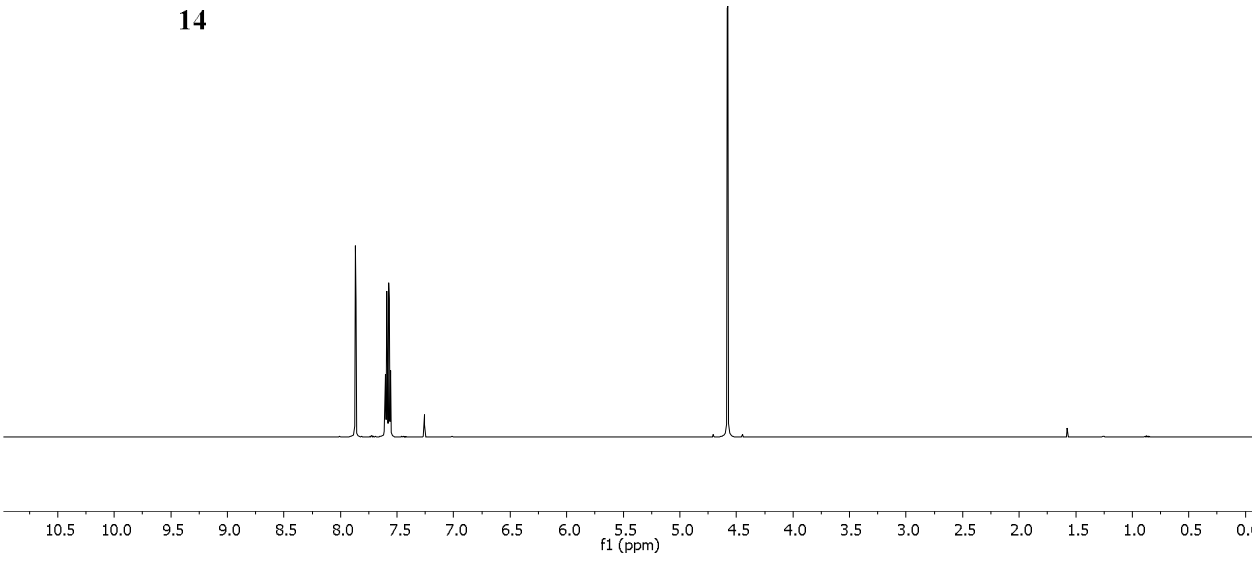
10.5 10.0 9.5 9.0 8.5 8.0 7.5 7.0 6.5 6.0 5.5 5.0 4.5 4.0 3.5 3.0 2.5 2.0 1.5 1.0 0.5
f1 (ppm)

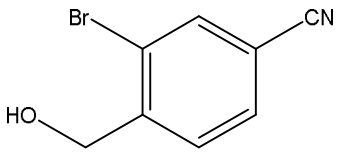

15

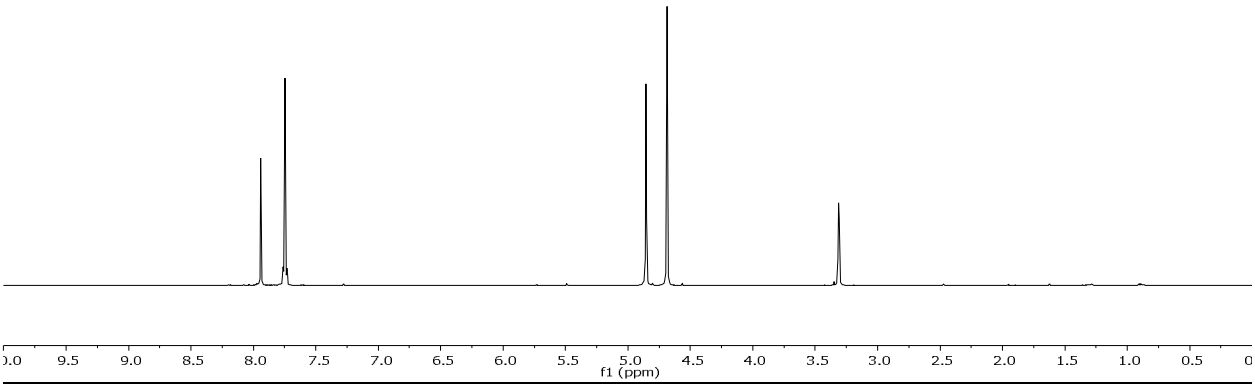

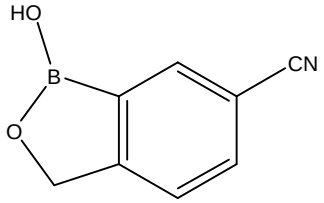

16

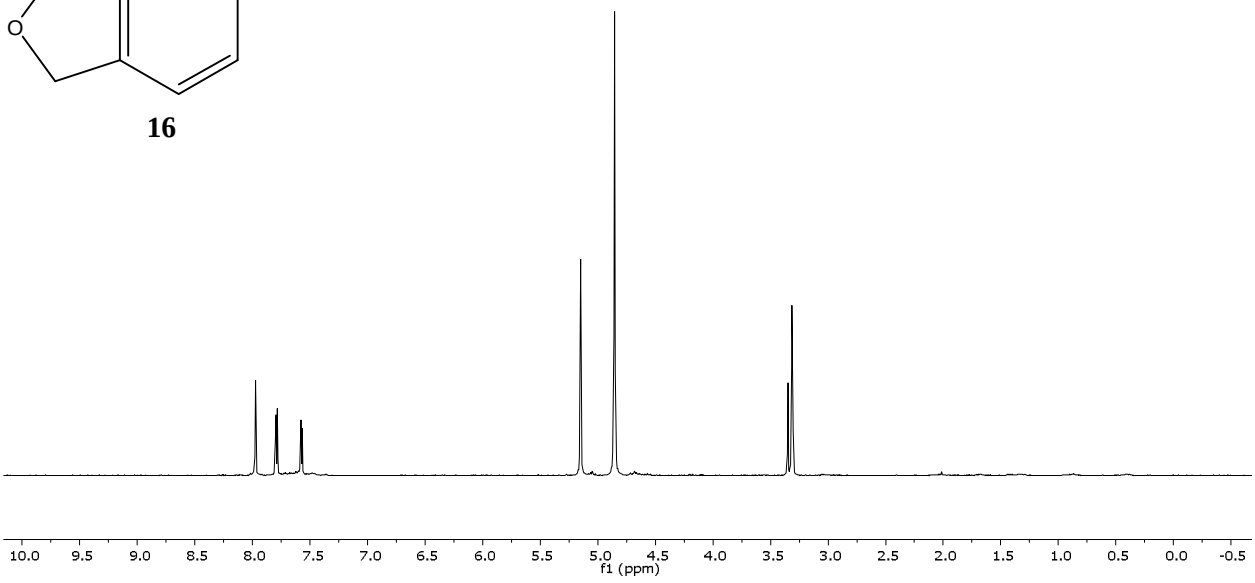

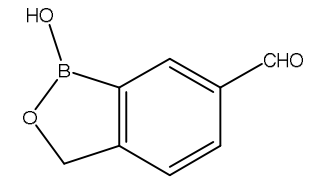
HO
B
O
CHO

17

11.5 11.0 10.5 10.0 9.5 9.0 8.5 8.0 7.5 7.0 6.5 6.0 5.5 5.0 4.5 4.0 3.5 3.0 2.5 2.0 1.5 1.0 0.5
f1 (ppm)

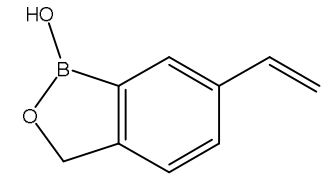
HO
B
O

4

11.0 10.5 10.0 9.5 9.0 8.5 8.0 7.5 7.0 6.5 6.0 5.5 5.0 4.5 4.0 3.5 3.0 2.5 2.0 1.5 1.0 0.5
f1 (ppm)

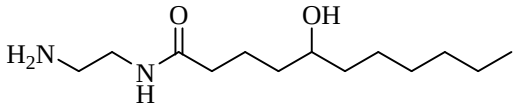

18

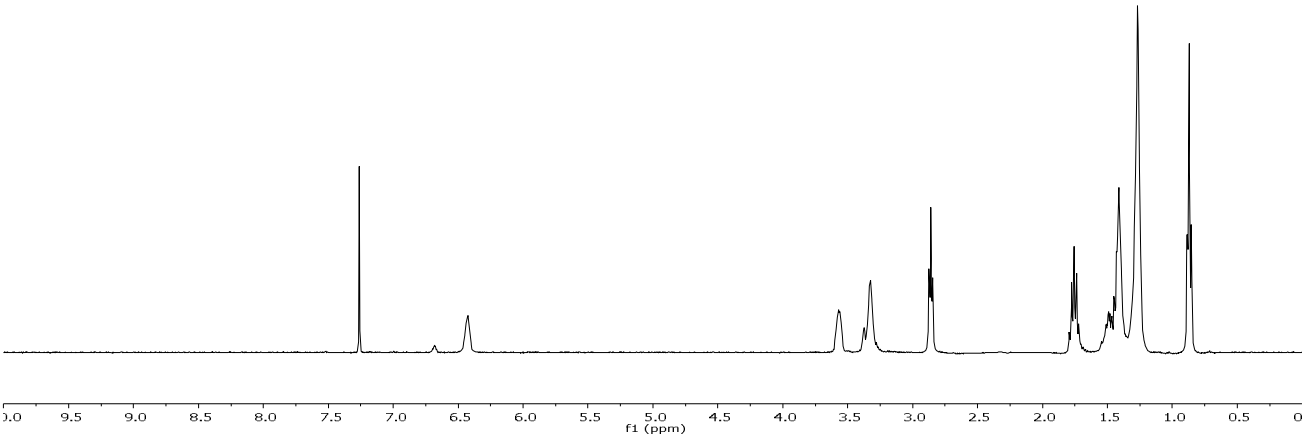

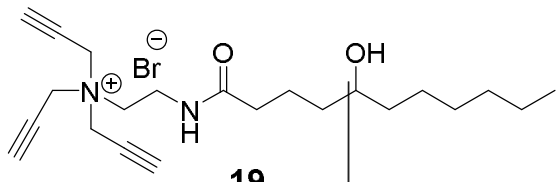

19

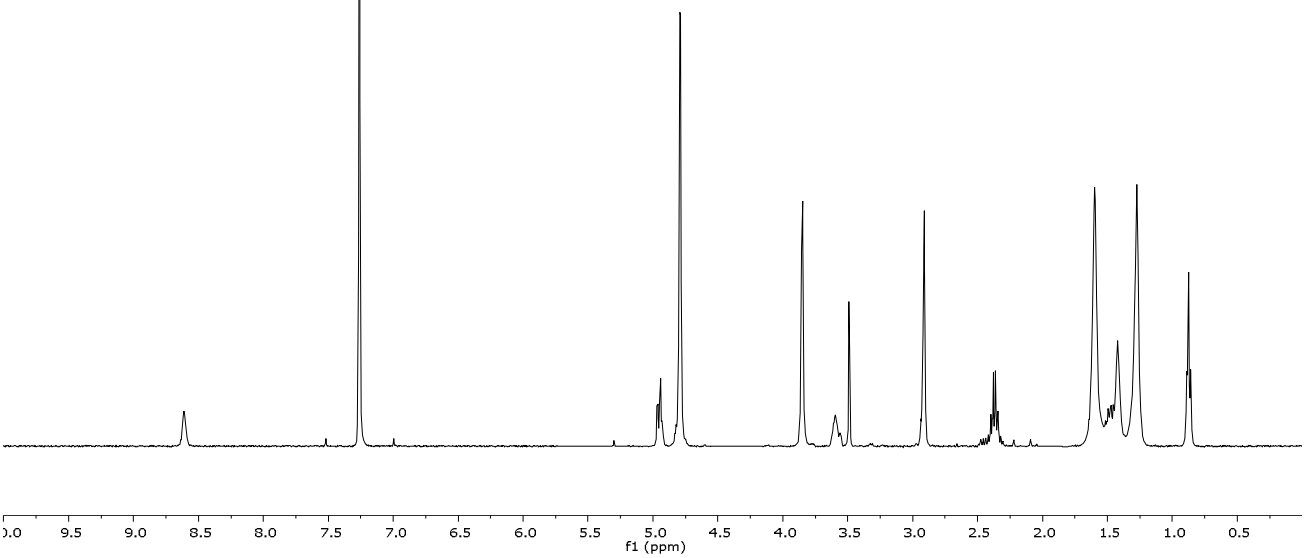

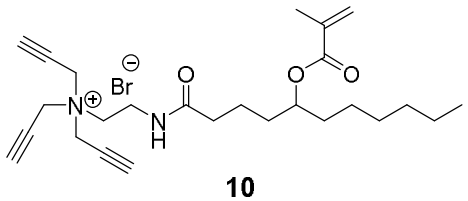

10

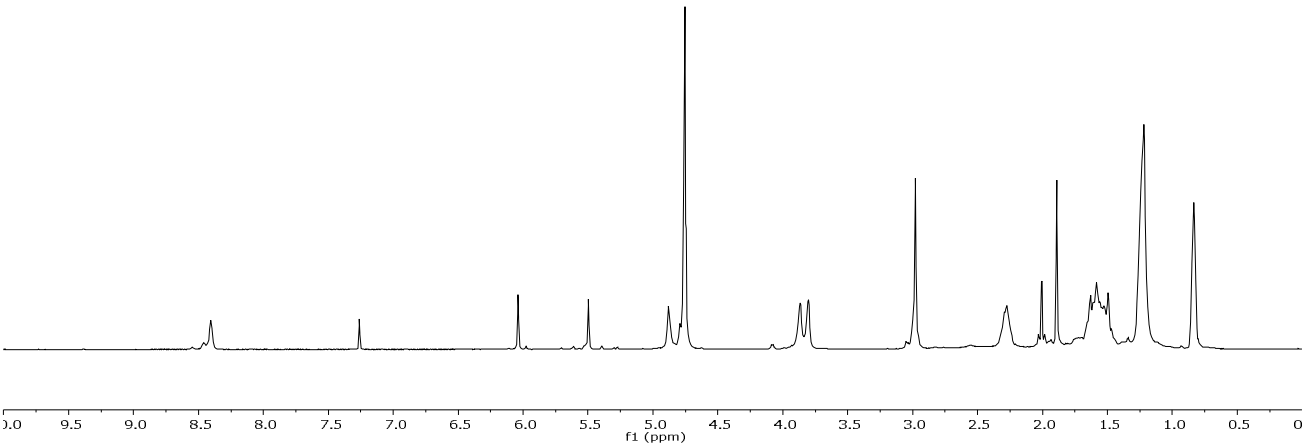

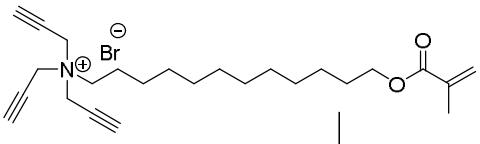

1

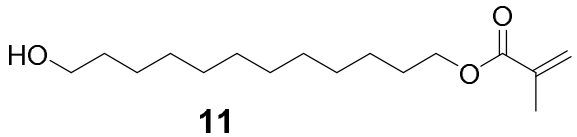

11